CONFIDENTIAL

NASA TECHNICAL MEMORANDUM

NASA TM X-2900

NASA TM X-2900

DYNAMIC STABILITY CHARACTERISTICS IN PITCH, YAW, AND ROLL OF A SUPERCRITICAL-WING RESEARCH AIRPLANE MODEL

by Richmond P. Boyden

Langley Research Center
Hampton, Va. 23665

NATIONAL AERONAUTICS AND SPACE ADMINISTRATION • WASHINGTON, D. C. • MAY 1974

CONFIDENTIAL

~~CONFIDENTIAL~~

1. Report No. NASA TM X-2900	2. Government Accession No.	3. Recipient's Catalog No.
4. Title and Subtitle DYNAMIC STABILITY CHARACTERISTICS IN PITCH, YAW, AND ROLL OF A SUPERCRITICAL-WING RESEARCH AIRPLANE MODEL (U)		5. Report Date May 1974
		6. Performing Organization Code
7. Author(s) Richmond P. Boyden		8. Performing Organization Report No. L-9006
		10. Work Unit No. 767-73-01-04
9. Performing Organization Name and Address NASA Langley Research Center Hampton, Va. 23665		11. Contract or Grant No.
		13. Type of Report and Period Covered Technical Memorandum
12. Sponsoring Agency Name and Address National Aeronautics and Space Administration Washington, D.C. 20546		14. Sponsoring Agency Code

15. Supplementary Notes

16. Abstract

The aerodynamic damping in pitch, yaw, and roll and the oscillatory stability in pitch and yaw of a supercritical-wing research airplane model have been determined for Mach numbers of 0.25 to 1.20 by using the small-amplitude forced-oscillation technique. The angle-of-attack range was from -2° to 20°. The effects of the underwing leading-edge vortex generators and the contributions of the wing, vertical tail, and horizontal tail to the appropriate damping and stability parameters were measured.

17. Key Words (Suggested by Author(s))
Dynamic stability
Transonic aerodynamics
Supercritical wing

DYNAMIC STABILITY CHARACTERISTICS IN PITCH, YAW, AND ROLL OF A SUPERCRITICAL-WING RESEARCH AIRPLANE MODEL*

By Richmond P. Boyden
Langley Research Center

SUMMARY

The aerodynamic damping in pitch, yaw, and roll and the oscillatory stability in pitch and yaw of a supercritical-wing research airplane model have been determined for Mach numbers of 0.25 to 1.20 by using the small-amplitude forced-oscillation technique. The angle-of-attack range was from -2° to 20°. The effects of the underwing leading-edge vortex generators and the contributions of the wing, vertical tail, and horizontal tail to the appropriate damping and stability parameters were measured.

INTRODUCTION

In order to verify the aerodynamic gains predicted in small-scale wind-tunnel tests for the supercritical-wing concept (refs. 1 and 2), the National Aeronautics and Space Administration has conducted a flight test program utilizing a fighter-type airplane with a modified wing having a supercritical airfoil section (ref. 3). In support of this flight test program, the Langley Research Center has determined the dynamic stability characteristics of a model of the research airplane configuration as modified for the flight test program.

The purpose of this paper is to present the results of these tests made in the Langley 8-foot transonic pressure tunnel to determine the aerodynamic damping in pitch, yaw, and roll, the oscillatory stability in pitch and yaw, and the effective-dihedral parameter. In addition, the normal-force stability derivatives in phase and out of phase with pitch rate were determined as were the lateral cross-derivative parameters. The tests were made over a Mach number range from 0.25 to 1.20 with a variation in Reynolds number, based on the mean geometric chord, from 0.83×10^6 to 1.55×10^6. The angle of attack was varied from about -2° to 20°. The tests were made by using a forced-oscillation technique with an oscillation amplitude of about 1° in pitch and yaw and about $2\frac{1}{2}^{\circ}$ in roll.

The wing vortex generators (used to decrease a pitch-up problem), wing, horizontal tail, and vertical tail were removed for certain portions of the tests to determine the

*Title, Unclassified.

contribution of these individual components to the various stability derivatives. Because the restrictions on the size of the model precluded any flow-through ducts, the engine inlet was filled and faired into the lines of the fuselage.

SYMBOLS

The aerodynamic parameters presented in this paper are referred to the body system of axes as shown in figure 1, in which the coefficients, angles, and angular velocities are shown in the positive sense. These axes originate at the center of oscillation which was located at the quarter-chord point of the mean geometric chord of the basic wing panel. The basic wing panel is formed by extending the leading and trailing edges of the outboard portion of the wing inward to the center line (see fig. 2(a)). The equations which were used to reduce the dimensional aerodynamic parameters of the model to nondimensional aerodynamic parameters are presented in appendix A, entitled "Measurements and Reduction of Data."

Units of measurement are given in the International System of Units (SI) with U.S. Customary Units given parenthetically. Measurements were made in U.S. Customary Units, and calculations were made in SI. Details on the use of SI, together with physical constants and conversion factors, are given in reference 4.

b reference span, 82.144 cm (32.340 in.)

C_l rolling-moment coefficient, $\dfrac{\text{Rolling moment}}{q_\infty Sb}$

$C_{l_p} = \dfrac{\partial C_l}{\partial\left(\dfrac{pb}{2V}\right)}$, per radian

$C_{l_{\dot{p}}} = \dfrac{\partial C_l}{\partial\left(\dfrac{\dot{p}b^2}{4V^2}\right)}$, per radian

$C_{l_p} + C_{l_{\dot{\beta}}} \sin\alpha$ damping-in-roll parameter, per radian

$C_{l_r} = \dfrac{\partial C_l}{\partial\left(\dfrac{rb}{2V}\right)}$, per radian

$C_{l_{\dot{r}}} = \dfrac{\partial C_l}{\partial\left(\dfrac{\dot{r}b^2}{4V^2}\right)}$, per radian

$C_{l_r} - C_{l_{\dot{\beta}}} \cos \alpha$ rolling moment due to yaw rate parameter, per radian

$C_{l_\beta} = \dfrac{\partial C_l}{\partial \beta}$, per radian

$C_{l_{\dot{\beta}}} = \dfrac{\partial C_l}{\partial\left(\dfrac{\dot{\beta}b}{2V}\right)}$, per radian

$C_{l_\beta} \sin \alpha - k^2 C_{l_{\dot{p}}}$ rolling moment due to roll displacement parameter, per radian

$C_{l_\beta} \cos \alpha + k^2 C_{l_{\dot{r}}}$ effective-dihedral parameter, per radian

C_m pitching-moment coefficient, $\dfrac{\text{Pitching moment}}{q_\infty S\bar{c}}$

$C_{m_q} = \dfrac{\partial C_m}{\partial\left(\dfrac{q\bar{c}}{2V}\right)}$, per radian

$C_{m_{\dot{q}}} = \dfrac{\partial C_m}{\partial\left(\dfrac{\dot{q}\bar{c}^2}{4V^2}\right)}$, per radian

$C_{m_q} + C_{m_{\dot{\alpha}}}$ damping-in-pitch parameter, per radian

$C_{m_\alpha} = \dfrac{\partial C_m}{\partial \alpha}$, per radian

$C_{m_{\dot{\alpha}}} = \dfrac{\partial C_m}{\partial\left(\dfrac{\dot{\alpha}\bar{c}}{2V}\right)}$, per radian

$C_{m_\alpha} - k^2 C_{m_{\dot{q}}}$ oscillatory longitudinal-stability parameter, per radian

C_N normal-force coefficient, $\dfrac{\text{Normal force}}{q_\infty S}$

$C_{N_q} = \dfrac{\partial C_N}{\partial\left(\dfrac{q\bar{c}}{2V}\right)}$, per radian

$C_{N_{\dot{q}}} = \dfrac{\partial C_N}{\partial\left(\dfrac{\dot{q}\bar{c}^2}{4V^2}\right)}$, per radian

$C_{N_q} + C_{N_{\dot{\alpha}}}$ normal force due to pitch rate parameter, per radian

$C_{N_\alpha} = \dfrac{\partial C_N}{\partial \alpha}$, per radian

$C_{N_{\dot{\alpha}}} = \dfrac{\partial C_N}{\partial\left(\dfrac{\dot{\alpha}\bar{c}}{2V}\right)}$, per radian

$C_{N_\alpha} - k^2 C_{N_{\dot{q}}}$ normal force due to pitch displacement parameter, per radian

C_n yawing-moment coefficient, $\dfrac{\text{Yawing moment}}{q_\infty Sb}$

$C_{n_p} = \dfrac{\partial C_n}{\partial\left(\dfrac{pb}{2V}\right)}$, per radian

$C_{n_{\dot{p}}} = \dfrac{\partial C_n}{\partial\left(\dfrac{\dot{p}b^2}{4V^2}\right)}$, per radian

$C_{n_p} + C_{n_{\dot{\beta}}} \sin \alpha$ yawing moment due to roll rate parameter, per radian

$C_{n_r} = \frac{\partial C_n}{\partial\left(\frac{rb}{2V}\right)}$, per radian

$C_{n_{\dot{r}}} = \frac{\partial C_n}{\partial\left(\frac{\dot{r}b^2}{4V^2}\right)}$, per radian

$C_{n_r} - C_{n_{\dot{\beta}}} \cos \alpha$ damping-in-yaw parameter, per radian

$C_{n_\beta} = \frac{\partial C_n}{\partial \beta}$, per radian

$C_{n_{\dot{\beta}}} = \frac{\partial C_n}{\partial\left(\frac{\dot{\beta}b}{2V}\right)}$, per radian

$C_{n_\beta} \cos \alpha + k^2 C_{n_{\dot{r}}}$ oscillatory directional-stability parameter, per radian

$C_{n_\beta} \sin \alpha - k^2 C_{n_{\dot{p}}}$ yawing moment due to roll displacement parameter, per radian

c local streamwise chord, cm (in.)

$\bar{c}$ reference chord, 13.015 cm (5.124 in.)

f frequency of oscillation, hertz

k reduced-frequency parameter, $\omega\bar{c}/2V$ in pitch; $\omega b/2V$ in roll and yaw, radians

M free-stream Mach number

p angular velocity of model about X-axis, radians per second

q	angular velocity of model about Y-axis, radians per second
q_∞	free-stream dynamic pressure, newtons per meter^2
R	Reynolds number based on $\bar{c}$
r	angular velocity of model about Z-axis, radians per second
S	reference area, 998.1 cm^2 (154.7 in^2)
t/c	thickness-chord ratio
V	free-stream velocity, meters per second
α	angle of attack, degrees or radians
β	angle of sideslip, radians
ω	angular velocity, $2\pi f$, radians per second

Configuration nomenclature:

F	fuselage
H	horizontal tail
V	vertical tail
W	wing
X	vortex generators

A dot over a quantity indicates a first derivative with respect to time.

MODEL DESCRIPTION

The 1/16-scale model of the fighter-type configuration with a modified wing planform (similar to proposed advanced transport configurations) utilizing supercritical

airfoil sections is shown in the drawings of figure 2 and in the photographs of figure 3. The model was based on configuration 140 of reference 5, and a complete set of nondimensional wing coordinates is contained in reference 5. For these tests, two modifications were made to the basic lines of the model described in reference 5. Because there was insufficient room in the fuselage for flow-through ducts, the fuselage engine inlet was closed and faired into the fuselage lines. The second modification required was an enlargement of the rear fuselage lines in the vicinity of the exhaust exit to allow for sting clearance. Both of the modifications are indicated in figure 2(a).

The forward portion of the fuselage including part of the wing glove was of fiberglass construction. The rear portion of the fuselage and the wing and tail surfaces were made of aluminum. A steel strongback was used to carry the wing loads through to the small-amplitude forced-oscillation balance. For testing with the wing removed, an alternate fuselage nose was used which did not include any portion of the wing glove (figs. 3(c) and 3(d)). Provisions were also made for removing the vertical and horizontal tails. A fixed incidence of 0° was used for the horizontal tail.

Underwing leading-edge vortex generators were used for part of the tests. These vortex generators were located at 60 percent of the wing semispan and are small 10-percent-thick Clark Y airfoils oriented with the flat lower surface facing inboard (fig. 2(b) and ref. 6).

TESTS AND PRESENTATION OF DATA

The small-amplitude forced-oscillation balance mechanisms used for these tests are shown in figures 4 and 5 and some detail of their operation is given in appendix B.

The tests reported herein were made in the Langley 8-foot transonic pressure tunnel. The characteristics and operating conditions of this tunnel are covered in reference 7. The dynamic-stability parameters were measured at selected Mach numbers from 0.25 to 1.20 over an angle-of-attack range extending from -2° to 20°. All tests at $M = 1.20$ were limited to an angle of attack of about 10° because of the reflected shock from the model nose impinging on the vertical tail. The amplitude of the oscillation for the pitch and the yaw tests was about 1° whereas it was about $2\frac{1}{2}^{\circ}$ for the roll tests. Nominal test conditions are listed in the following table. The Reynolds number is based on the mean geometric chord of the wing outer panel extended to the fuselage center line (see fig. 2).

The range of reduced-frequency parameter was from 0.0038 to 0.0240 in pitch, 0.020 to 0.134 in yaw, and 0.034 to 0.348 in roll.

Mach number, M	Dynamic pressure, kN/m^2 (lb/ft^2)	Stagnation temperature, K (^oF)	Reynolds number, R
0.25	5.51 (115)	322 (120)	0.83×10^6
.50	15.56 (325)	↓	1.23
.80	28.73 (600)	↓	1.55
.90	↓	↓	1.43
.95	↓	↓	1.39
.99	↓	↓	1.35
1.02	↓	↓	1.33
1.20	↓	↓	1.23

For all tests, the balance oscillation center was located at the model station corresponding to $0.25\bar{c}$. Tests were made with various components removed from the complete configuration. These included the wing, underwing leading-edge vortex generators, horizontal tail, and vertical tail.

In order to insure a turbulent boundary layer over the model, carborundum grains were applied as three-dimensional roughness to the model nose, to the leading edge of the wing, and to the leading edges of the horizontal- and vertical-tail surfaces. The roughness size and location were computed by using the method of reference 8. Strips of No. 120 carborundum grains were applied around the fuselage 2.54 cm (1.00 in.) rearward from the nose for all tests. On the horizontal and vertical tails, transition strips of No. 120 carborundum grains were applied at 5 percent of the local streamwise chord for all tests. All the transition strips were 0.127 cm (0.05 in.) wide. The location and size of the carborundum transition strips on the wing were modified, based on the work in references 5, 9, and 10, in order to better simulate full-scale flow at the high Mach numbers. The fluorescent-oil film method of reference 11 was used to define the wing transition-strip location by avoiding the occurrence of any laminar separation ahead of the transition strip. The location and size of the transition roughness used on the wing are shown in figure 6. As shown in the figure, the size and location of the transition roughness on the wing upper surface were different for the two Mach number ranges of 0.25 to 0.90 and 0.95 to 1.20. The transition placement on the wing is referred to as "normal" in the data figures for the lower Mach number range and as "supercritical" for the higher Mach number range.

The basic principles of operation of the dynamic-stability system using the small-amplitude forced-oscillation mechanism and the equations used to compute the different dynamic-stability parameters are covered in appendix A.

RESULTS AND DISCUSSION

Pitching Characteristics

Basic configuration.- The results for the basic configuration (FWHV) are contained in figure 7. The configuration has positive damping in pitch (negative values of $C_{m_q} + C_{m_{\dot{\alpha}}}$) over most of the Mach number and angle-of-attack ranges except for negative damping at angles of attack greater than 12° for Mach numbers of 0.99 to 1.02. In the low angle-of-attack range, the basic configuration has positive oscillatory longitudinal stability (negative values of $C_{m_\alpha} - k^2 C_{m_{\dot{q}}}$) except for instabilities near angles of attack from 6° to 10° for subsonic and transonic Mach numbers. These regions of negative oscillatory longitudinal stability correlate well with the static data for this configuration reported in reference 5, where pitch-up problems were encountered for similar angles of attack and Mach numbers.

The normal-force characteristics measured during the pitching tests are shown in figure 8 for the basic configuration. The normal force due to pitching rate parameter $\left(C_{N_q} + C_{N_{\dot{\alpha}}}\right)$ generally increases negatively with increased Mach number in the low angle-of-attack range for subsonic Mach numbers. The trend reverses for the supersonic Mach numbers so that the parameter becomes less negative. The results for the normal force due to pitching displacement $\left(C_{N_\alpha} - k^2 C_{N_{\dot{q}}}\right)$ presented in figure 8 are generally in good agreement with the static lift-curve slopes for similar test conditions taken from reference 5 for the low angle-of-attack range.

Effect of vortex generators.- Because of the longitudinal-stability problems (pitch-up) with the basic supercritical-wing research airplane configuration discussed in reference 5 (and evident in the results presented in fig. 7), underwing leading-edge vortex generators were developed as reported in reference 6. The vortex generators were designed to delay any pitch-up tendency to higher angles of attack or to minimize the severity of the pitch-up. The vortex on the wing upper surface created by the vortex generator tends to prevent spanwise flow of the boundary layer and decreases the tendency of the flow to separate from the upper surface of the outboard wing panel.

The results for the damping in pitch and the oscillatory longitudinal stability for the basic configuration with the vortex generators added (FWHVX) are shown in figure 9. The addition of the vortex generators had little effect on the damping in pitch except at moderate to high angles of attack ($\alpha = 14^\circ$ to 20°) where there were large negative values in the pitch damping. However, the configuration with vortex generators (FWHVX) has improved oscillatory longitudinal stability over the low to moderate angle-of-attack range as compared with the basic configuration (FWHV). A region of negative longitudinal stability (positive values of $C_{m_\alpha} - k^2 C_{m_{\dot{q}}}$) is still evident near $\alpha = 8^\circ$ for $M = 0.90$, but

the magnitude has been reduced by the addition of the vortex generators as can be seen by comparing figures 7 and 9. There are some areas of negative longitudinal stability at the higher angles of attack for configuration FWHVX for Mach numbers of 0.25 to 0.95 but these are above the normal flight values of angle of attack. Coincident with each of these areas of instability is a sharp increase in the pitch damping which is probably a result of separated flow on the wing.

The normal-force-parameter results for the basic configuration with the vortex generators (FWHVX) are in figure 10 and generally show the same trends with Mach number and angle of attack as were found for configuration FWHV.

Effect of configuration components.- The component-breakdown results for Mach numbers of 0.25, 0.90, 0.99, and 1.20 are shown in figures 11 and 12. The horizontal tail generally made the largest contribution to the damping in pitch as would be expected. However, near angles of attack of 8° to 10° at subsonic speeds the wing (configuration FWV) had a large positive damping contribution. This damping was apparently a result of a flow separation on the outer wing panels as it coincided with a decrease in the oscillatory longitudinal-stability parameter $\left(C_{m_\alpha} - k^2 C_{m_{\dot{q}}}\right)$ to large positive or unstable values. Increased damping in pitch due to the wing near the stall has previously been found for a variable-sweep-wing fighter model with the wing at the 50° sweep position as reported in reference 12. The fuselage contribution (configuration FV) to the pitch damping was positive and showed only a small variation with angle of attack throughout the Mach number range.

The normal-force components both in phase and out of phase with displacement are primarily determined by the wing contribution as seen in figure 12.

Yawing Characteristics

Basic configuration.- The damping-in-yaw parameter $\left(C_{n_r} - C_{n_{\dot{\beta}}} \cos \alpha\right)$ and the oscillatory directional-stability parameter $\left(C_{n_\beta} \cos \alpha + k^2 C_{n_{\dot{r}}}\right)$ are shown in figure 13 for the basic configuration (FWHV). At angles of attack from 8° to 12° at $M = 0.90$ for this configuration, no data were obtained because of some model-sting vibrations in the vertical plane which were apparently caused by large unsteady aerodynamic loads on the model. The basic configuration had positive damping in yaw (negative values of $C_{n_r} - C_{n_{\dot{\beta}}} \cos \alpha$) throughout the entire angle-of-attack and Mach number ranges except at $\alpha = 20^{\circ}$ for $M = 0.99$ and $M = 1.02$. The oscillatory directional-stability parameter has positive values, indicating a stabilizing effect, up to angles of attack of 15° to 20° depending on the particular Mach number.

The rolling moment due to yaw rate parameter and the effective-dihedral parameter for the basic configuration (FWHV) are in figure 14. Generally, the rolling moment due

to yaw rate parameter is seen to have positive values and to increase in magnitude with increasing angle of attack up to moderate angles of attack. However, some large negative values were found at $M = 0.95$ at $\alpha = 10^{\circ}$ and 14°. The reason for these extreme values has not been determined. The effective-dihedral parameter shows that there is positive dihedral effect over the entire range of angle of attack and Mach number, but there is considerable variation in the magnitude with angle of attack and Mach number.

The vortex generators appear to have only minor effects on the yawing characteristics, especially at low angles of attack, as can be seen by comparing figures 13 and 14 with figures 15 and 16.

Effect of configuration components.- The component-breakdown results for the damping in yaw and the oscillatory directional stability are shown in figure 17 for Mach numbers of 0.25, 0.90, 0.99, and 1.20. The small differences due to the vortex generators can also be seen from a comparison of configurations FWHV and FWHVX. The large contributions of the vertical tail to the yaw damping and to the directional stability throughout the Mach number range are evident from a comparison of the differences between the configurations with the vertical tail on and off. The addition of the wing to configuration FHV had a destabilizing effect on the directional-stability parameter at the lower angles of attack. However, at angles of attack above 10° to 12° for the subsonic Mach numbers, the addition of the wing resulted in a stabilizing contribution to the directional-stability parameter and a negative damping contribution.

The results for the component breakdown for the rolling moment due to yaw rate parameter and the effective-dihedral parameter are contained in figure 18. The vertical tail and the wing appear to be the primary components responsible for the rolling moment due to yaw rate parameter. For configuration FHV, this cross-derivative parameter is seen to increase positively with increasing angle of attack and this increase is assumed to be due largely to the vertical tail. For configuration FWH, the rolling moment due to yaw rate parameter generally increases positively with angle of attack up to 12° to 16° and then the values become more negative. The overall trends for configuration FWH with angle of attack are generally similar to those of the basic configuration (FWHV) for both the rolling moment due to yaw rate parameter and the effective-dihedral parameter. For the configuration with the wing removed (FHV), the effective-dihedral parameter has about the same value as for the basic configuration at $\alpha = -2^{\circ}$ and then the values for configuration FHV increase positively with angle of attack for all Mach numbers.

Rolling Characteristics

Basic configuration.- The damping-in-roll parameter $\left(C_{l_p} + C_{l_{\dot{\beta}}} \sin \alpha\right)$ for the basic configuration (FWHV) as shown in figure 19 has negative values (positive damping)

throughout the range of test parameters with the exception of 10° angle of attack at a Mach number of 0.99. The roll damping generally decreases with increasing angle of attack for Mach numbers of 0.80 and less in the moderate range of angle of attack, whereas for Mach numbers above 0.80, the roll damping first increases with angle of attack up to 2° to 4° and then decreases. This change in the roll damping with angle of attack implies a similar variation in the lift-curve slope which is evident in references 5 and 6. The rolling moment due to roll displacement parameter, $C_{l_\beta} \sin \alpha - k^2 C_{l_{\dot{p}}}$ where $C_{l_\beta} \sin \alpha$ is the aerodynamic "spring" term resulting from the rolling motion about the body axis at an angle of attack, is also presented for completeness. However, because of the "sin α" multiplier this parameter is not as useful as the effective-dihedral parameter $\left(C_{l_\beta} \cos \alpha + k^2 C_{l_{\dot{r}}}\right)$ presented earlier in the section "Yawing Characteristics."

The yawing moment due to roll rate parameter $\left(C_{n_p} + C_{n_{\dot{\beta}}} \sin \alpha\right)$ for configuration FWHV is in figure 20 and generally has a negative slope between angles of attack of 0° and 4° or 0° and 6° for the subsonic Mach numbers with positive or near-zero values at the higher angles of attack. The yawing moment due to roll displacement parameter $\left(C_{n_\beta} \sin \alpha - k^2 C_{n_{\dot{p}}}\right)$ is also shown but again the "sin α" multiplier makes this parameter less useful than the oscillatory directional-stability parameter $\left(C_{n_\beta} \cos \alpha + k^2 C_{n_{\dot{r}}}\right)$.

Effect of vortex generators.- The roll-damping results for the basic configuration with the vortex generators (FWHVX) are shown in figure 21. The addition of the vortex generators resulted in improved roll damping at the higher angles of attack in that the damping did not drop off as much with increased angle of attack as it did for configuration FWHV (see figs. 19 and 21). This is an indication of improved flow conditions on the outboard section of the wing because of the vortex generators.

The yawing moment due to roll rate results for configuration FWHVX are in figure 22. The apparent effect of the vortex generators on this parameter at subsonic Mach numbers was to extend slightly the angle of attack at which the curve breaks and the values become more positive.

Effect of configuration components.- The component-breakdown roll-damping results are in figure 23 and the beneficial effect of the vortex generators on the roll damping is evident, especially for the lower subsonic Mach numbers. The damping in roll of the basic configuration (FWHV) was usually only slightly larger in magnitude than the damping of just the fuselage and the wing (FW). For the basic configuration minus the wing (FHV), the roll damping is positive $\left(\text{negative values of } C_{l_p} + C_{l_{\dot{\beta}}} \sin \alpha\right)$ and there is little variation with either angle of attack or Mach number.

The yawing moment due to roll rate parameter results for the different configuration are shown in figure 24. The results for the fuselage plus the horizontal- and vertical-tail surfaces (FHV) have been omitted as the data did not appear to be consistent. It is thought

that the higher frequency of oscillation for this configuration might have caused a model-sting vibration problem in the yaw plane. The results for the basic configuration (FWHV) are seen to follow the trends of the fuselage-plus-wing configuration (FW) in the low angle-of-attack range for all Mach numbers. The increment in $C_{n_p} + C_{n_{\dot{\beta}}} \sin \alpha$ between these two configurations should be that due to the vertical tail.

Comparison of Experimental Data With Vortex-Lattice Estimates

A vortex-lattice computer program, described in reference 13, was used to make theoretical estimates of some of the subsonic aerodynamic parameters for comparison with the experimentally determined parameters. The FORTRAN program utilizes a vortex-lattice representation of a zero-thickness lifting planform. The program will handle two planforms so that a wing—horizontal-tail combination can be studied. The parameters of interest which were determined by the use of reference 13 for a planform representation of this configuration are C_{m_q}, $C_{m_{\dot{\alpha}}}$, C_{N_q}, $C_{N_{\dot{\alpha}}}$, and C_{l_p}. The results of the vortex-lattice program are based on the assumption of an attached-flow condition and are therefore only valid in the linear range of the lift-curve slope.

Figure 25(a) is a comparison between the experimental pitching-moment parameters from the pitch tests and theoretical estimates from the vortex-lattice program. The experimental data are for $\alpha = 0^\circ$ and the individual data points at $\alpha = 0^\circ$ have been averaged for the sake of clarity. The experimental values of $C_{m_q} + C_{m_{\dot{\alpha}}}$ for the basic configuration without the vortex generators (FWHV) are seen to have more positive damping over the subsonic Mach number range than the vortex-lattice values of C_{m_q} for the corresponding configuration (FWH). (The vertical tail cannot be represented in the vortex-lattice program but this lack of representation should have no effect on the pitching-moment results.) The difference between the experimental values and the vortex-lattice-program results is probably a result of the $C_{m_{\dot{\alpha}}}$ term not being included in the theoretical values shown here. The large decrease in the experimental damping-in-pitch parameter for configuration FWHV with Mach number between 0.95 and 1.02 is very evident in figure 25(a). The pitch-damping comparisons for the fuselage—horizontal-tail, fuselage-wing, and fuselage-alone configurations are seen to be good but with small differences in the level of damping. The experimental values for the fuselage and wing configuration showed negative damping at $M = 0.99$ which could not be predicted by theory.

The comparison of the experimental oscillatory longitudinal-stability parameter $\left(C_{m_\alpha} - k^2 C_{m_{\dot{q}}}\right)$ with the vortex-lattice values of C_{m_α} is also shown in figure 25(a). The theoretical values are shown to be slightly more stable than the experimental results. The best agreement was obtained for the fuselage-wing configuration where the differences between the experimental points for $M = 0.25$ and 0.90 and the vortex-lattice predictions were small.

The comparison of the normal force due to pitch rate parameter $\left(C_{N_q} + C_{N_{\dot{\alpha}}}\right)$ measured experimentally with the vortex-lattice C_{N_q} for the different configurations (or planforms) is shown in figure 25(b) for $\alpha = 0^{\circ}$. The experimental data for the two winged configurations are seen to depart drastically from the theoretical trends and go to large negative values. The reason for this change has not been determined. There is some experimental evidence, however, that $C_{N_{\dot{\alpha}}}$ could have negative values as in reference 14 where an effort was made to separate the terms in $C_{N_q} + C_{N_{\dot{\alpha}}}$. The results for the fuselage and horizontal tail and just the fuselage are seen to be in good agreement with the vortex-lattice predictions.

The vortex-lattice results for C_{N_α} are shown in comparison with the experimental $C_{N_\alpha} - k^2 C_{N_{\dot{q}}}$ values in the bottom plot in figure 25(b). The agreement for the fuselage—wing—horizontal-tail configuration is very good for Mach numbers less than 0.80 but is not as good for the higher subsonic Mach numbers. The agreement for the fuselage-wing configuration is not as good, the experimental values being higher than the vortex-lattice results. The fuselage—horizontal-tail configuration only showed fair agreement between experiment and the predicted values but the fuselage alone showed good agreement.

The comparison of the damping-in-roll parameters as a function of Mach number for the forced-oscillation tests and for the vortex-lattice program is shown in figure 25(c). For the basic configuration without the vortex generators (FWHV), the experimental damping-in-roll parameter is compared with the vortex-lattice results for FWH, since the vertical tail cannot be included in the vortex-lattice program. The agreement is good at the lower Mach numbers, is not as good at $M = 0.80$, and then becomes better at the high subsonic Mach numbers. The same trends seem to exist for the FW configuration. The experimental damping in roll for the FHV configuration was higher than the vortex-lattice FH configuration and the difference should be the contribution of the vertical tail as the fuselage effects are generally negligible. The small differences between the experimental data for FWHV and FW as well as the small differences in the vortex-lattice results for FWH and FW indicate, as would be expected, that the tail surfaces do not contribute much to the damping in roll while immersed in the wing wake.

CONCLUDING REMARKS

The aerodynamic damping about all three axes, the oscillatory stability in pitch and yaw, and the cross-derivative parameters of a supercritical-wing research airplane model have been determined for Mach numbers of 0.25 to 1.20 by using the small-amplitude forced-oscillation technique. The angle-of-attack range covered was from -2° to 20°. The effects of underwing leading-edge vortex generators, wing, vertical tail, and horizontal tail on the appropriate damping and stability parameters were measured.

The results of the investigation indicate that the basic configuration has positive aerodynamic damping in pitch, roll, and yaw over most of the range of test conditions. The use of a supercritical airfoil for the wing did not appear to result in any unusual trends for the dynamic-stability parameters in pitch, yaw, and roll. The addition of the wing vortex generators resulted in improved oscillatory longitudinal stability up to moderate values of angle of attack. The vortex generators were found to have little effect on the damping in pitch except at the higher angles of attack where there were large negative values in the pitch-damping results. The vortex generators improved the roll-damping characteristics, especially at the higher angles of attack.

Comparison of the experimental pitch- and roll-damping results for 0° angle of attack with the results from a vortex-lattice digital computer program showed generally good agreement over the range of subsonic Mach numbers.

Langley Research Center,
National Aeronautics and Space Administration,
Hampton, Va., January 15, 1974.

APPENDIX A

MEASUREMENTS AND REDUCTION OF DATA

Basic Principles

Strain-gage bridges are used to measure the torque required to oscillate the model and the angular displacement of the model with respect to the fixed portion of the sting. Additional bridges are provided on the pitch-yaw balance to provide signals proportional to normal force and rolling moment and on the roll balance to provide signals proportional to yawing moment. The constant components of the bridge outputs are removed by using conventional bridge-balance circuits. The nonconstant components are amplified and passed through mechanically coupled but electrically independent sine-cosine resolvers which rotate with constant angular velocity at the frequency of model oscillation and resolve each signal into orthogonal components. The components are rectified by phase-sensitive demodulators and read on damped digital voltmeters to provide direct-current voltages proportional to the amplitudes of the orthogonal components. The individual resolvers are electrically alined so that the phase angle between the torque required to oscillate the model and angular displacement and between the secondary signal (rolling moment, yawing moment, or normal force) and angular displacement may also be determined from the orthogonal components.

The resolver-damped voltmeter system acts as an extremely narrow bandpass filter with the center frequency always being the frequency of oscillation of the model. In this way, as explained in reference 15, the effects of random signal inputs due to tunnel turbulence or other causes are eliminated and only those components of the desired torques, forces, and angular displacement which occur at the frequency of oscillation are used in computing the dynamic stability characteristics of the model.

The frequency of oscillation was measured by an electronic counter which counted for 1 second the pulses generated by a photocell device which had a slotted disk attached to the shaft of the motor turning the resolvers.

The computation of the various parameters presented is an extension of the material in reference 16.

Computation of Pitching Parameters

For the pitching tests, measurements were made of the amplitude of the torque required to oscillate the model in pitch T_Y, the amplitude of the angular displacement in pitch of the model with respect to the sting Θ, the phase angle η between T_Y and Θ, and the angular velocity of the forced oscillation ω. The viscous-damping-moment

APPENDIX A

coefficient in pitch for this single-degree-of-freedom system was computed as

$$C_Y = \frac{T_Y \sin \eta}{\omega \Theta} \tag{1}$$

and the spring-inertia parameter in pitch was computed as

$$K_Y - I_Y \omega^2 = \frac{T_Y \cos \eta}{\Theta} \tag{2}$$

where K_Y is the torsional-spring coefficient of the system and I_Y is the moment of inertia of the system about the body Y-axis.

For these tests, the damping-in-pitch parameter was computed as

$$C_{m_q} + C_{m_{\dot{\alpha}}} = \frac{-2V}{q_\infty S \bar{c}^2} \left[(C_Y)_{\text{wind on}} - (C_Y)_{\text{wind off}} \right] \tag{3}$$

and the oscillatory longitudinal-stability parameter was computed as

$$C_{m_\alpha} - k^2 C_{m_{\dot{q}}} = - \frac{1}{q_\infty S \bar{c}} \left[(K_Y - I_Y \omega^2)_{\text{wind on}} - (K_Y - I_Y \omega^2)_{\text{wind off}} \right] \tag{4}$$

The wind-off value of C_Y is determined at the frequency of wind-off velocity resonance since the value of C_Y is independent of frequency and can be determined most accurately at the frequency of velocity resonance. The wind-on and wind-off values of $K_Y - I_Y \omega^2$ are determined at the same frequency since $K_Y - I_Y \omega^2$ is a function of frequency.

During the pitch-oscillation tests, measurements were also made of the normal force N induced by the pitching oscillation and of the phase angle ζ between N and the pitching displacement. The normal-force coefficient in phase with pitching velocity for this system was computed as

$$C_{N,Z} = \frac{N \sin \zeta}{\omega \Theta} \tag{5}$$

APPENDIX A

and the force-acceleration parameter (in phase with pitching displacement) in pitch was computed as

$$\frac{K_Y}{l} - mx\omega^2 = \frac{N \cos \zeta}{\Theta} \tag{6}$$

where K_Y is the torsional-spring coefficient of the system, l is its effective length with respect to the balance pivot, m is the model mass, and x is the distance from the balance pivot to the center of the model mass (positive forward).

The normal force due to pitch rate parameter was computed as

$$C_{N_q} + C_{N_{\dot{\alpha}}} = - \frac{2V}{q_\infty S\bar{c}} \left[(C_{N,Z})_{\text{wind on}} - (C_{N,Z})_{\text{wind off}} \right] \tag{7}$$

and the normal force due to pitch displacement parameter was computed as

$$C_{N_\alpha} - k^2 C_{N_{\dot{q}}} = - \frac{1}{q_\infty S} \left[\left(\frac{K_Y}{l} - mx\omega^2 \right)_{\text{wind on}} - \left(\frac{K_Y}{l} - mx\omega^2 \right)_{\text{wind off}} \right] \tag{8}$$

The wind-off and wind-on values of $\frac{K_Y}{l} - mx\omega^2$ are determined at the same frequency. The normal-force data for wind-on conditions are taken simultaneously with the pitch data at the frequency for velocity resonance in pitch of the system.

Computation of Yawing Parameters

For the yawing tests, measurements were made of the torque required to oscillate the model in yaw T_Z, the amplitude of the angular displacement in yaw of the model with respect to the sting Ψ, the phase angle λ between T_Z and Ψ, and the angular velocity of the forced oscillation ω. The viscous-damping-moment coefficient in yaw C_Z for this single-degree-of-freedom system was computed in a manner similar to the pitch case as

$$C_Z = \frac{T_Z \sin \lambda}{\omega \Psi} \tag{9}$$

and the spring-inertia parameter in yaw was computed as

$$K_Z - I_Z\omega^2 = \frac{T_Z \cos \lambda}{\Psi} \tag{10}$$

where K_Z is the torsional-spring coefficient of the system and I_Z is the moment of inertia of the system about the body Z-axis.

For these tests, the damping-in-yaw parameter was computed as

$$C_{n_r} - C_{n_{\dot{\beta}}} \cos \alpha = - \frac{2V}{q_\infty Sb^2} \left[(C_Z)_{\text{wind on}} - (C_Z)_{\text{wind off}} \right] \tag{11}$$

and the oscillatory directional-stability parameter was computed as

$$C_{n_\beta} \cos \alpha + k^2 C_{n_{\dot{r}}} = \frac{1}{q_\infty Sb} \left[(K_Z - I_Z\omega^2)_{\text{wind on}} - (K_Z - I_Z\omega^2)_{\text{wind off}} \right] \tag{12}$$

The wind-off value of C_Z is determined at the frequency of wind-off velocity resonance, and the wind-off and wind-on values of $K_Z - I_Z\omega^2$ are determined at the same frequency.

As part of the yawing oscillation tests, measurements were made of the amplitude of the rolling torque T_X induced by the yawing oscillation and the phase angle γ between T_X and the yawing displacement Ψ. The rolling-moment coefficient in phase with yawing velocity for this system was

$$C_{l,Z} = \frac{T_X \sin \gamma}{\omega \Psi} \tag{13}$$

and the rolling-moment parameter in phase with yawing displacement was

$$A + I_{XZ}\omega^2 = \frac{T_X \cos \gamma}{\Psi} \tag{14}$$

where A is the torsional-spring coefficient in roll induced by a yawing displacement and I_{XZ} is the product of inertia of the system.

APPENDIX A

For these tests the rolling moment due to yaw rate parameter was computed as

$$C_{l_r} - C_{l_{\dot{\beta}}} \cos \alpha = - \frac{2V}{q_\infty Sb^2} \left[(C_{l,Z})_{\text{wind on}} - (C_{l,Z})_{\text{wind off}} \right] \tag{15}$$

and the effective-dihedral parameter was computed as

$$C_{l_\beta} \cos \alpha + k^2 C_{l_{\dot{r}}} = \frac{1}{q_\infty Sb} \left[(A + I_{XZ}\omega^2)_{\text{wind on}} - (A + I_{XZ}\omega^2)_{\text{wind off}} \right] \tag{16}$$

The wind-off and wind-on values of $A + I_{XZ}\omega^2$ are determined at the same frequency since $A + I_{XZ}\omega^2$ is a function of frequency.

Computation of Rolling Parameters

For the rolling tests, measurements were made of the amplitude of the torque required to oscillate the model in roll T_X, the amplitude of the angular displacement in roll of the model with respect to the fixed portion of the sting Φ, the phase angle σ between T_X and Φ, and the angular velocity of the forced oscillation ω. The viscous-damping coefficient in roll C_X for this single-degree-of-freedom system was computed in a manner similar to the pitch and yaw cases as

$$C_X = \frac{T_X \sin \sigma}{\omega \Phi} \tag{17}$$

and the spring-inertia parameter in roll was computed as

$$K_X - I_X \omega^2 = \frac{T_X \cos \sigma}{\Phi} \tag{18}$$

where K_X is the torsional-spring coefficient of the system and I_X is the moment of inertia of the system about the body X-axis.

For these tests, the damping-in-roll parameter was computed as

$$C_{l_p} + C_{l_{\dot{\beta}}} \sin \alpha = - \frac{2V}{q_\infty Sb^2} \left[(C_X)_{\text{wind on}} - (C_X)_{\text{wind off}} \right] \tag{19}$$

and the rolling moment due to roll displacement parameter was computed as

$$C_{l_\beta} \sin \alpha - k^2 C_{l_{\dot{p}}} = - \frac{1}{q_\infty Sb} \left[\left(K_X - I_X \omega^2 \right)_{\text{wind on}} - \left(K_X - I_X \omega^2 \right)_{\text{wind off}} \right] \tag{20}$$

As in the pitch and yaw cases, the wind-off value of C_X is determined at the frequency of wind-off velocity resonance since the value of C_X is independent of frequency and can be determined most accurately at the frequency of velocity resonance. The wind-on and wind-off values of $K_X - I_X \omega^2$ are determined at the same frequency since $K_X - I_X \omega^2$ is a function of frequency.

As part of the rolling-oscillation tests, measurements were made of the amplitude of the yawing torque T_Z induced by the rolling oscillation and the phase angle ϵ between T_Z and rolling displacement Φ. The yawing-moment coefficient in phase with rolling velocity for this system was

$$C_{n,X} = \frac{T_Z \sin \epsilon}{\omega \Phi} \tag{21}$$

and the yawing-moment parameter in phase with rolling displacement was

$$B + I_{XZ} \omega^2 = \frac{T_Z \cos \epsilon}{\Phi} \tag{22}$$

where B is the torsional-spring coefficient in yaw induced by a roll displacement and I_{XZ} is the product of inertia of the system.

For these tests, the yawing moment due to roll rate parameter was computed as

$$C_{n_p} + C_{n_{\dot{\beta}}} \sin \alpha = - \frac{2V}{q_\infty Sb^2} \left[\left(C_{n,X} \right)_{\text{wind on}} - \left(C_{n,X} \right)_{\text{wind off}} \right] \tag{23}$$

and the yawing moment due to roll displacement parameter was computed as

$$C_{n_\beta} \sin \alpha - k^2 C_{n_{\dot{p}}} = - \frac{1}{q_\infty Sb} \left[\left(B + I_{XZ} \omega^2 \right)_{\text{wind on}} - \left(B + I_{XZ} \omega^2 \right)_{\text{wind off}} \right] \tag{24}$$

APPENDIX A

The wind-off and the wind-on values of $B + I_{XZ}\omega^2$ are determined at the same frequency since $B + I_{XZ}\omega^2$ is a function of frequency.

It should be emphasized that the measurement of the primary damping coefficients $\left(C_{m_q} + C_{m_{\dot{\alpha}}},\ C_{n_r} - C_{n_{\dot{\beta}}} \cos \alpha, \text{ and } C_{l_p} + C_{l_{\dot{\beta}}} \sin \alpha\right)$ where the system is operated at the frequency for velocity resonance, so that the component of torque in phase with displacement is zero, is inherently more accurate than the measurement of the secondary-type damping coefficients $\left(C_{N_q} + C_{N_{\dot{\alpha}}},\ C_{l_r} - C_{l_{\dot{\beta}}} \cos \alpha, \text{ and } C_{n_p} + C_{n_{\dot{\beta}}} \sin \alpha\right)$ where the damping parameters are measured in the presence of large forces and moments in phase with displacement.

APPENDIX B

FORCED-OSCILLATION BALANCE MECHANISMS

Pitch-Yaw Balance

The small-amplitude forced-oscillation balance used for the pitch and the yaw tests is shown in the photograph of figure 4. An offset crank which fits into the balance crosshead mechanism is driven in a rotary motion by a variable-frequency electric motor. This rotary motion serves to oscillate the movable portion of the balance (and thereby the model) about the pivot axis in an essentially sinusoidal motion. The amplitude of the motion is dependent on the throw of the particular crank used as the allowable range is from $1/2^{\circ}$ to 2°. An amplitude of about 1° was used for both the pitch and the yaw tests.

The instrumented torque beams which measure the torque required to oscillate the model are located between the pivot axis and the model mounting surface. This torque-bridge location eliminates the pivot-friction characteristics from the model system and thereby eliminates the need to correct the data for varying pivot friction associated with changing aerodynamic load. Although this bridge is physically forward of the pivot axis, all torques are measured with respect to the pivot axis.

A mechanical spring, which is an integral part of the fixed balance support, is connected to the oscillation balance forward of the torque beams by means of a flexure plate which is electron-beam welded to both the front of the spring and the forward portion of the oscillation balance. Welding the spring in this manner minimizes the mechanical friction which would arise from using mechanical fasteners. A strain-gage bridge mounted on the mechanical spring provides a signal proportional to the model angular displacement with respect to the sting. Although the forced-oscillation balance may be oscillated through a frequency range from about 1 to 30 hertz, the most accurate measurement of the damping coefficient is obtained at the frequency of velocity resonance as noted in reference 15.

Strain-gage bridges also are located on the oscillation-balance torque beams to measure normal force and rolling moment in the pitching and yawing modes, respectively.

Roll Mechanism

The small-amplitude oscillatory-roll mechanism used for the rolling tests is sketched in figure 5. The basic principles of operation of the oscillatory-roll mechanism are the same as those for the pitch-yaw mechanism previously discussed. An electric motor with eccentric drive oscillates the sting and model in an essentially sinusoidal

APPENDIX B

motion. The model is rigidly forced in a fixed $2\frac{1}{2}^{\circ}$ amplitude oscillation about the sting axis at a variable frequency. A mechanical torsion spring internal to the sting is attached to the front of the strain-gage balance section to permit the model to be oscillated at the frequency for velocity resonance, whereby the mechanical torsion spring, plus any aerodynamic spring turn, balances out the model inertia. The only torque then required to oscillate the model at that particular frequency is equal to that due to aerodynamic damping (see ref. 15). The strain gages are located forward of all the bearings and other friction-producing devices. In addition to rolling moment, the torque beams are instrumented with strain-gage bridges to measure yawing moment due to rolling. A strain-gage bridge is mounted on the mechanical torsion spring to provide a signal proportional to the model angular displacement in roll.

REFERENCES

1. Whitcomb, Richard T.; and Clark, Larry R.: An Airfoil Shape for Efficient Flight at Supercritical Mach Numbers. NASA TM X-1109, 1965.

2. Harris, Charles D.: Wind-Tunnel Investigation of Effects of Trailing-Edge Geometry on a NASA Supercritical Airfoil Section. NASA TM X-2336, 1971.

3. Anon.: Supercritical Wing Technology – A Progress Report on Flight Evaluations. NASA SP-301, 1972.

4. Mechtly, E. A.: The International System of Units – Physical Constants and Conversion Factors (Second Revision). NASA SP-7012, 1973.

5. Bartlett, Dennis W.; and Re, Richard J.: Wind-Tunnel Investigation of Basic Aerodynamic Characteristics of a Supercritical-Wing Research Airplane Configuration. NASA TM X-2470, 1972.

6. Harris, Charles D.; and Bartlett, Dennis W.: Wind-Tunnel Investigation of Effects of Underwing Leading-Edge Vortex Generators on a Supercritical-Wing Research Airplane Configuration. NASA TM X-2471, 1972.

7. Schaefer, William T., Jr.: Characteristics of Major Active Wind Tunnels at the Langley Research Center. NASA TM X-1130, 1965.

8. Braslow, Albert L.; and Knox, Eugene C.: Simplified Method for Determination of Critical Height of Distributed Roughness Particles for Boundary-Layer Transition at Mach Numbers From 0 to 5. NACA TN 4363, 1958.

9. Loving, Donald L.: Wind-Tunnel—Flight Correlation of Shock-Induced Separated Flow. NASA TN D-3580, 1966.

10. Blackwell, James A., Jr.: Preliminary Study of Effects of Reynolds Number and Boundary-Layer Transition Location on Shock-Induced Separation. NASA TN D-5003, 1969.

11. Loving, Donald L.; and Katzoff, S.: The Fluorescent-Oil Film Method and Other Techniques for Boundary-Layer Flow Visualization. NASA MEMO 3-17-59L, 1959.

12. Wiley, Harleth G.: The Significance of Nonlinear Damping Trends Determined for Current Aircraft Configurations. Presented at the AGARD Flight Mechanics Panel's Specialists' Meeting on Stability and Control (Cambridge, England), Sept. 20-23, 1966.

13. Margason, Richard J.; and Lamar, John E.: Vortex-Lattice FORTRAN Program for Estimating Subsonic Aerodynamic Characteristics of Complex Planforms. NASA TN D-6142, 1971.

14. Statler, Irving C.: The Development and Evaluation of the CAL/Air Force Dynamic Wind-Tunnel Testing System. Part II – Dynamic Tests of an F-104 Model. AFFDL-TR-66-153, Pt. II, U.S. Air Force, Feb. 1967.

15. Braslow, Albert L.; Wiley, Harleth G.; and Lee, Cullen Q.: A Rigidly Forced Oscillation System for Measuring Dynamic-Stability Parameters in Transonic and Supersonic Wind Tunnels. NASA TN D-1231, 1962. (Supersedes NACA RM L58A28.)

16. Kilgore, Robert A.: Some Transonic and Supersonic Dynamic Stability Characteristics of a Variable-Sweep-Wing Tactical Fighter Model. NASA TM X-2163, 1971.

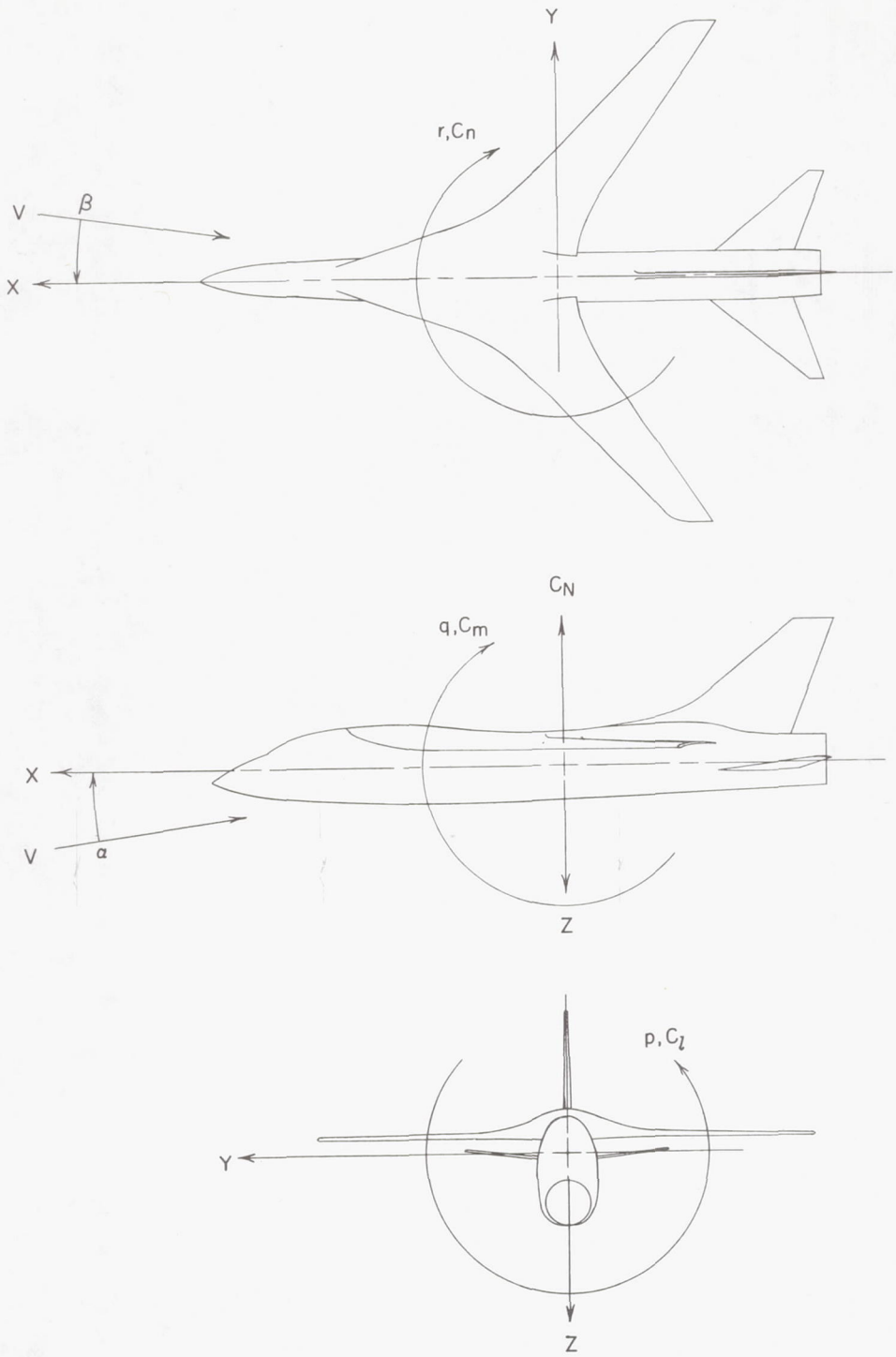

Figure 1.- Body system of axes with coefficients, angles, and angular velocities shown in positive sense.

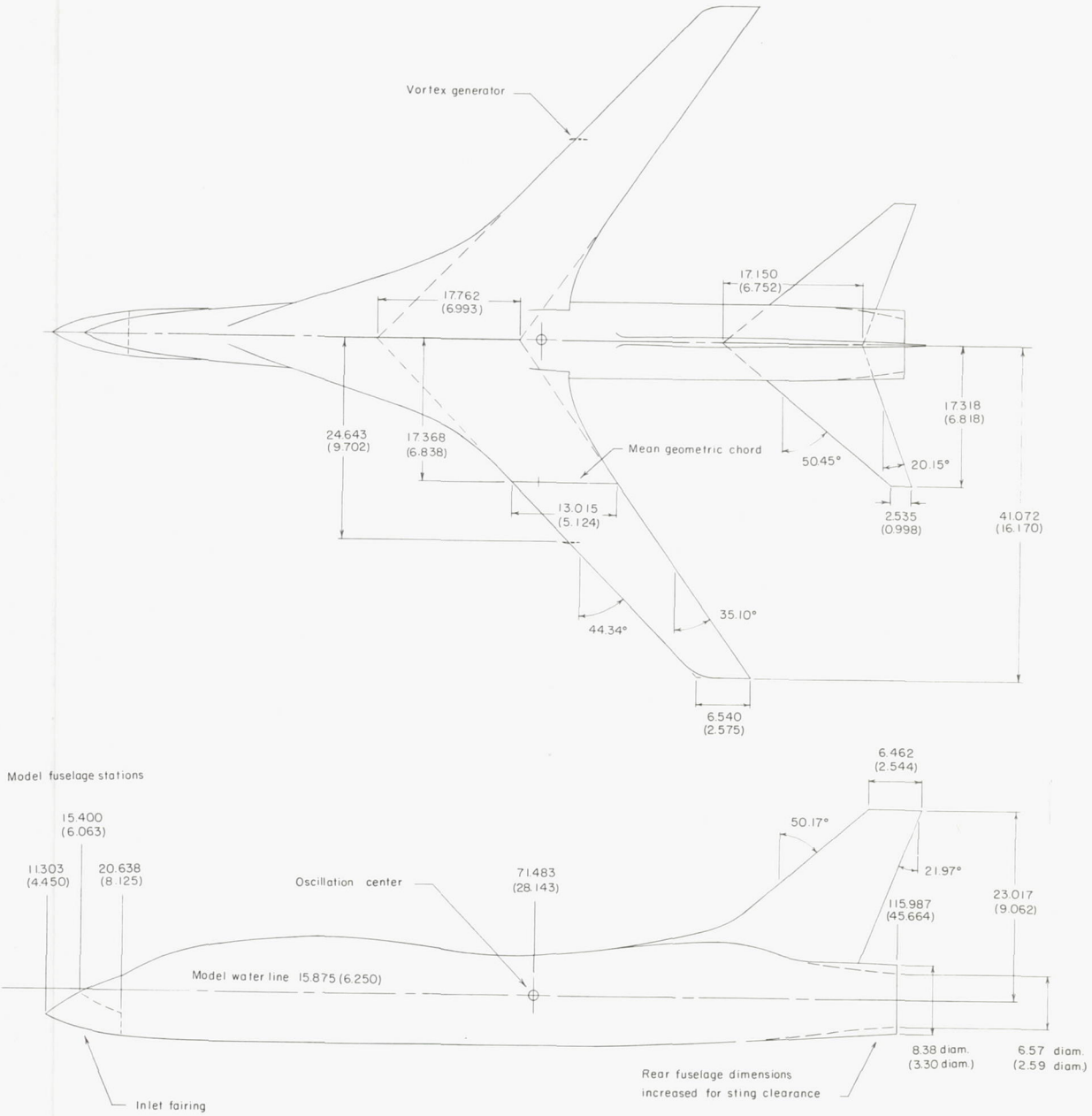

(a) General arrangement of 0.0625-scale dynamic-stability model.

Figure 2.- Design dimensions of model. All linear dimensions are in centimeters and parenthetically in inches.

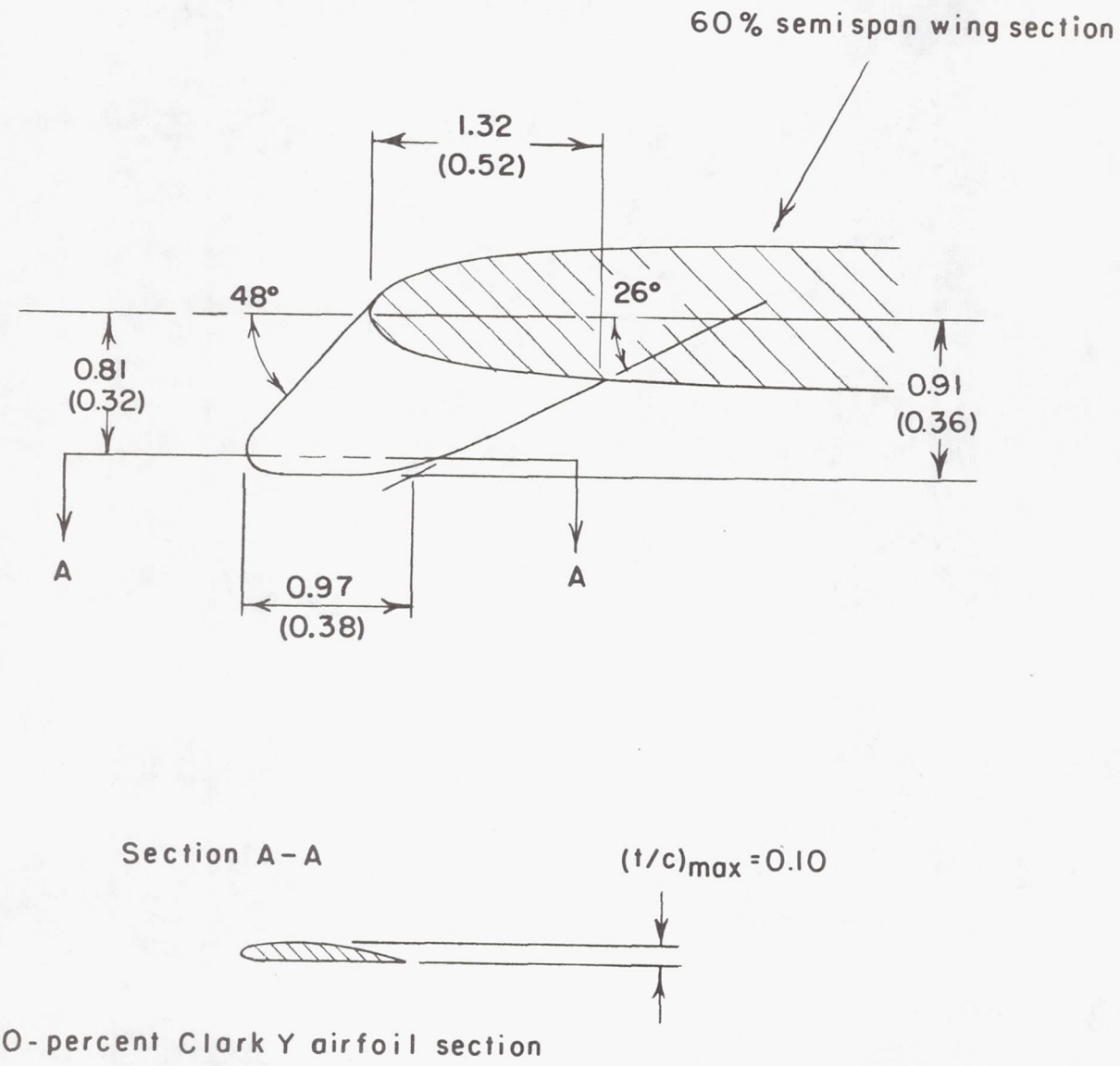

(b) Details of the underwing leading-edge vortex generator.

Figure 2.- Concluded.

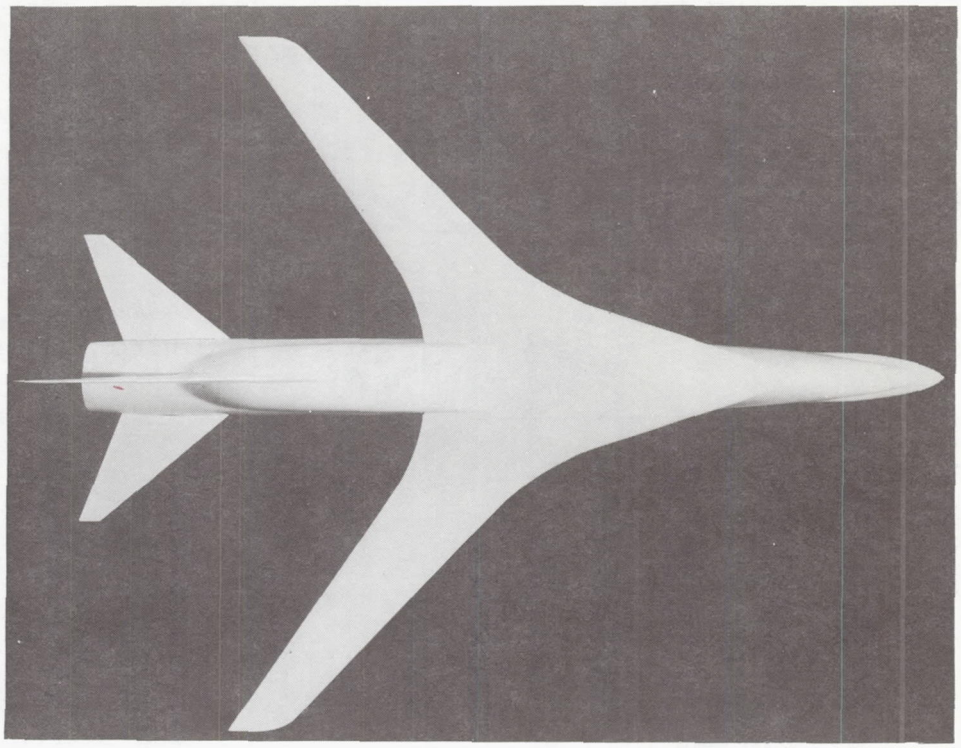

L-70-8733

(a) Plan view of configuration FWHV.

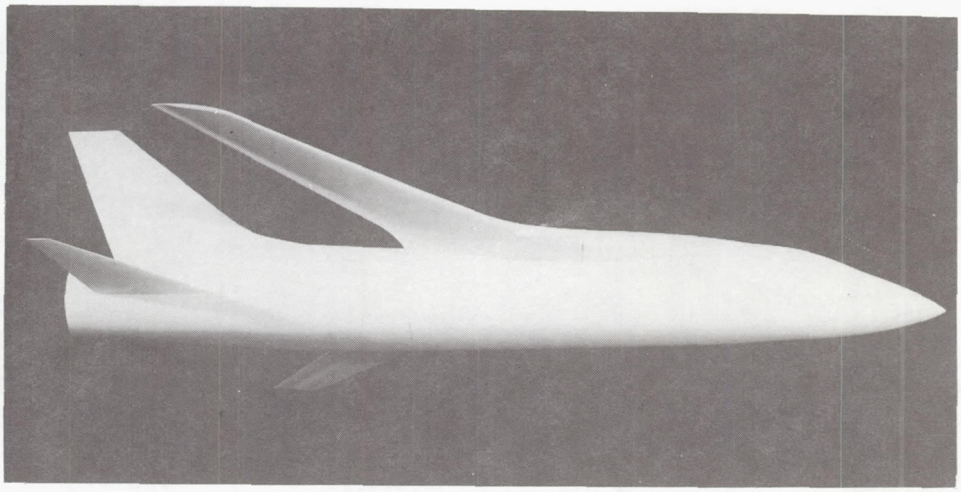

L-70-8729

(b) View from side and below configuration FWHV.

Figure 3.- Photographs of 0.0625-scale dynamic-stability model.

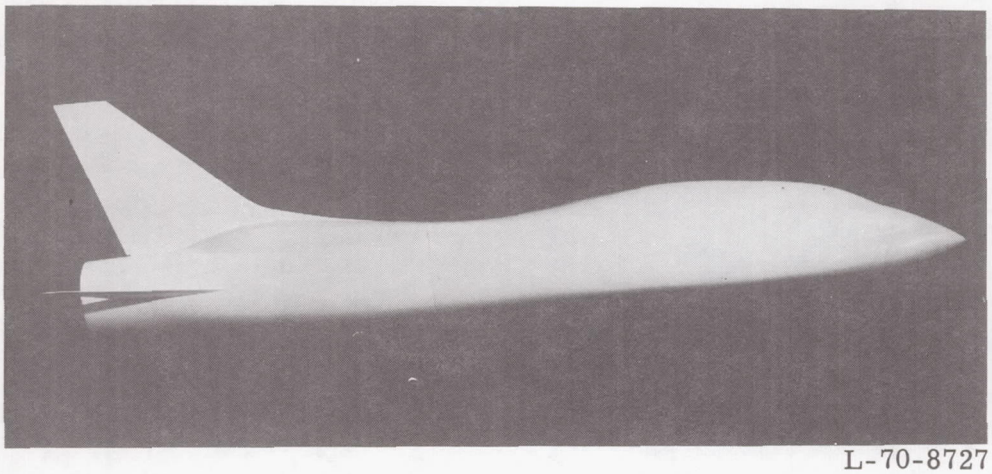

L-70-8727

(c) Side view of configuration FHV.

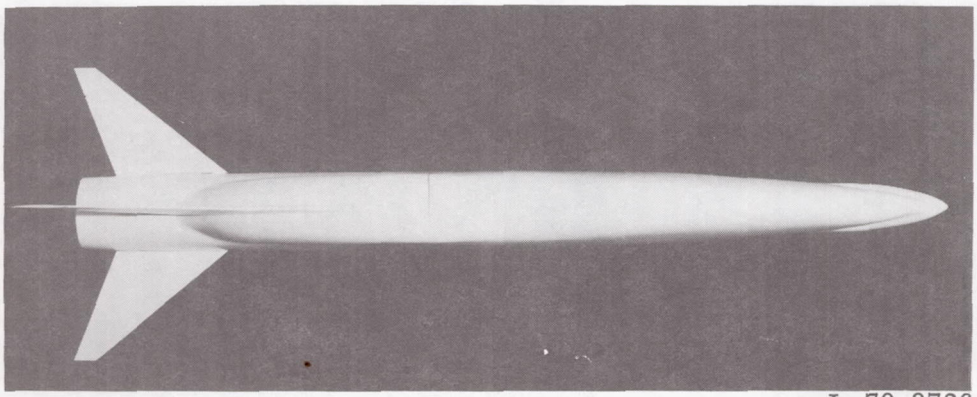

L-70-8726

(d) Plan view of configuration FHV.

Figure 3.- Concluded.

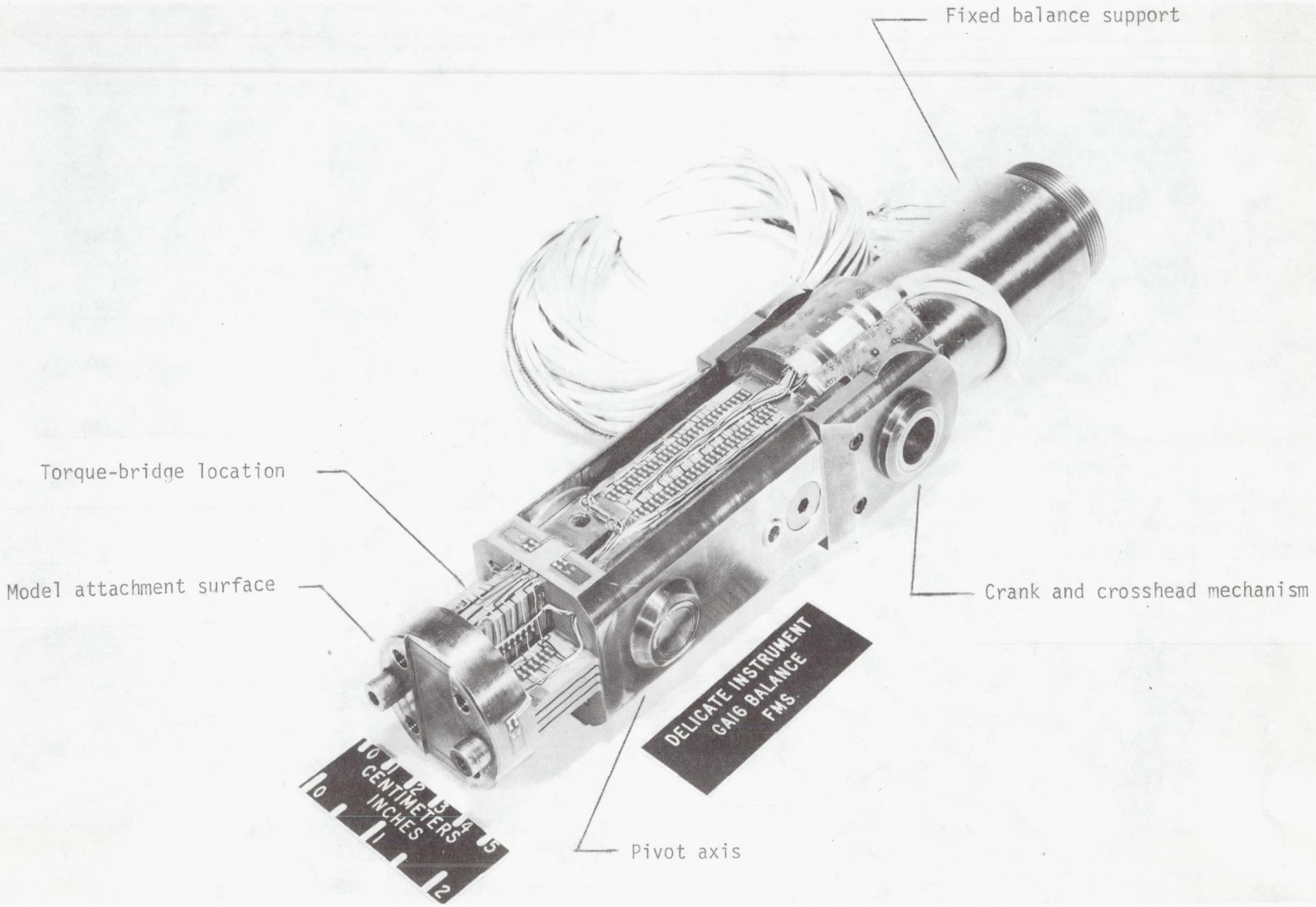

L-68-10 690

Figure 4.- Photograph of small-amplitude forced-oscillation pitch-yaw balance.

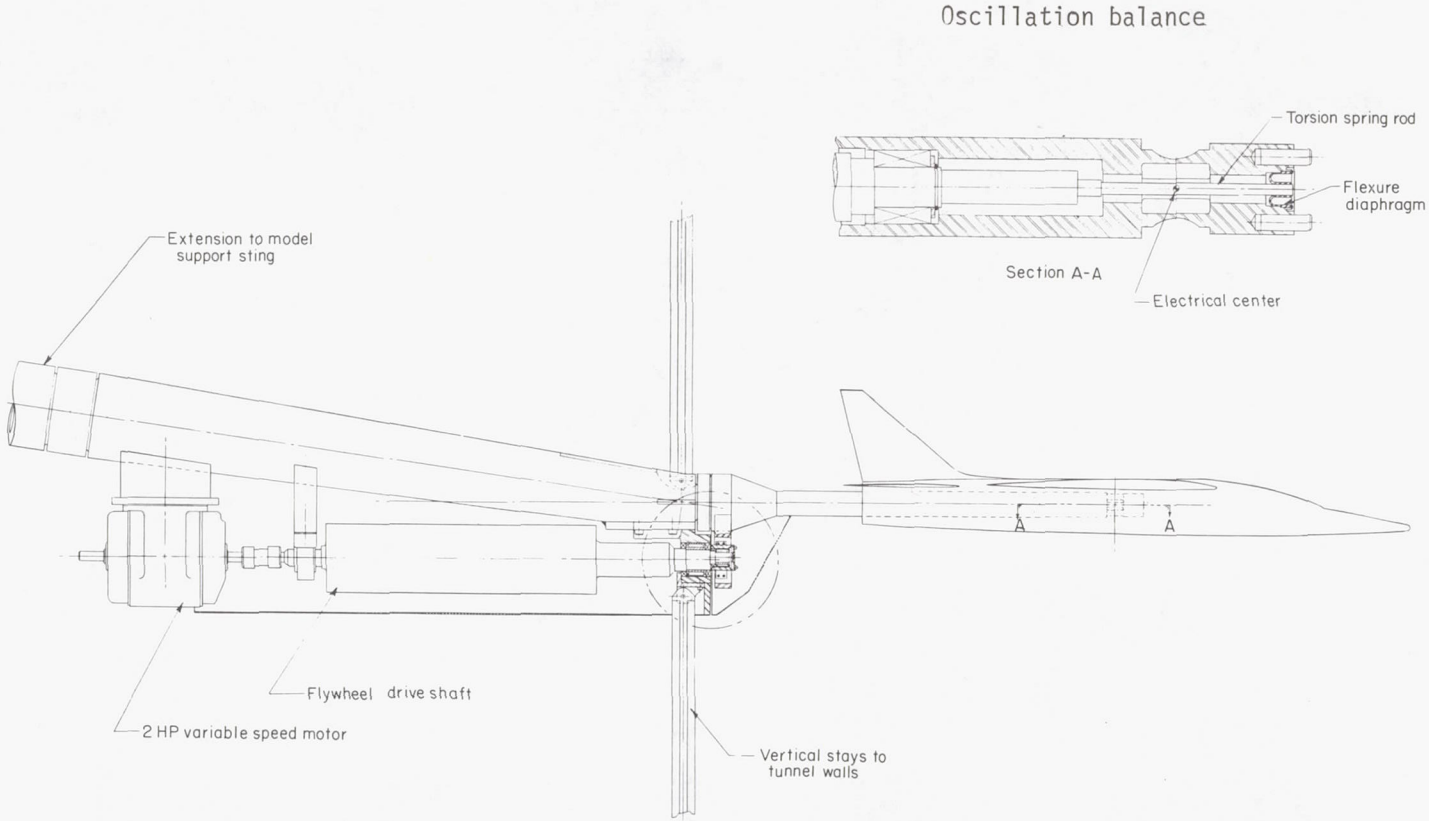

Figure 5.- Forced-oscillation roll mechanism and balance.

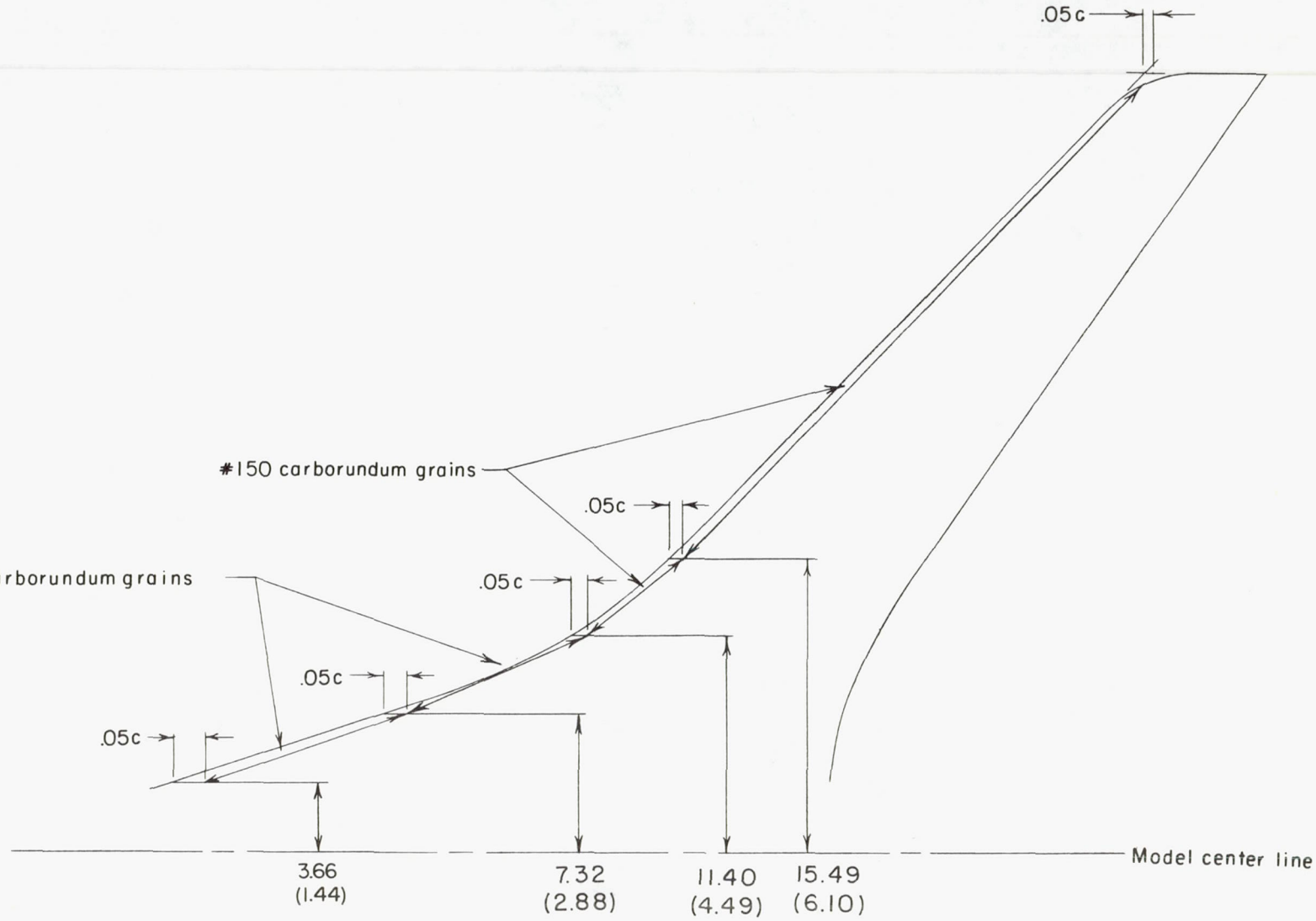

(a) Wing upper surface; M = 0.25 to 0.90 (normal transition).

Figure 6.- Location and size of boundary-layer transition strips on wing. All linear dimensions are in centimeters and parenthetically in inches.

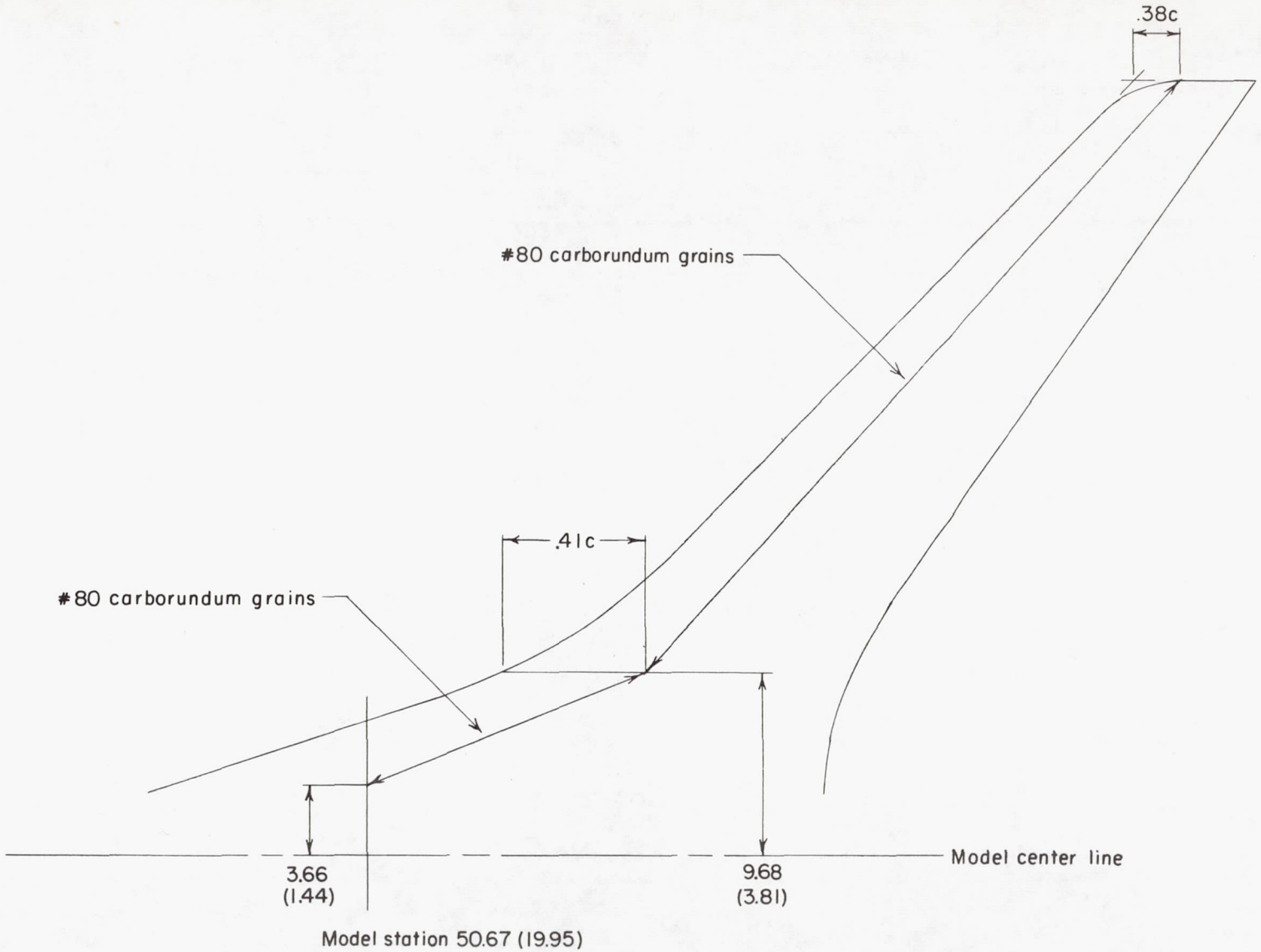

(b) Wing upper surface; M = 0.95 to 1.20 (supercritical transition).

Figure 6.- Continued.

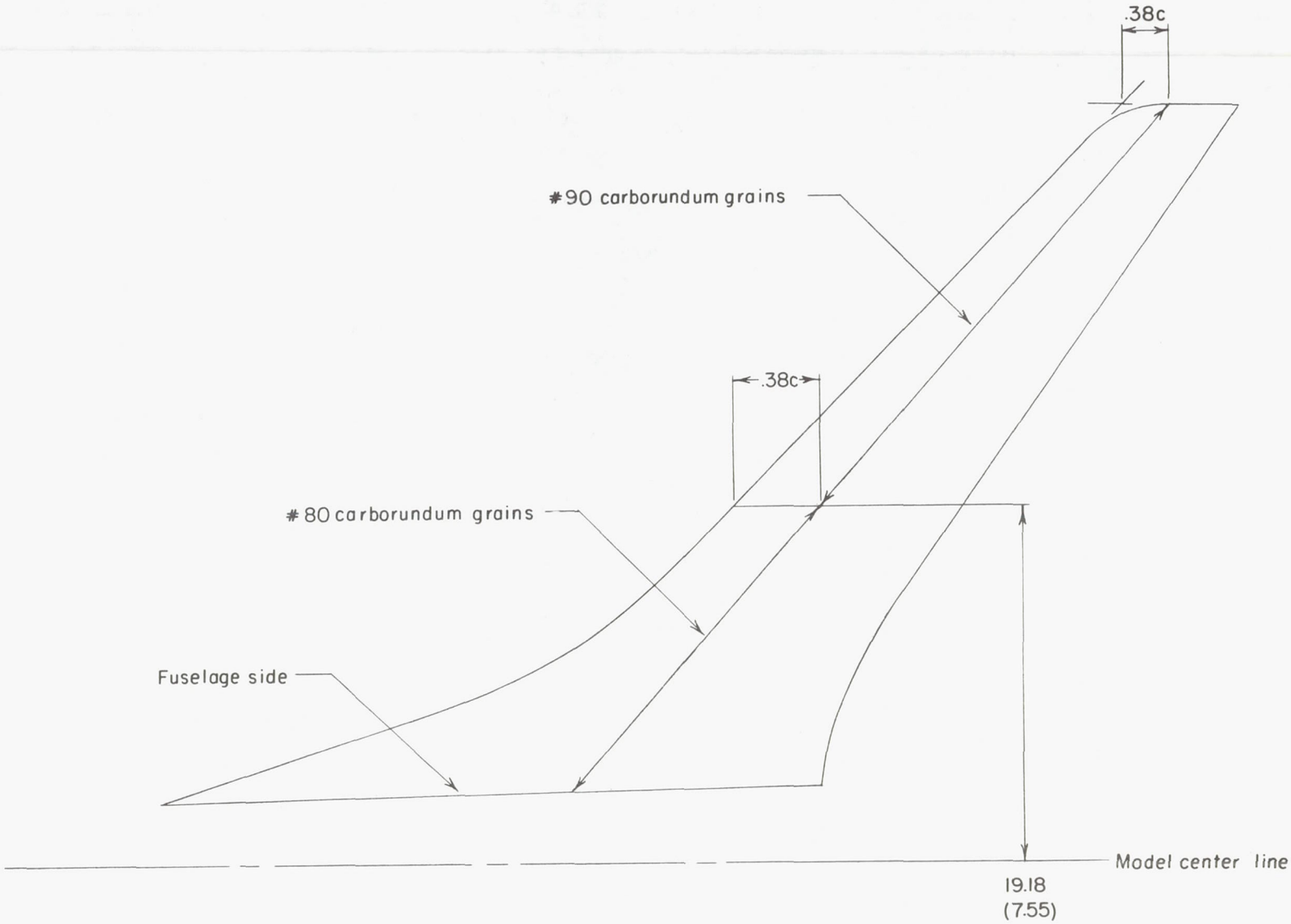

(c) Wing lower surface; M = 0.25 to 1.20 (normal and supercritical transition).

Figure 6.- Concluded.

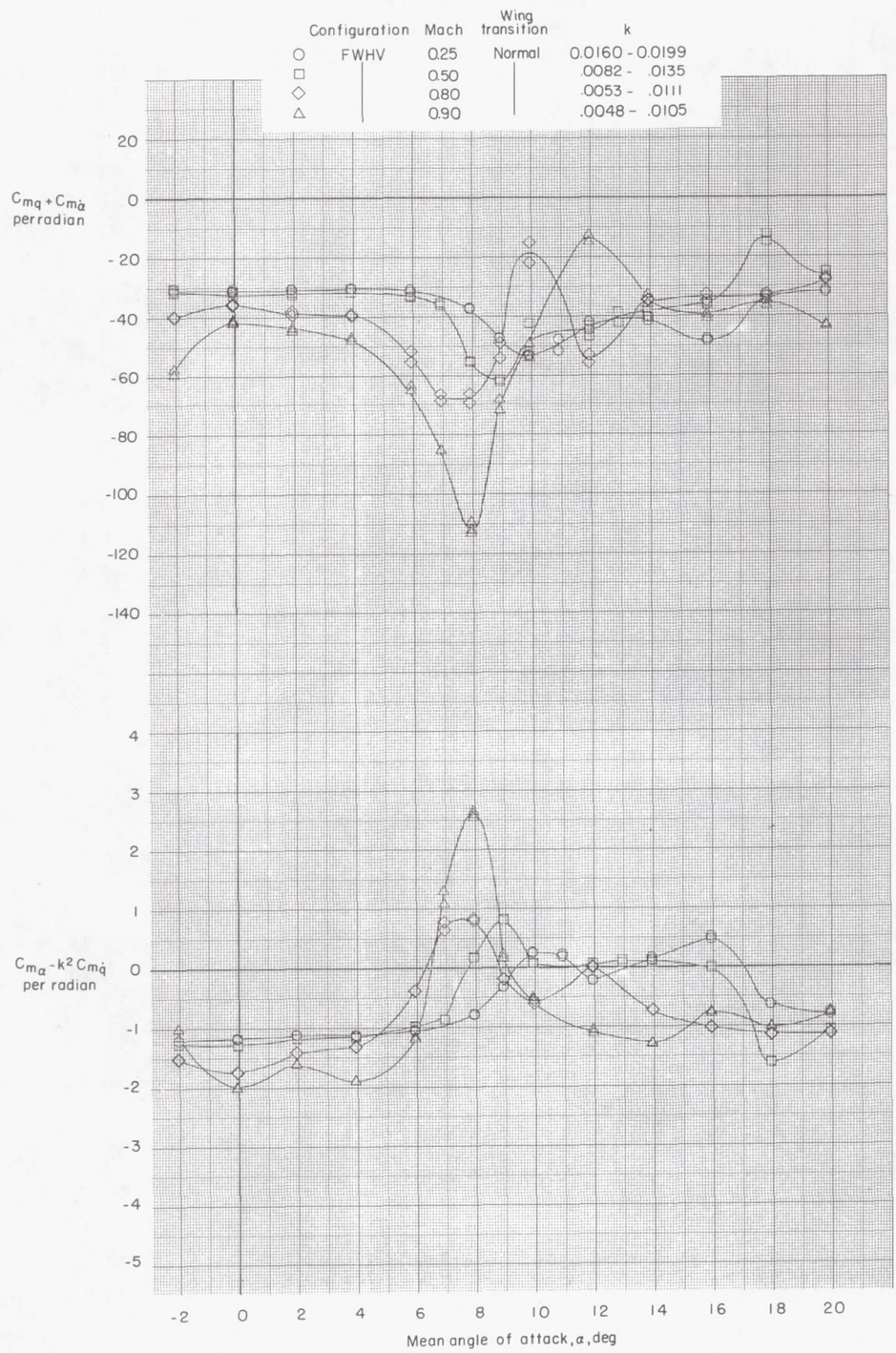

(a) M = 0.25, 0.50, 0.80, and 0.90.

Figure 7.- Variation of damping-in-pitch parameter and oscillatory longitudinal-stability parameter with mean angle of attack for basic configuration.

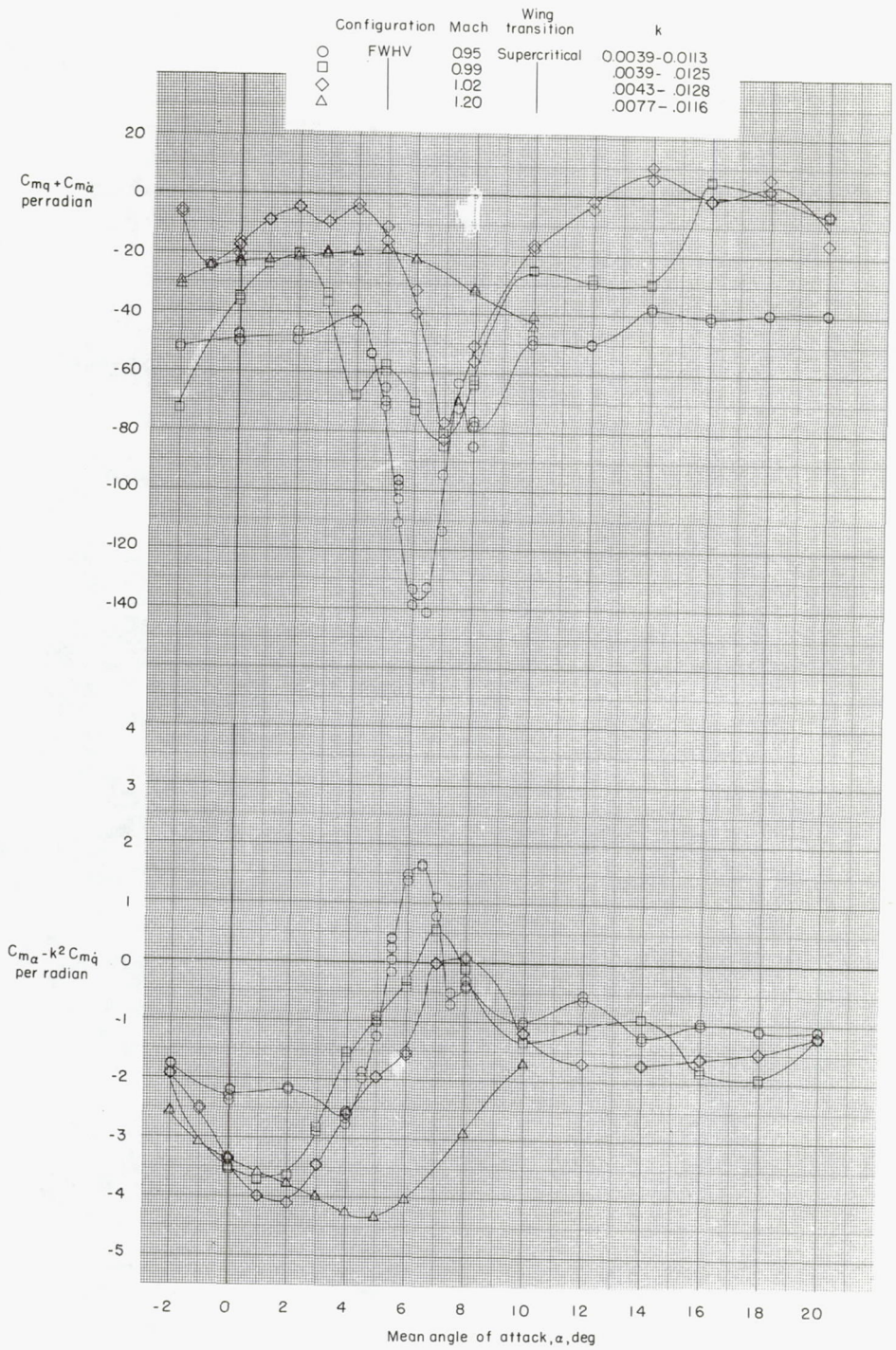

(b) M = 0.95, 0.99, 1.02, and 1.20.

Figure 7.- Concluded.

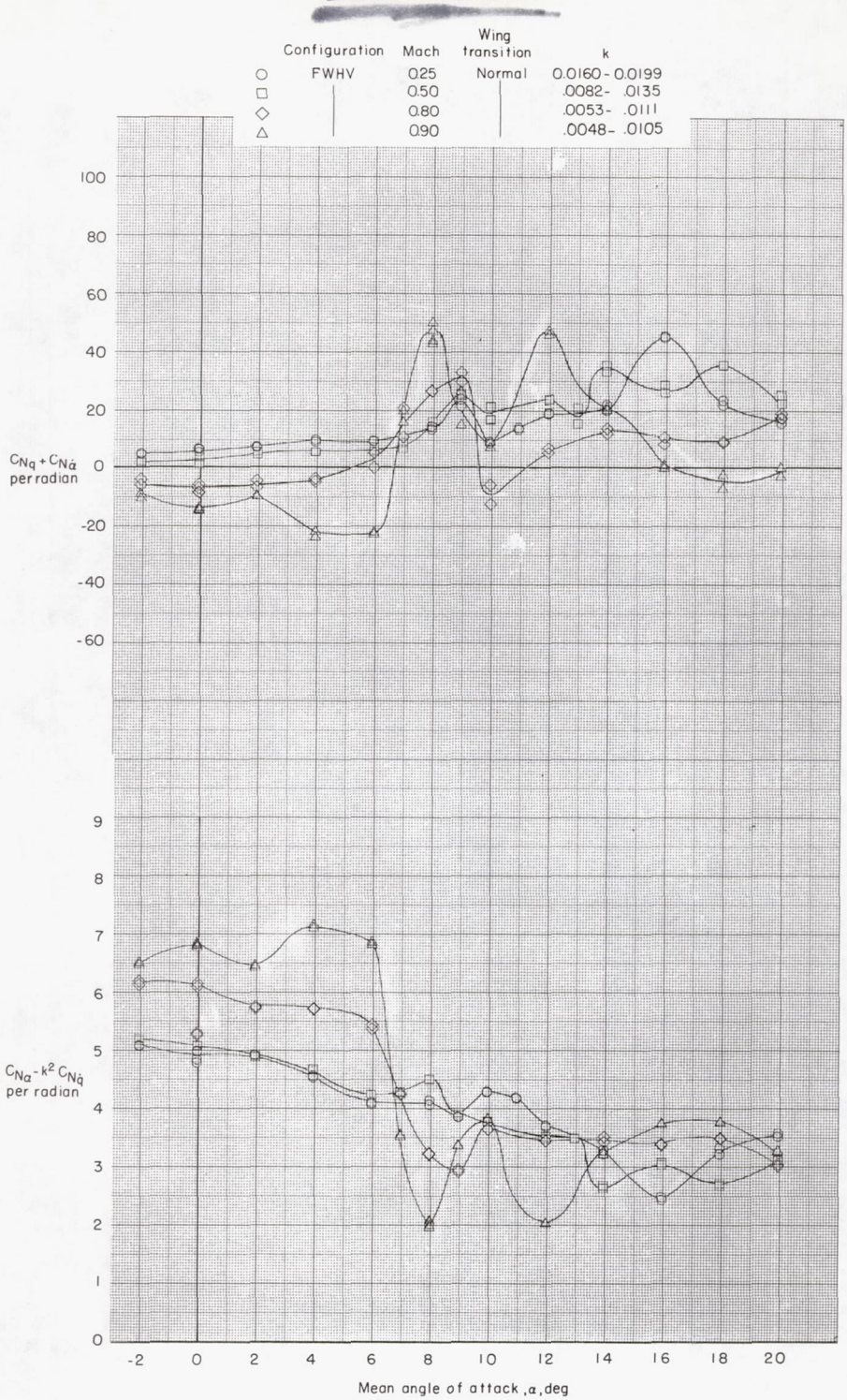

(a) M = 0.25, 0.50, 0.80, and 0.90.

Figure 8.- Variation of normal force due to pitching rate parameter and normal force due to pitch displacement parameter with mean angle of attack for basic configuration.

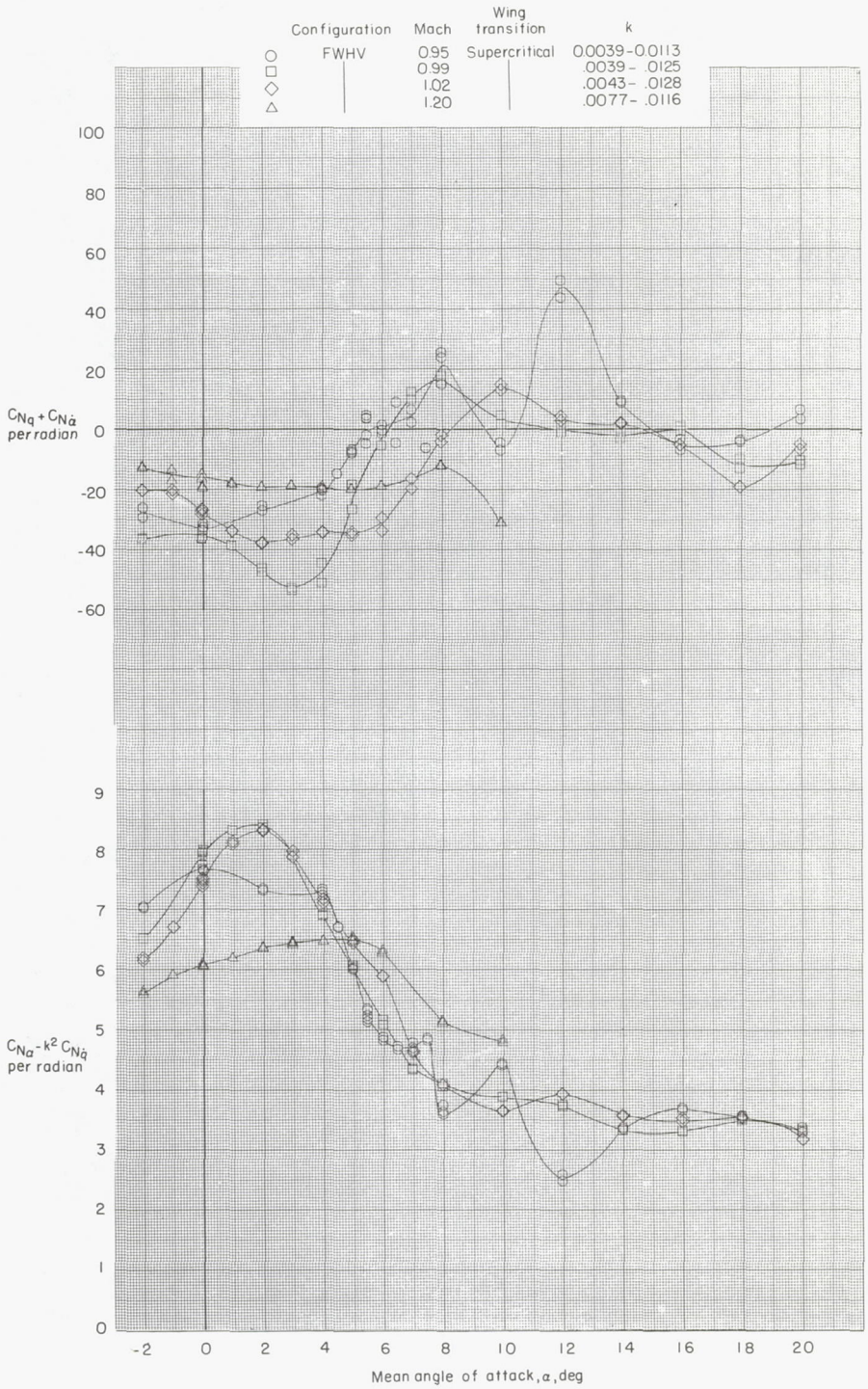

(b) M = 0.95, 0.99, 1.02, and 1.20.

Figure 8.- Concluded.

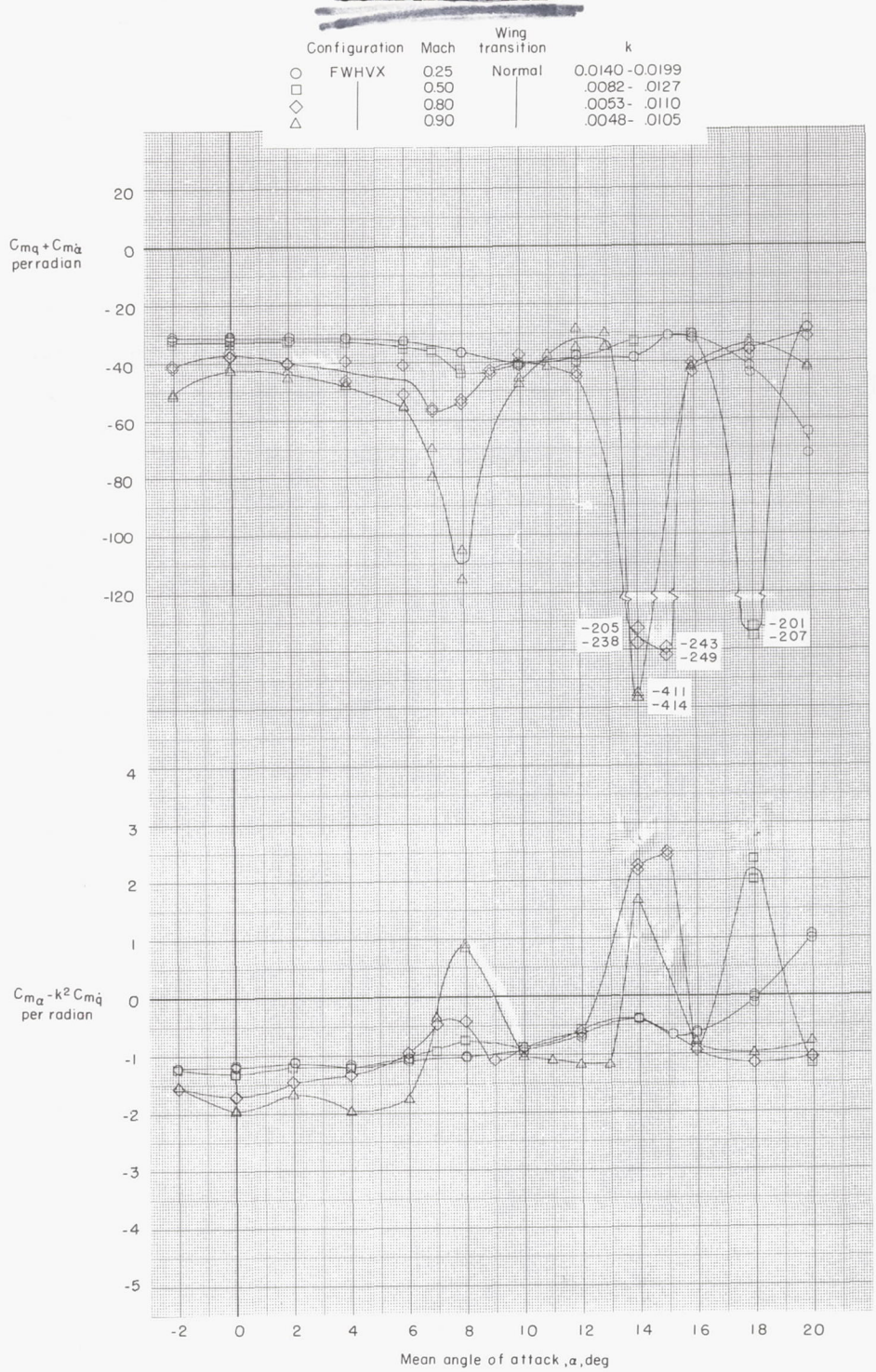

(a) M = 0.25, 0.50, 0.80, and 0.90.

Figure 9.- Variation of damping-in-pitch parameter and oscillatory longitudinal-stability parameter with mean angle of attack for basic configuration with vortex generators.

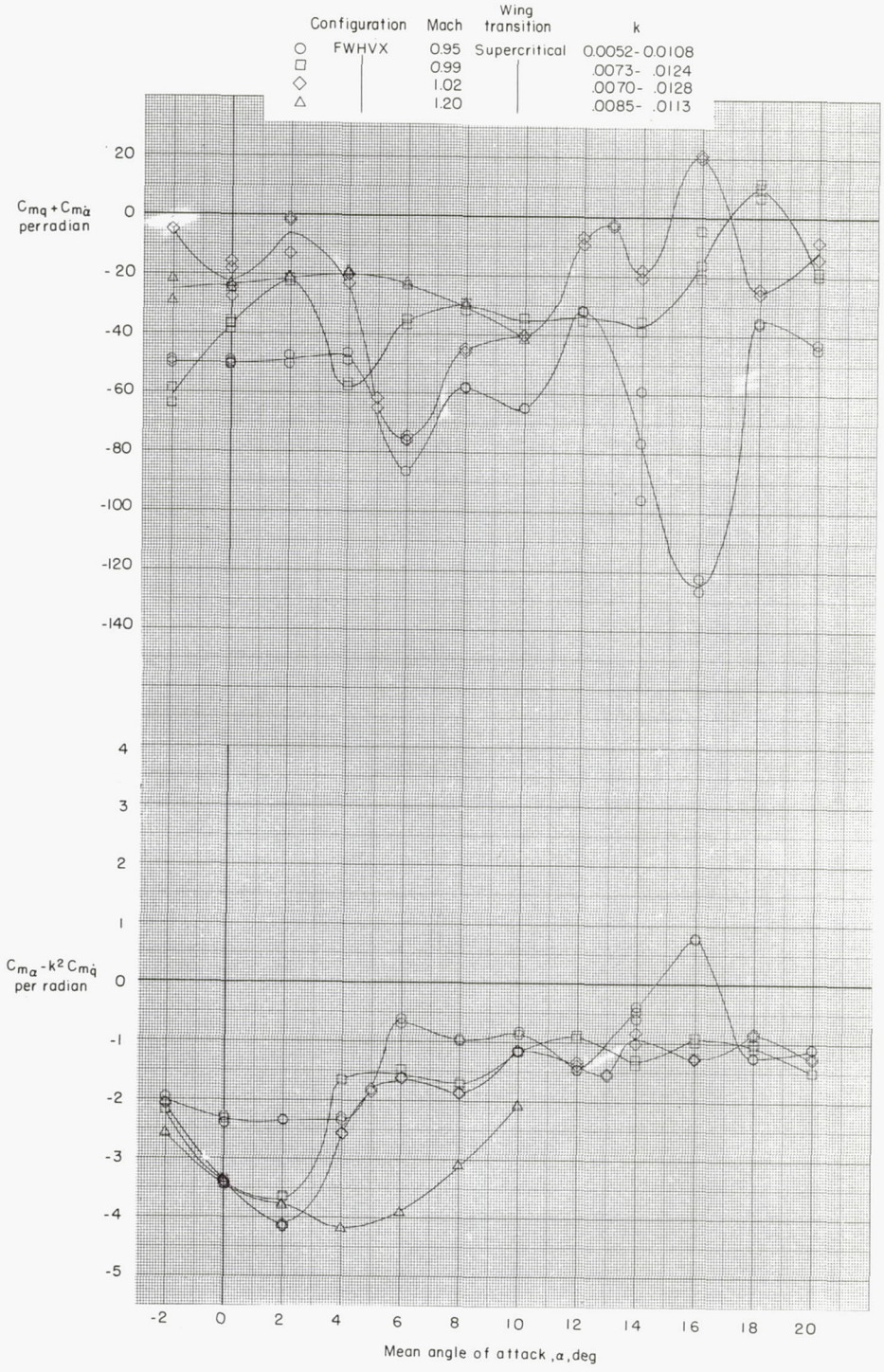

(b) M = 0.95, 0.99, 1.02, and 1.20.

Figure 9.- Concluded.

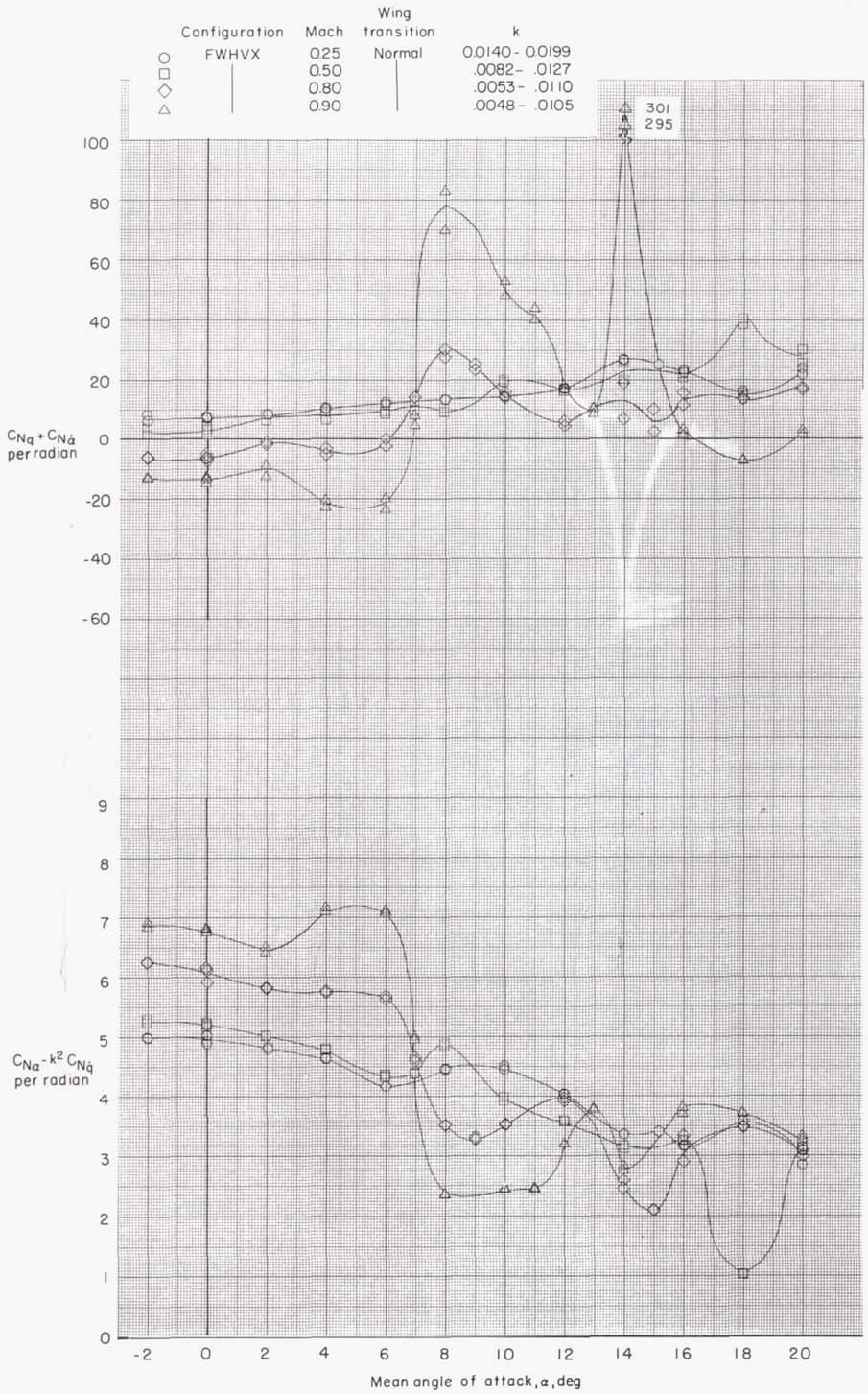

(a) M = 0.25, 0.50, 0.80, and 0.90.

Figure 10.- Variation of normal force due to pitching rate parameter and normal force due to pitch displacement parameter with mean angle of attack for basic configuration with vortex generators.

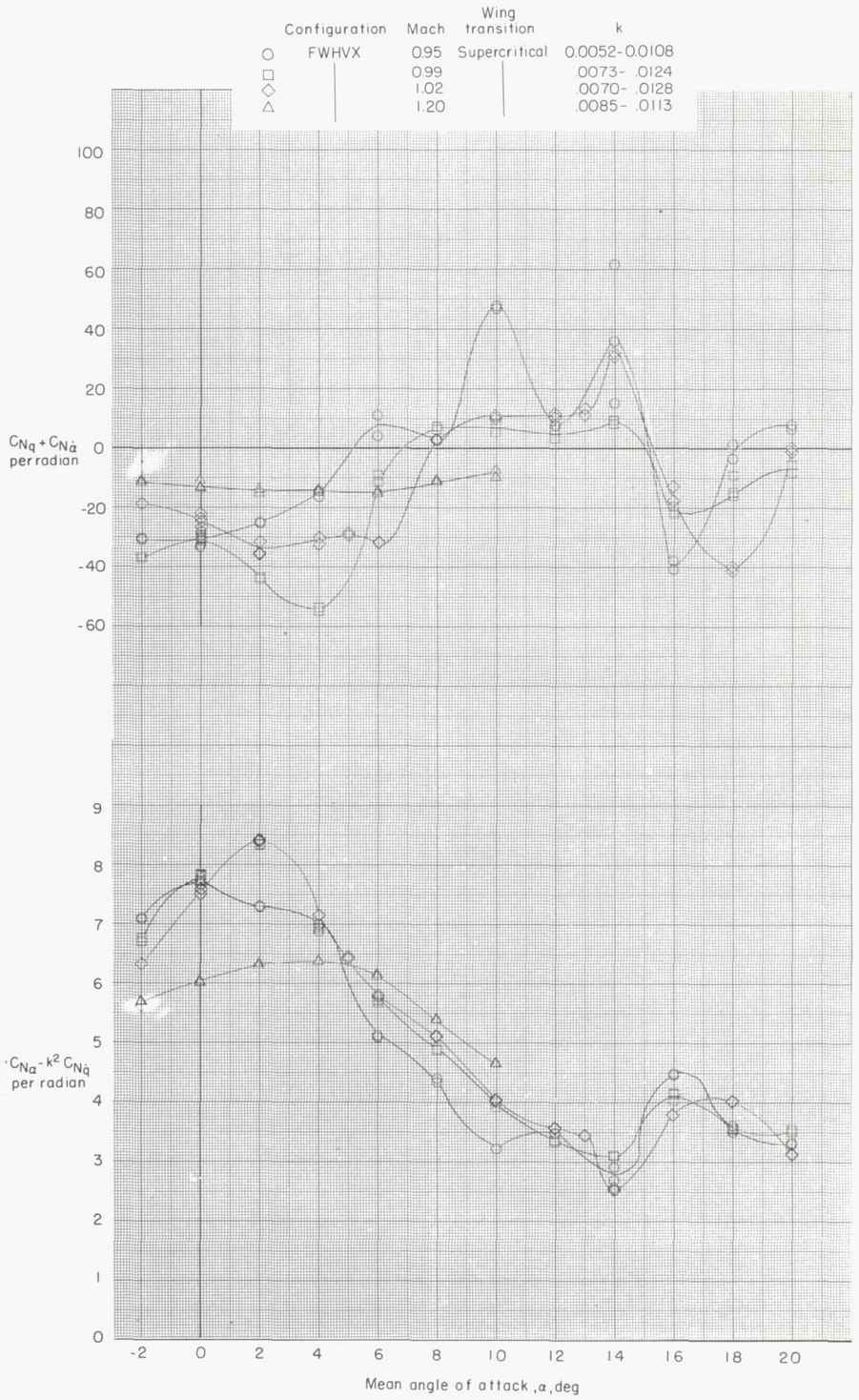

(b) M = 0.95, 0.99, 1.02, and 1.20.

Figure 10.- Concluded.

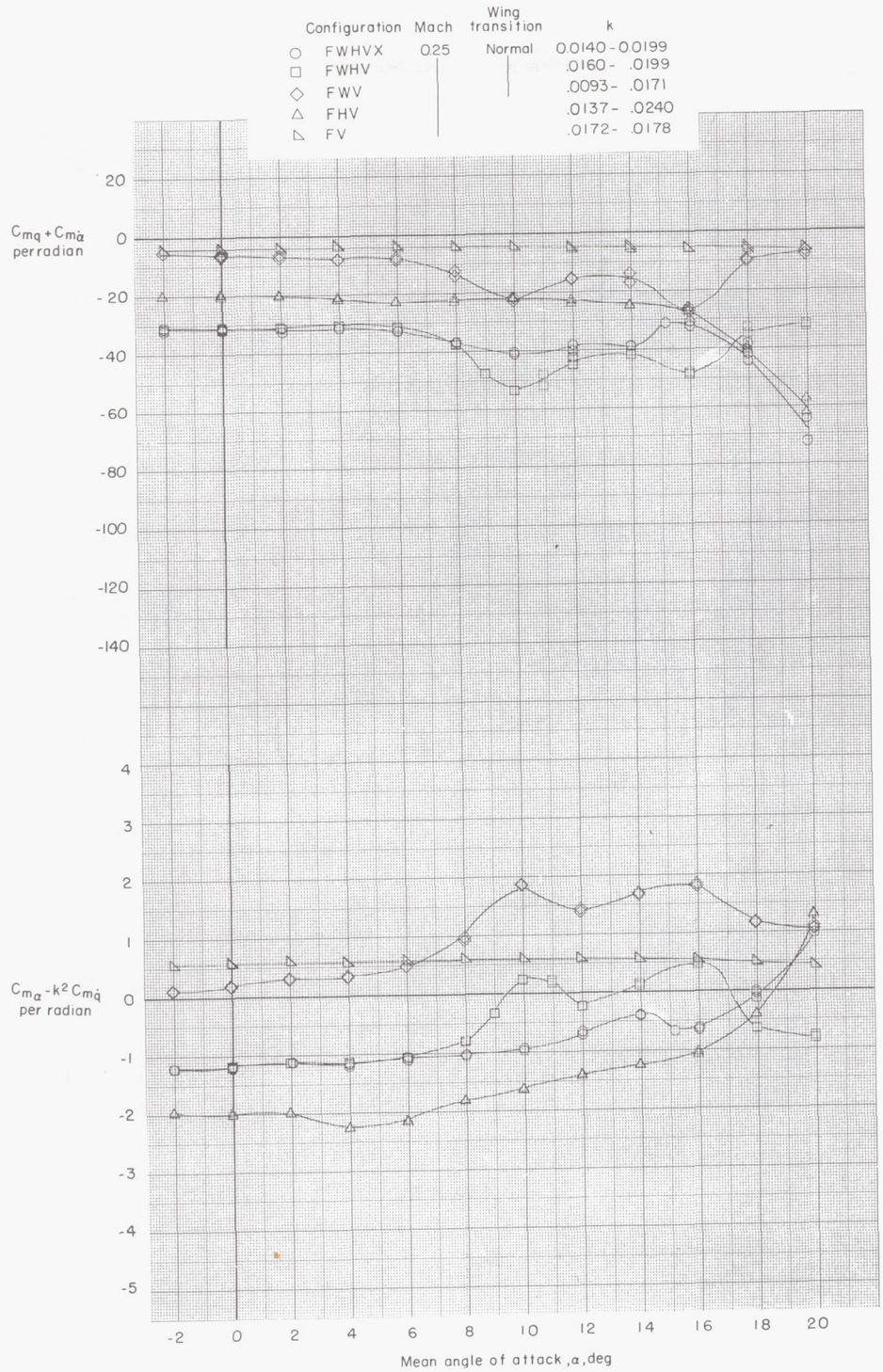

(a) M = 0.25.

Figure 11.- Variation of damping-in-pitch parameter and oscillatory longitudinal-stability parameter with mean angle of attack. Configuration component breakdown.

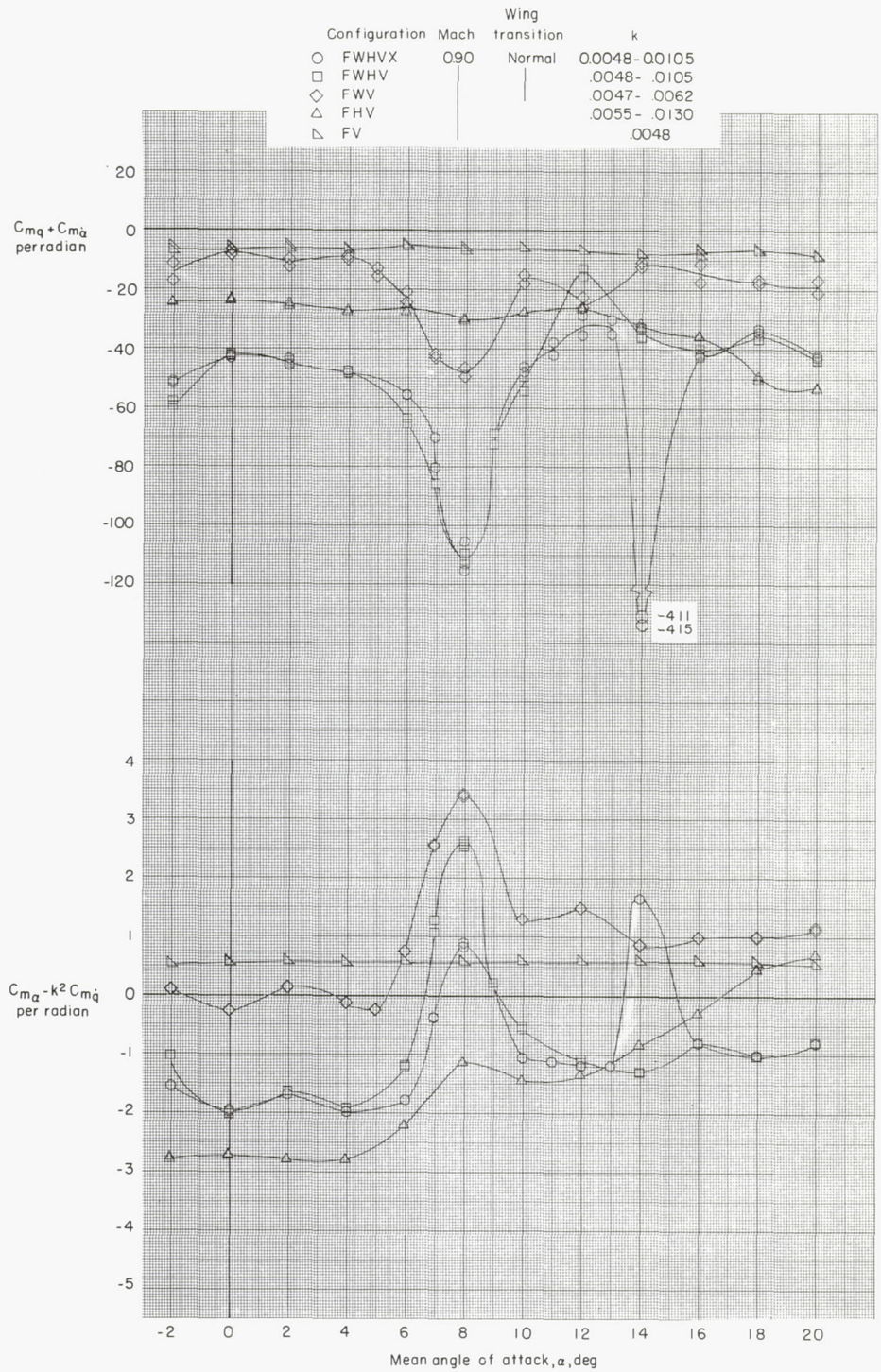

(b) M = 0.90.

Figure 11.- Continued.

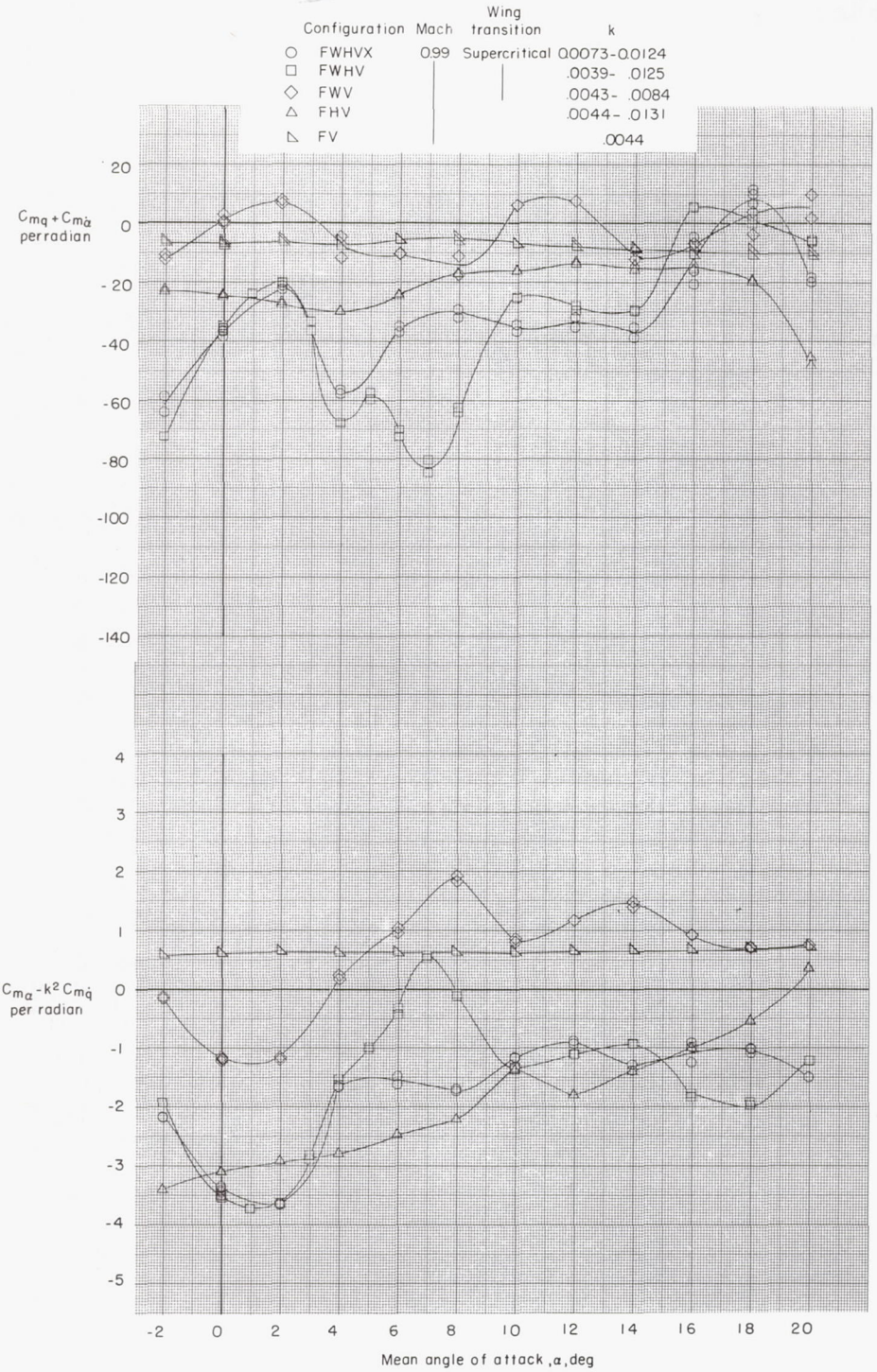

(c) M = 0.99.

Figure 11.- Continued.

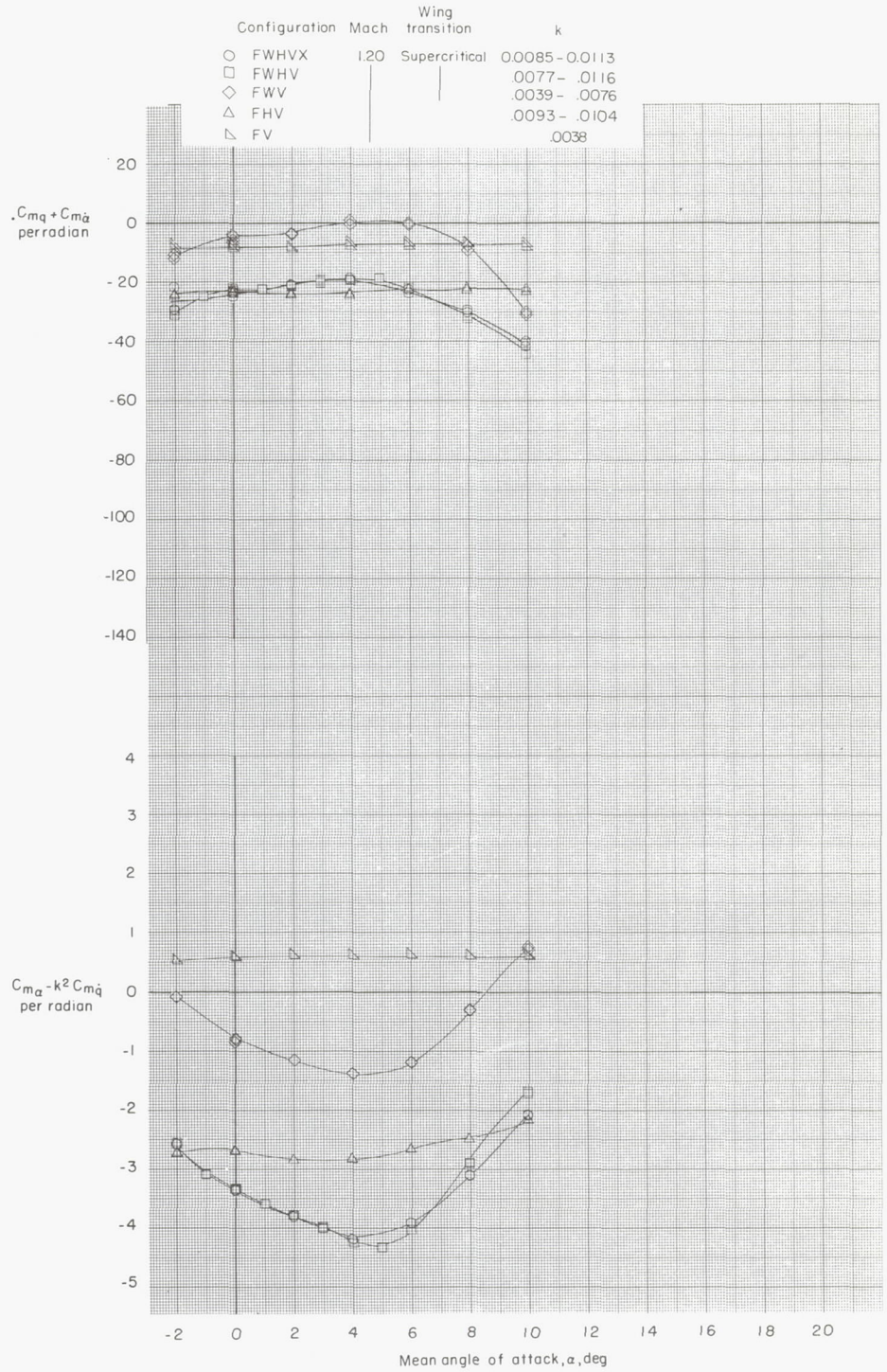

(d) M = 1.20.

Figure 11.- Concluded.

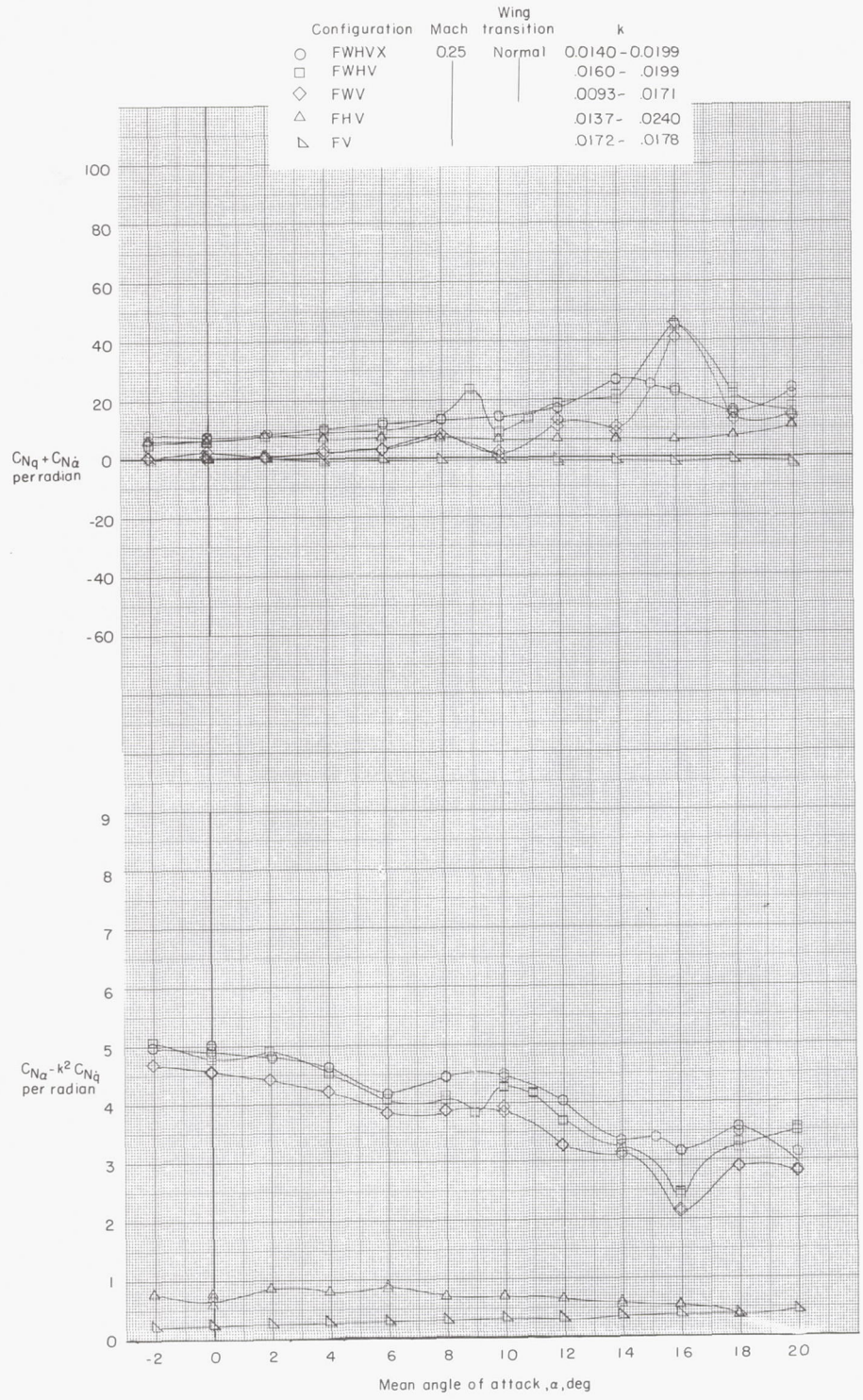

(a) M = 0.25.

Figure 12.- Variation of normal force due to pitching rate parameter and normal force due to pitch displacement parameter with mean angle of attack. Configuration component breakdown.

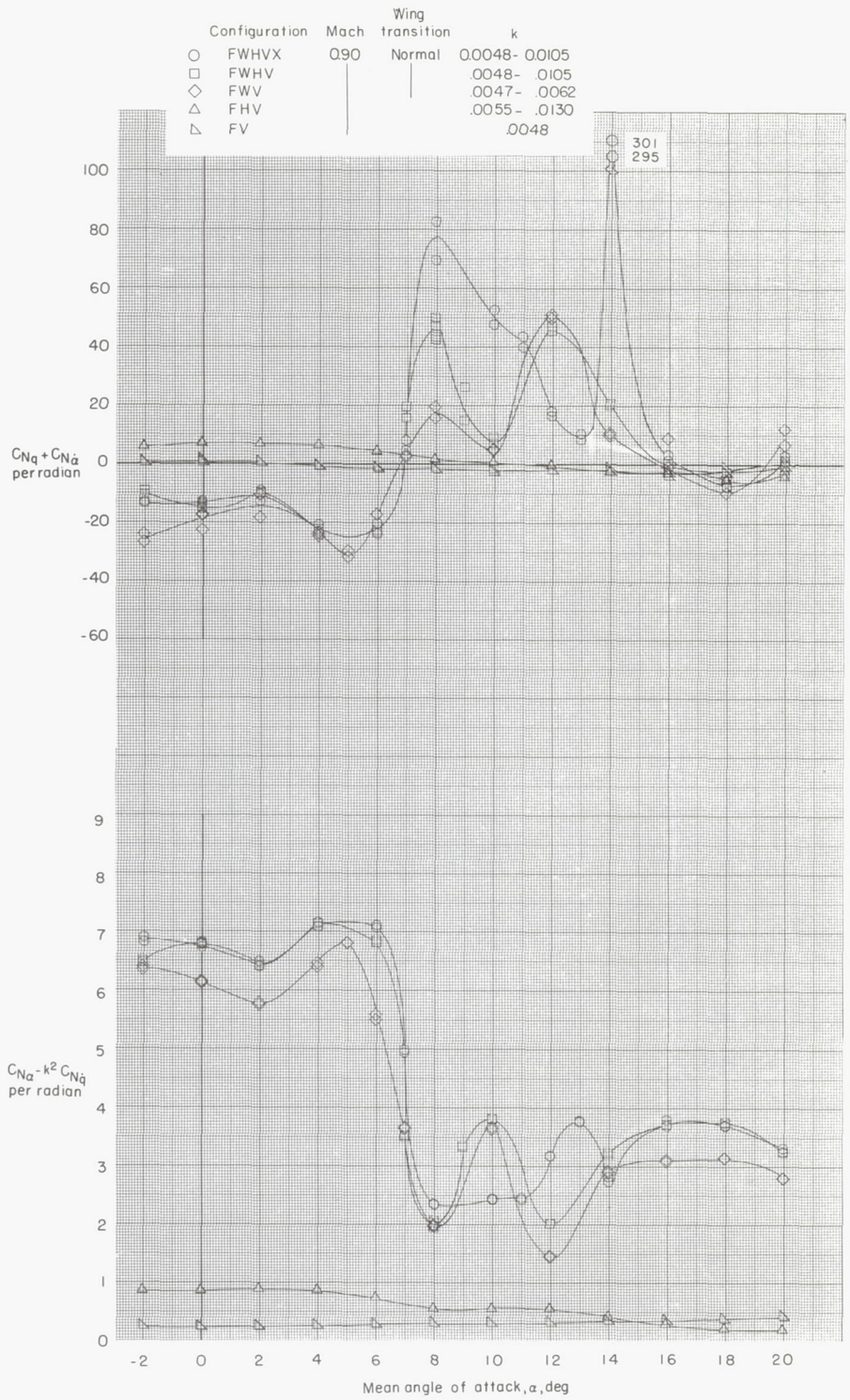

(b) M = 0.90.

Figure 12.- Continued.

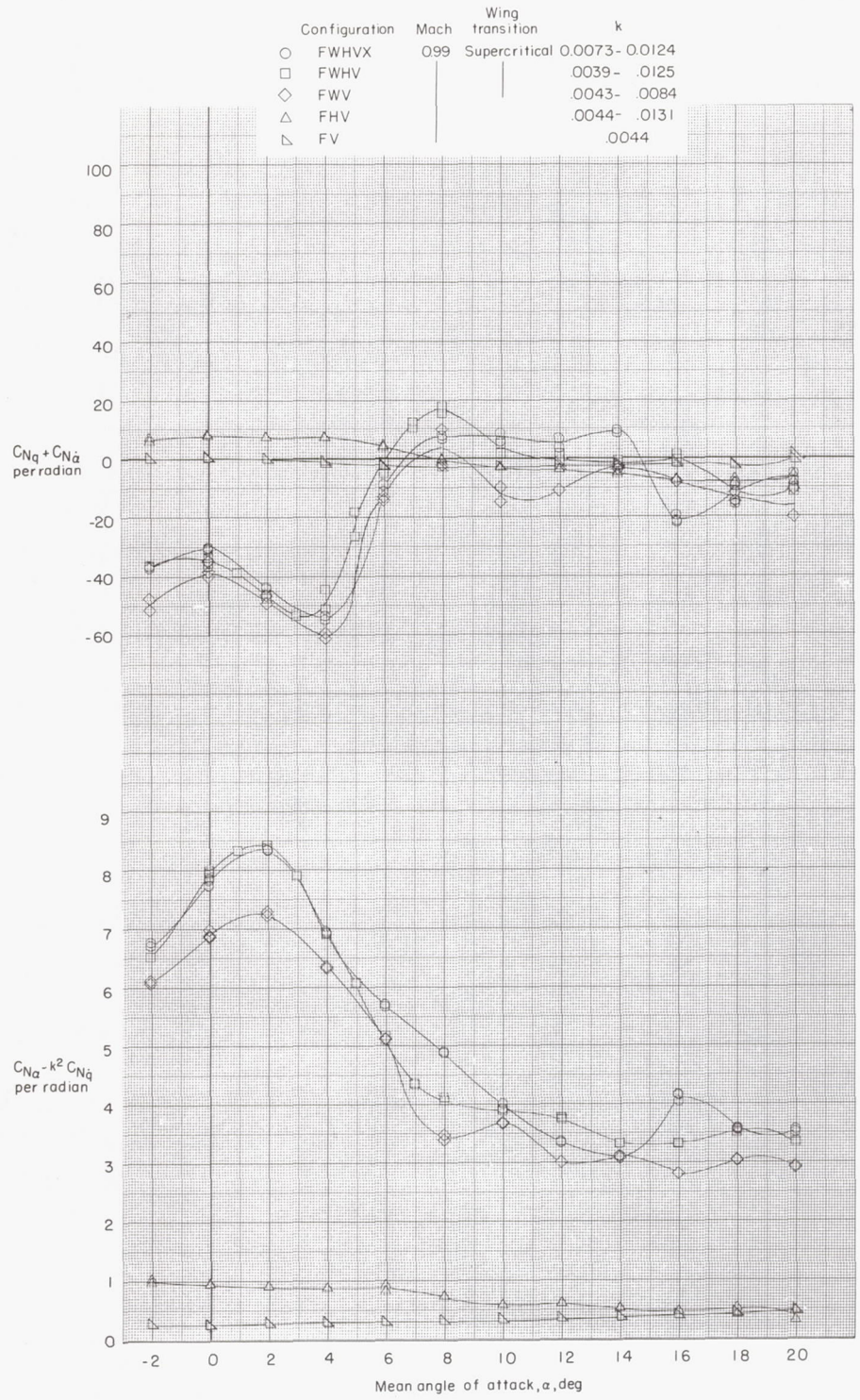

(c) M = 0.99.

Figure 12.- Continued.

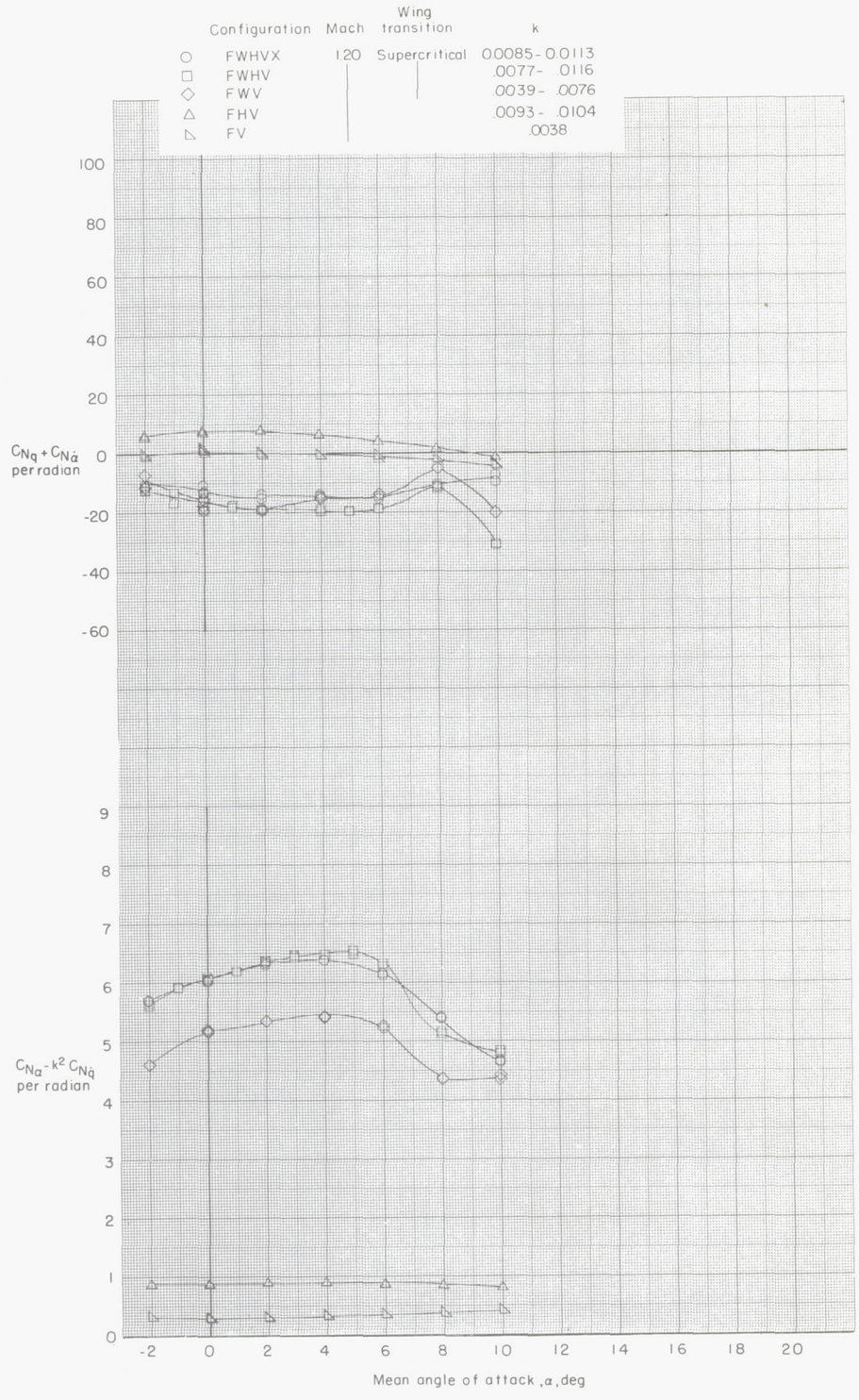

(d) M = 1.20.

Figure 12.- Concluded.

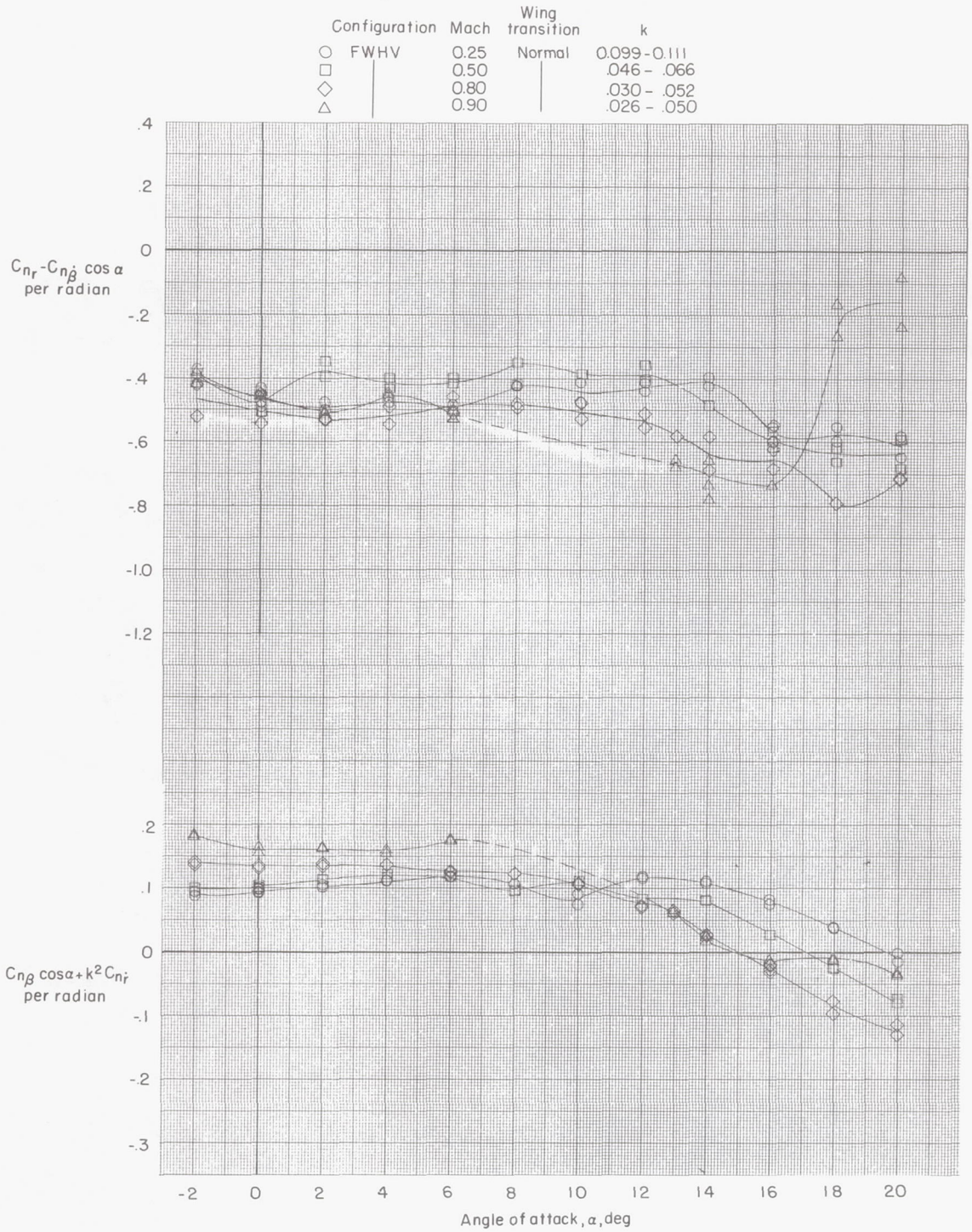

(a) M = 0.25, 0.50, 0.80, and 0.90.

Figure 13.- Variation of damping-in-yaw parameter and oscillatory directional-stability parameter with angle of attack for basic configuration.

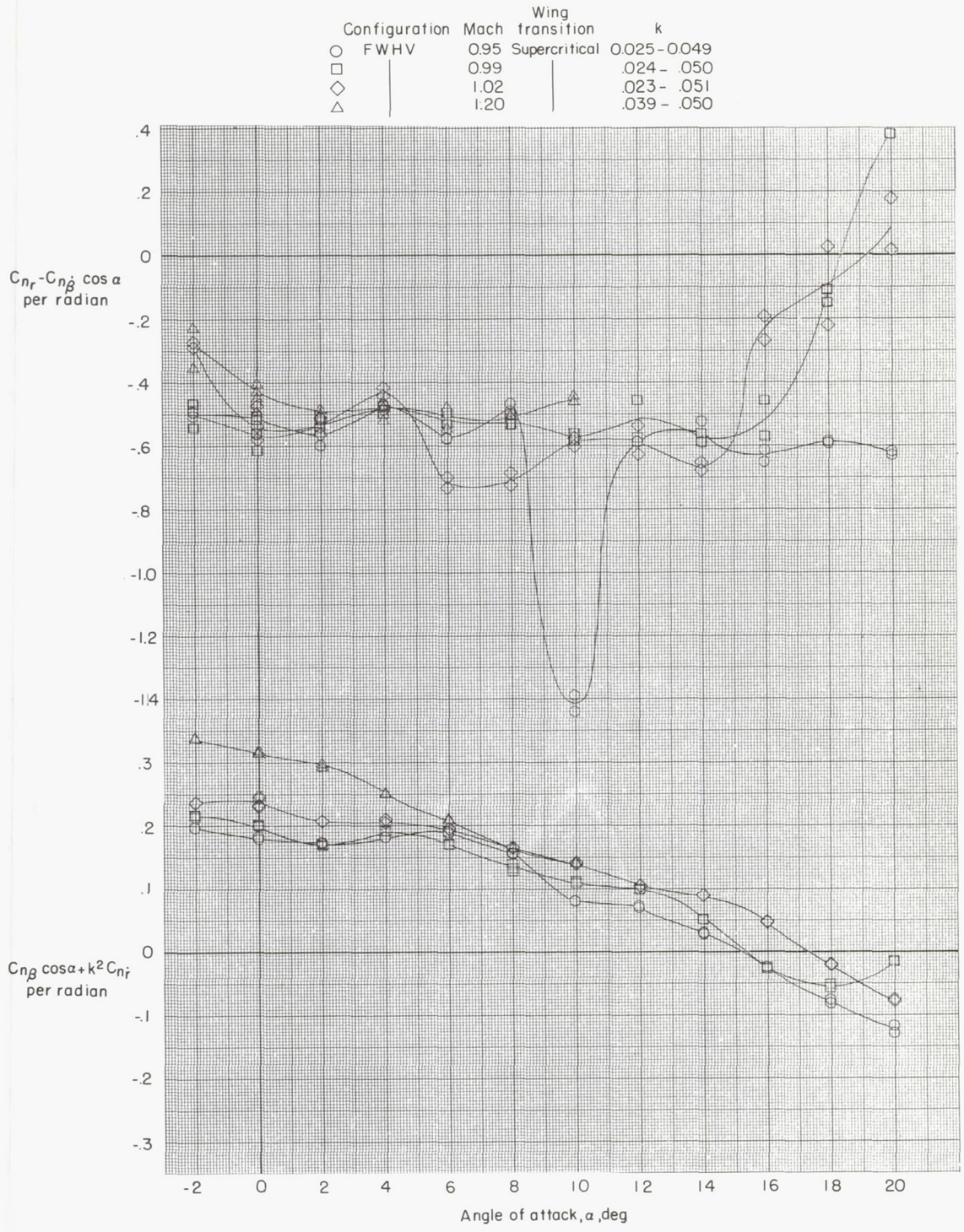

(b) M = 0.95, 0.99, 1.02, and 1.20.

Figure 13.- Concluded.

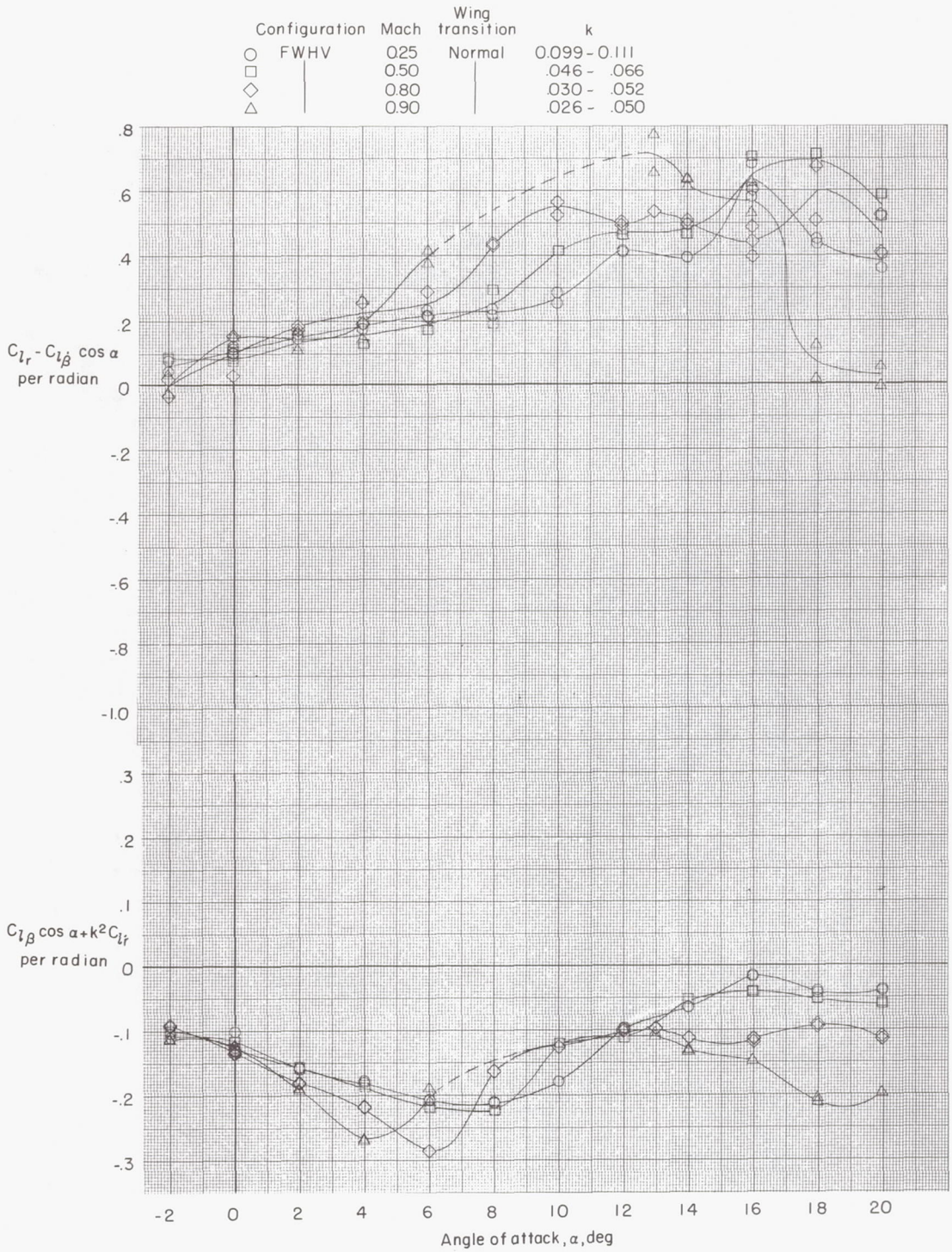

(a) M = 0.25, 0.50, 0.80, and 0.90.

Figure 14.- Variation of rolling moment due to yaw rate parameter and effective-dihedral parameter with angle of attack. Basic configuration.

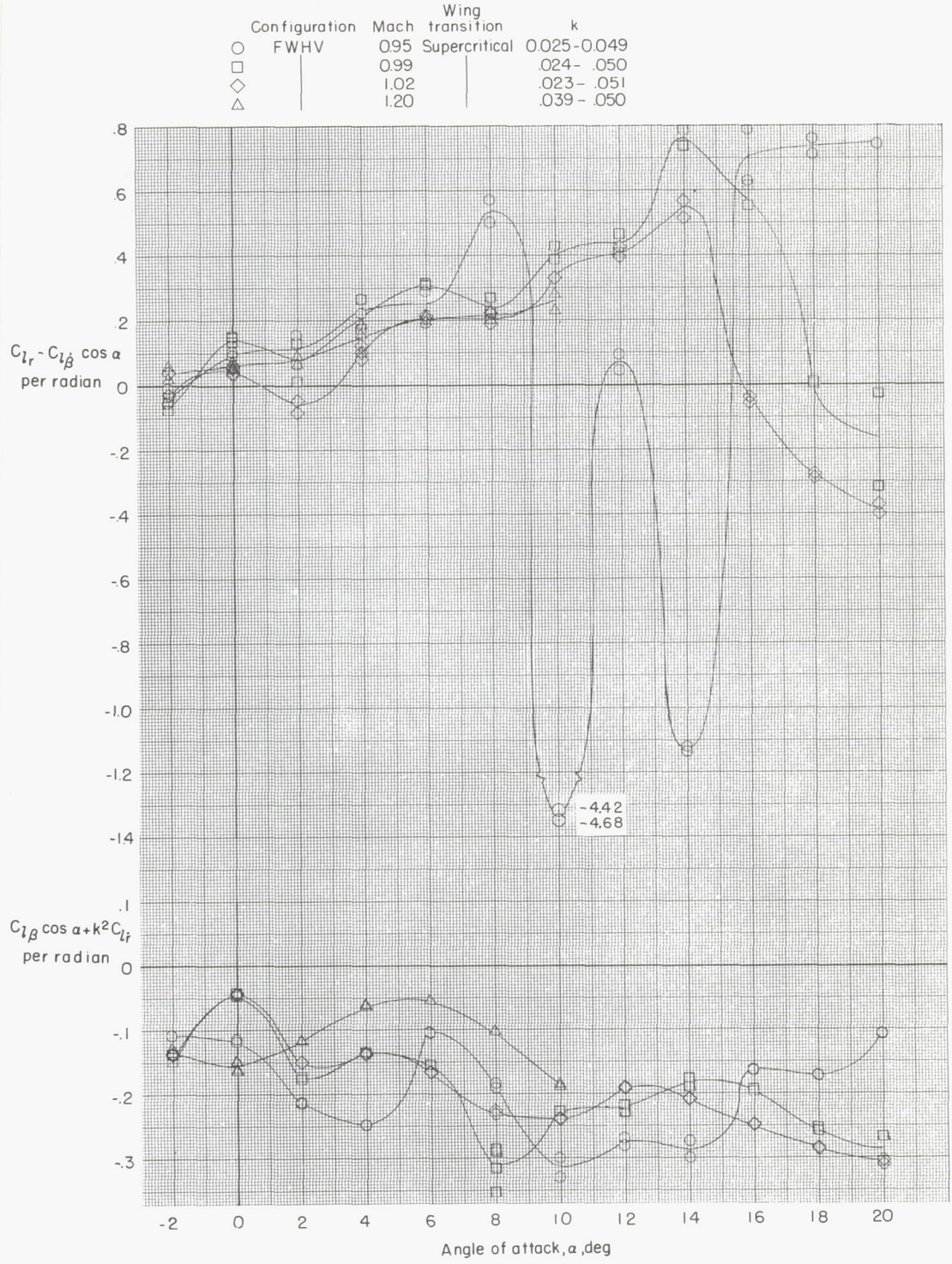

(b) M = 0.95, 0.99, 1.02, and 1.20.

Figure 14.- Concluded.

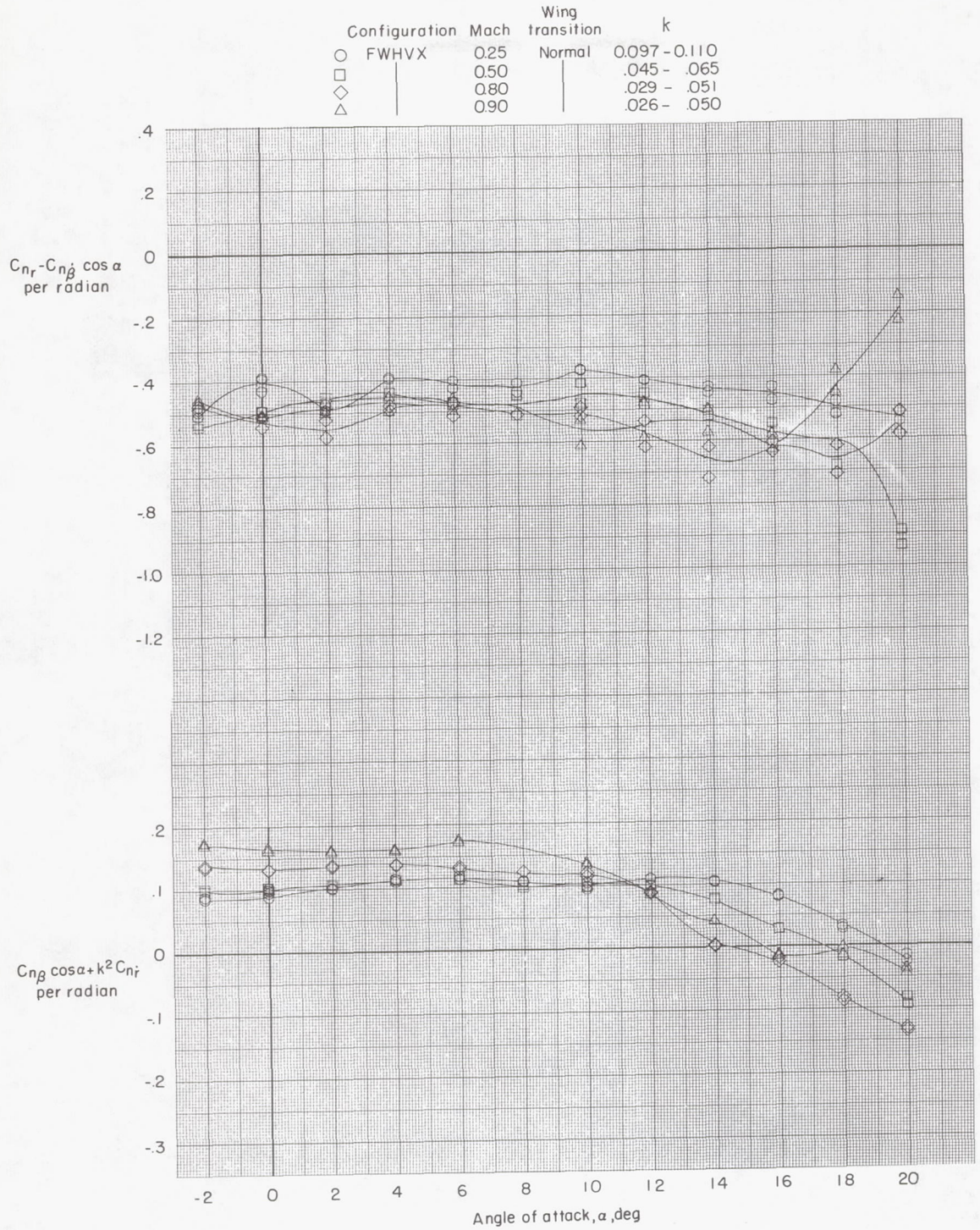

(a) M = 0.25, 0.50, 0.80, and 0.90.

Figure 15.- Variation of damping-in-yaw parameter and oscillatory directional-stability parameter with angle of attack for basic configuration with vortex generator.

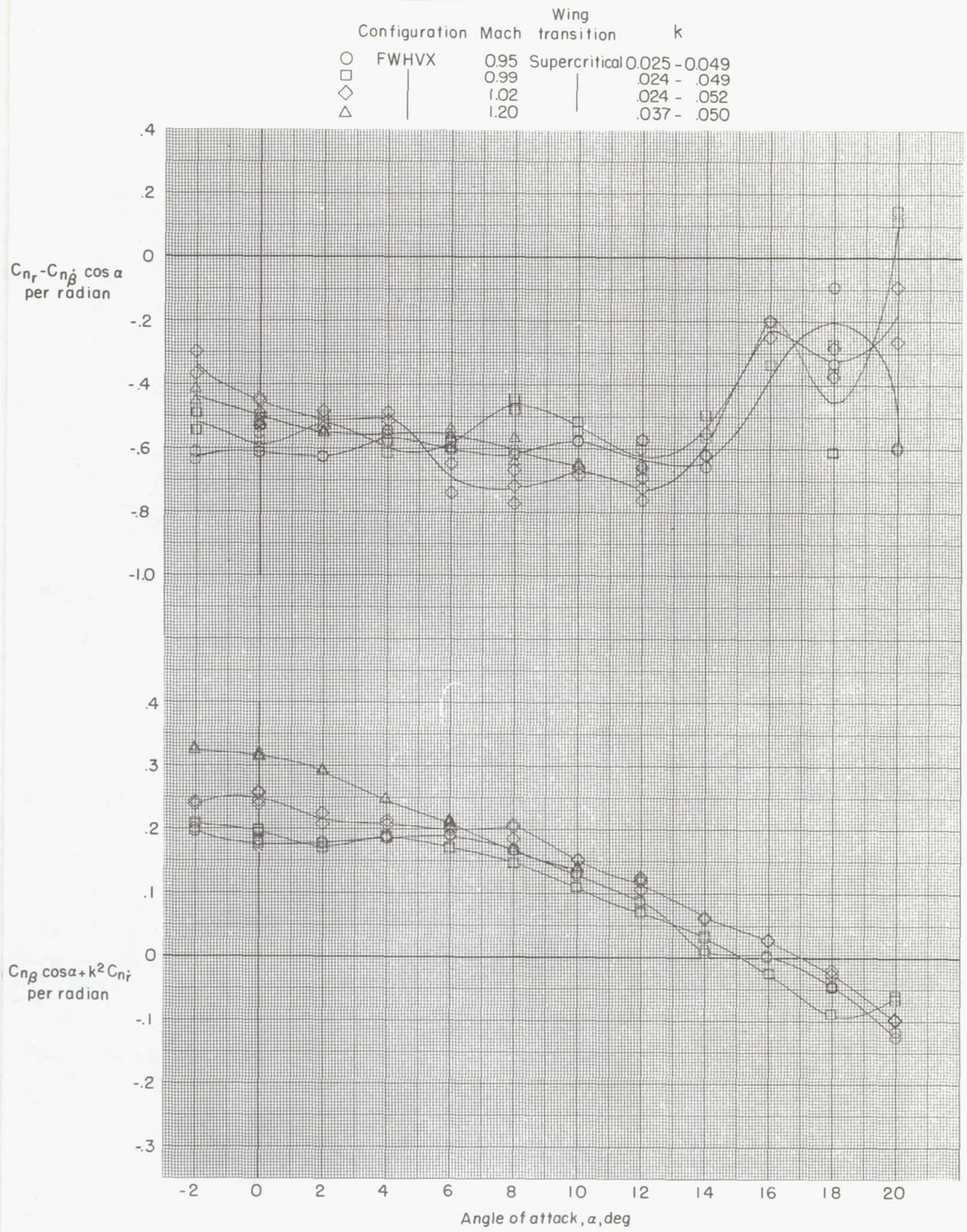

(b) M = 0.95, 0.99, 1.02, and 1.20.

Figure 15.- Concluded.

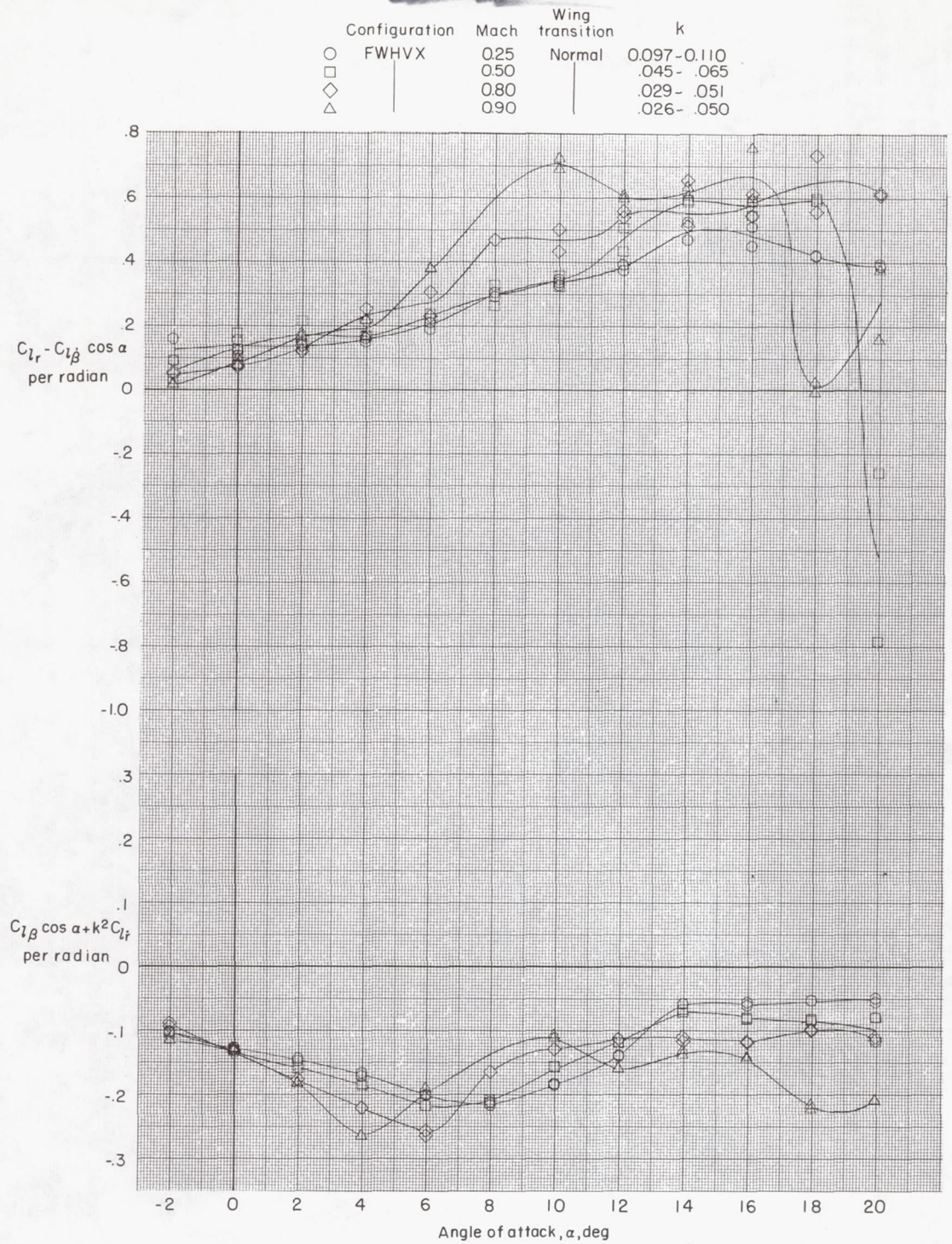

(a) M = 0.25, 0.50, 0.80, and 0.90.

Figure 16.- Variation of rolling moment due to yaw rate parameter and effective-dihedral parameter with angle of attack for basic configuration with vortex generator.

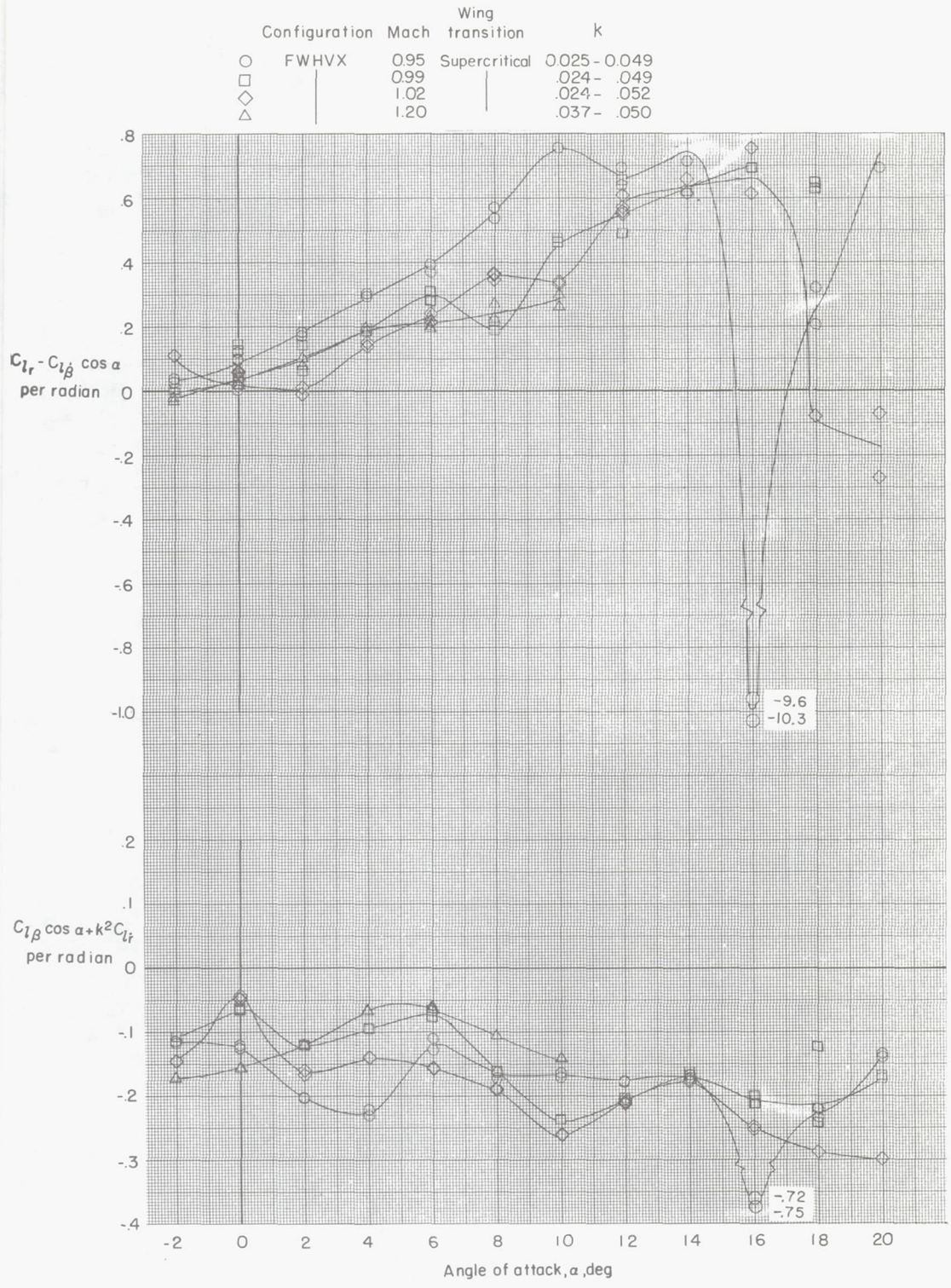

(b) M = 0.95, 0.99, 1.02, and 1.20.

Figure 16.- Concluded.

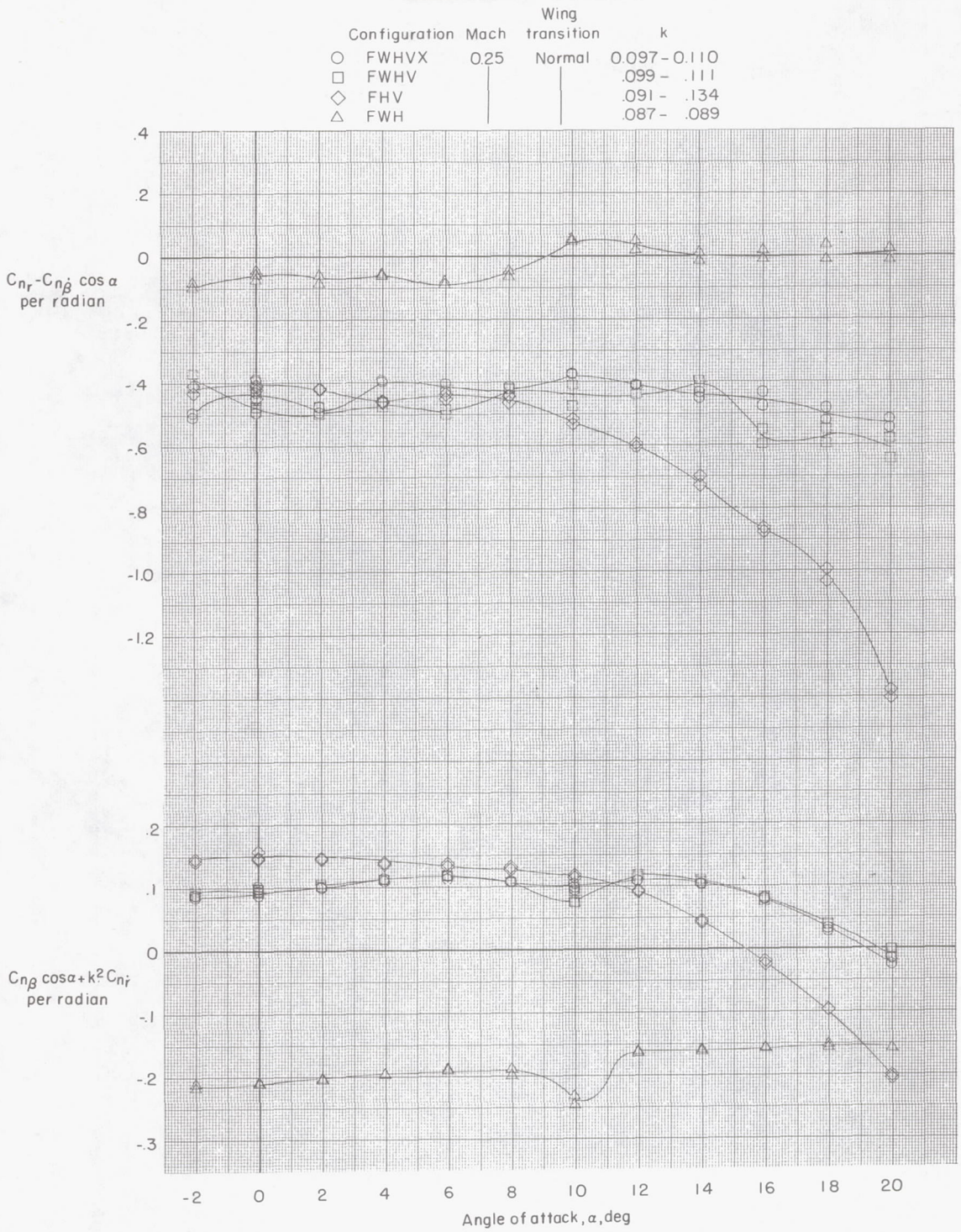

(a) M = 0.25.

Figure 17.- Variation of damping-in-yaw parameter and oscillatory directional-stability parameter with angle of attack. Configuration component breakdown.

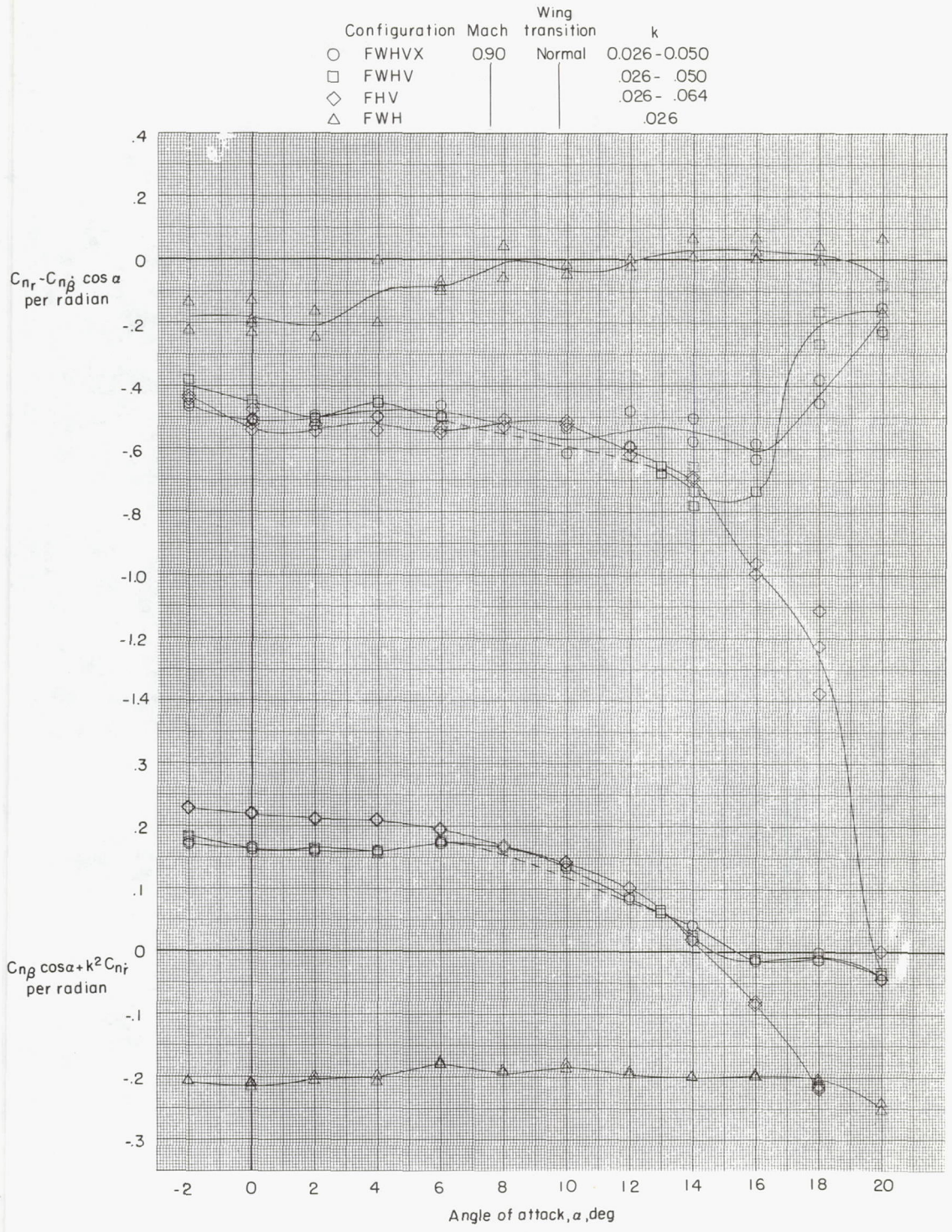

(b) M = 0.90.

Figure 17.- Continued.

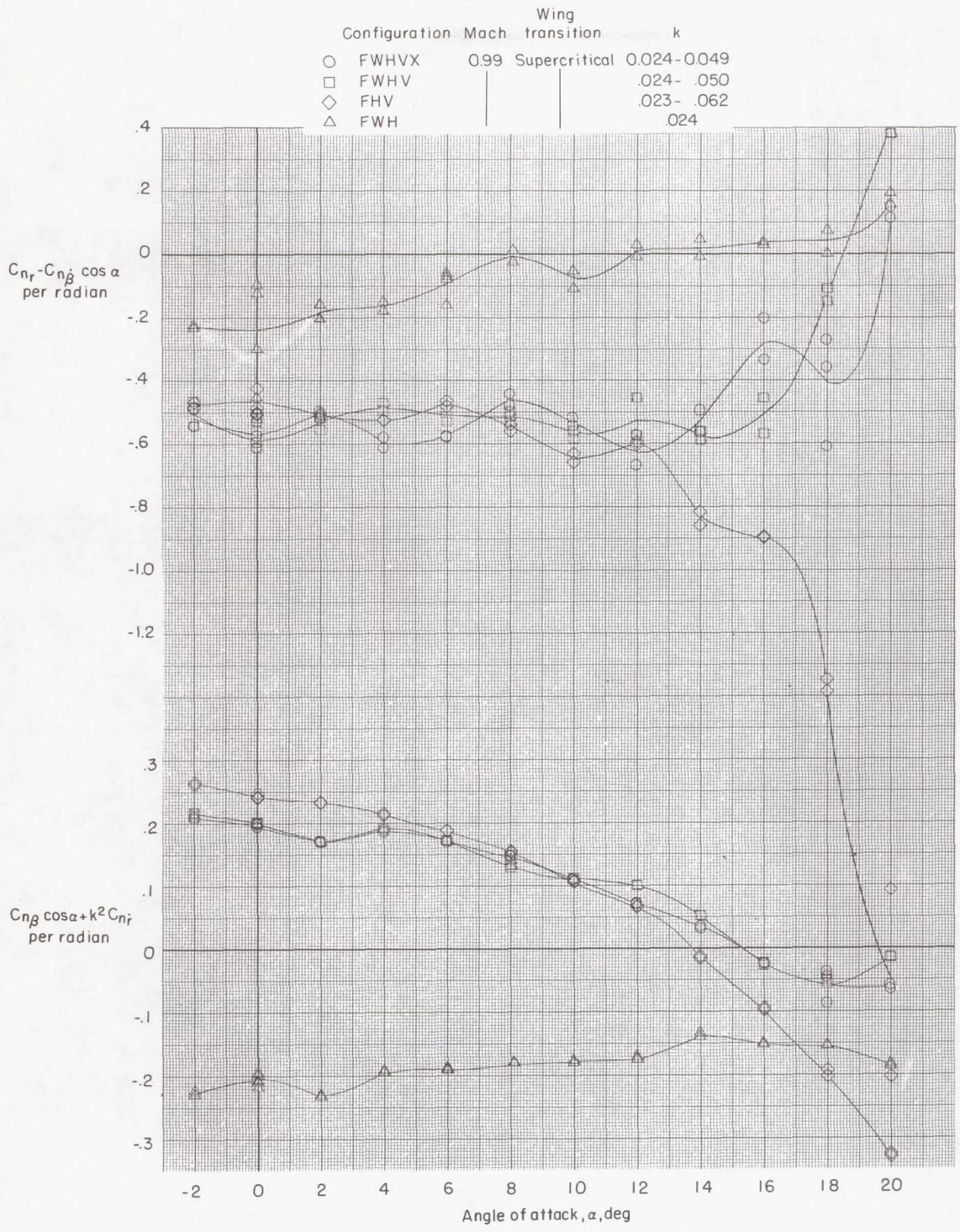

(c) M = 0.99.

Figure 17.- Continued.

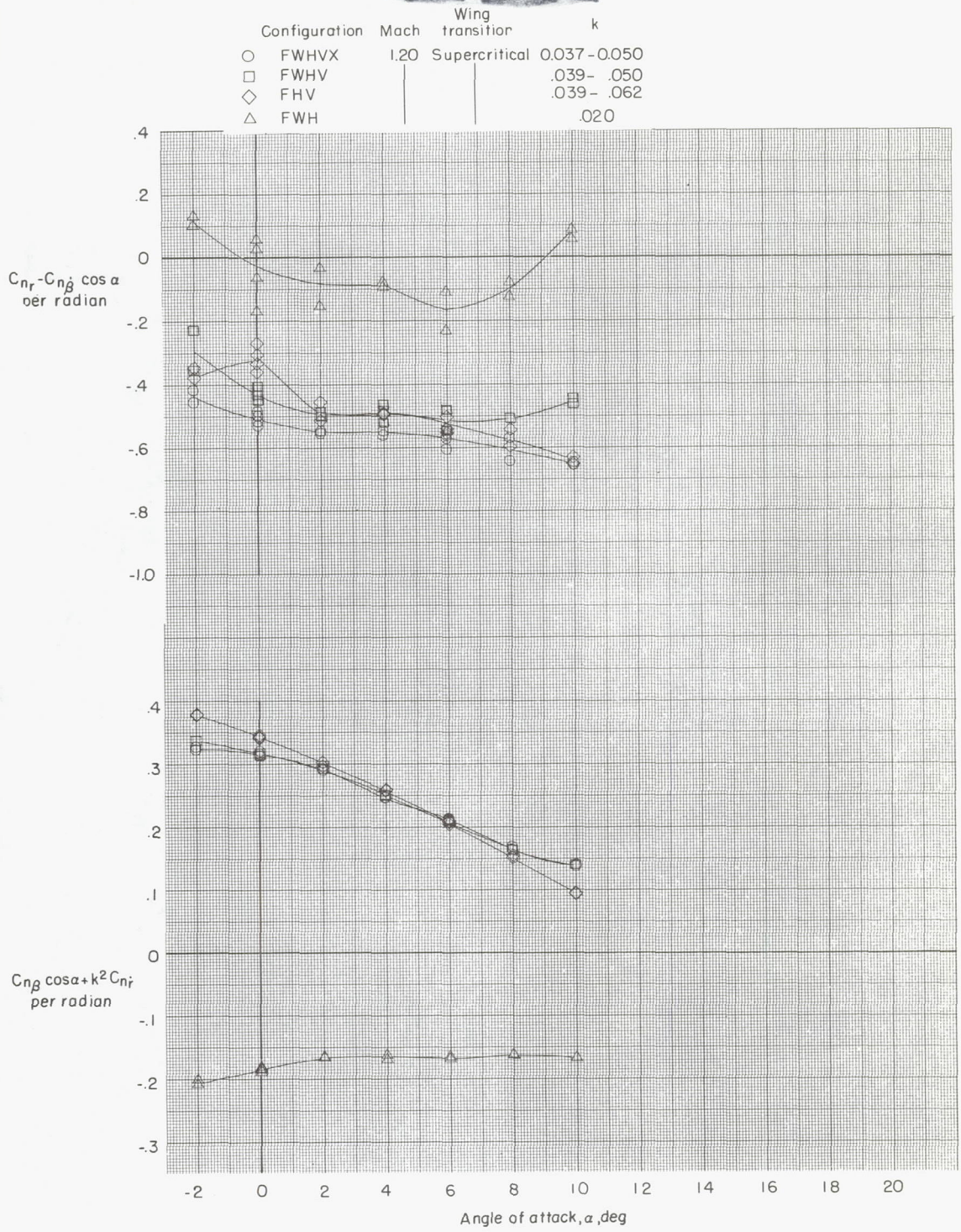

(d) M = 1.20.

Figure 17.- Concluded.

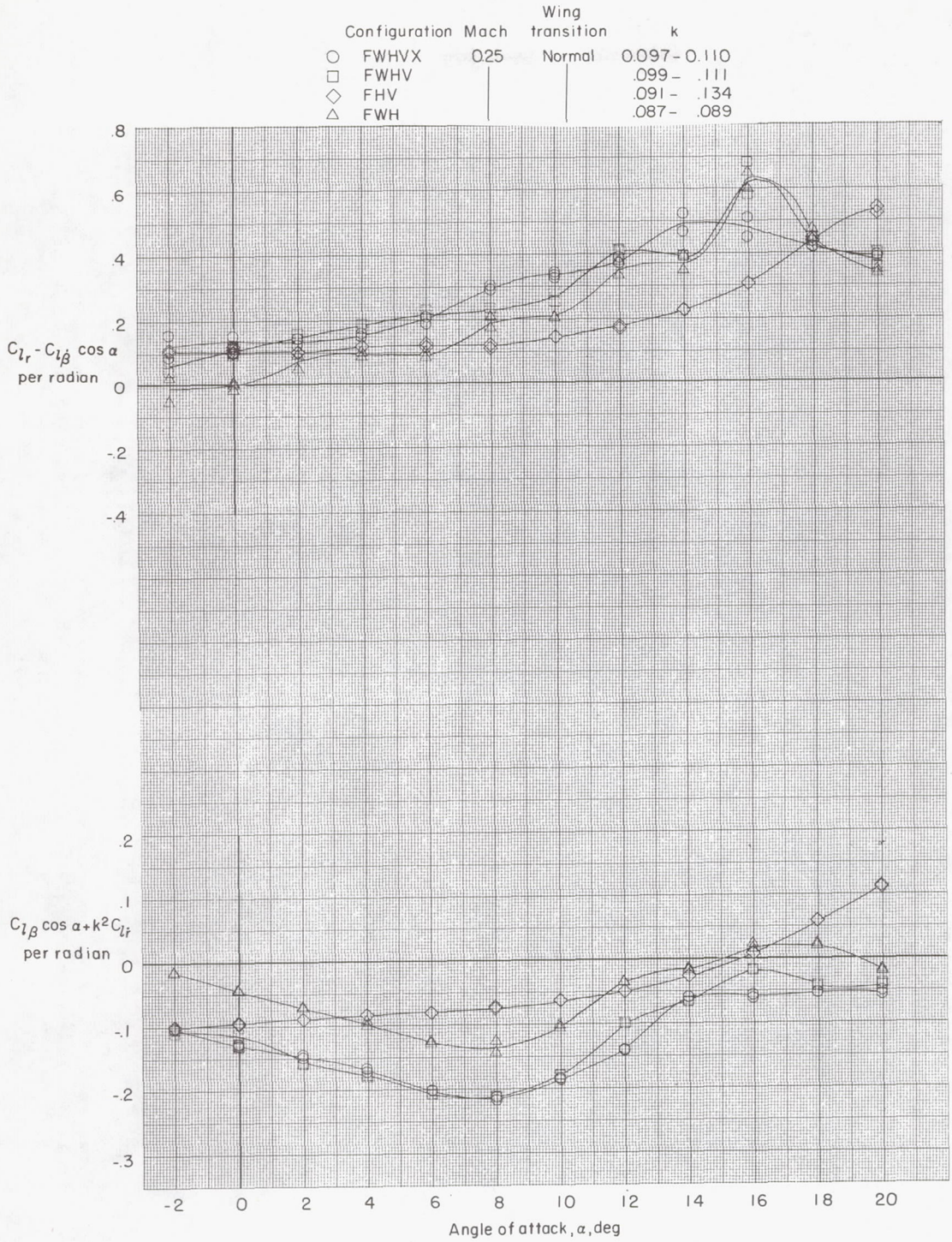

(a) M = 0.25.

Figure 18.- Variation of rolling moment due to yaw rate parameter and effective-dihedral parameter with angle of attack. Configuration component breakdown.

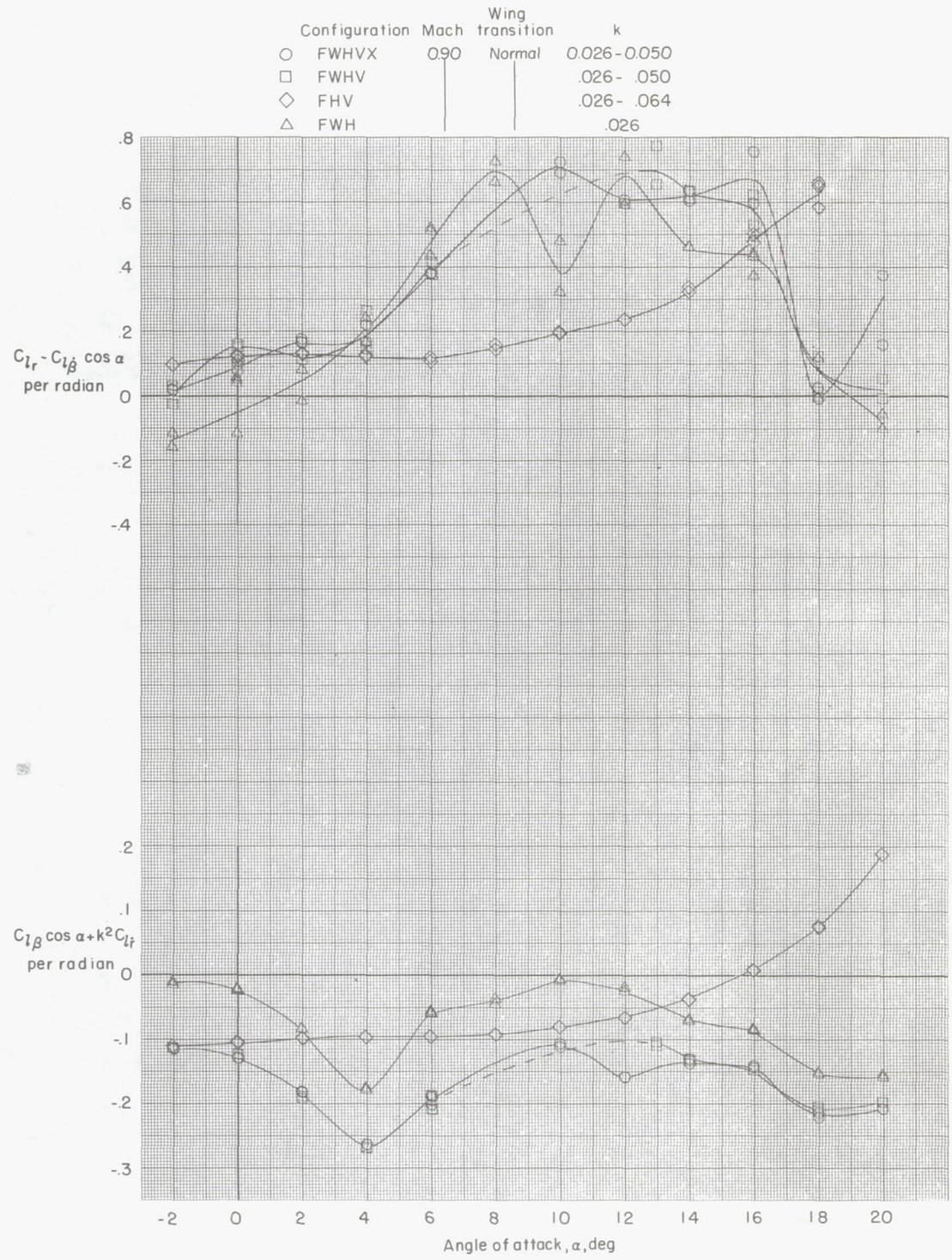

(b) M = 0.90.

Figure 18.- Continued.

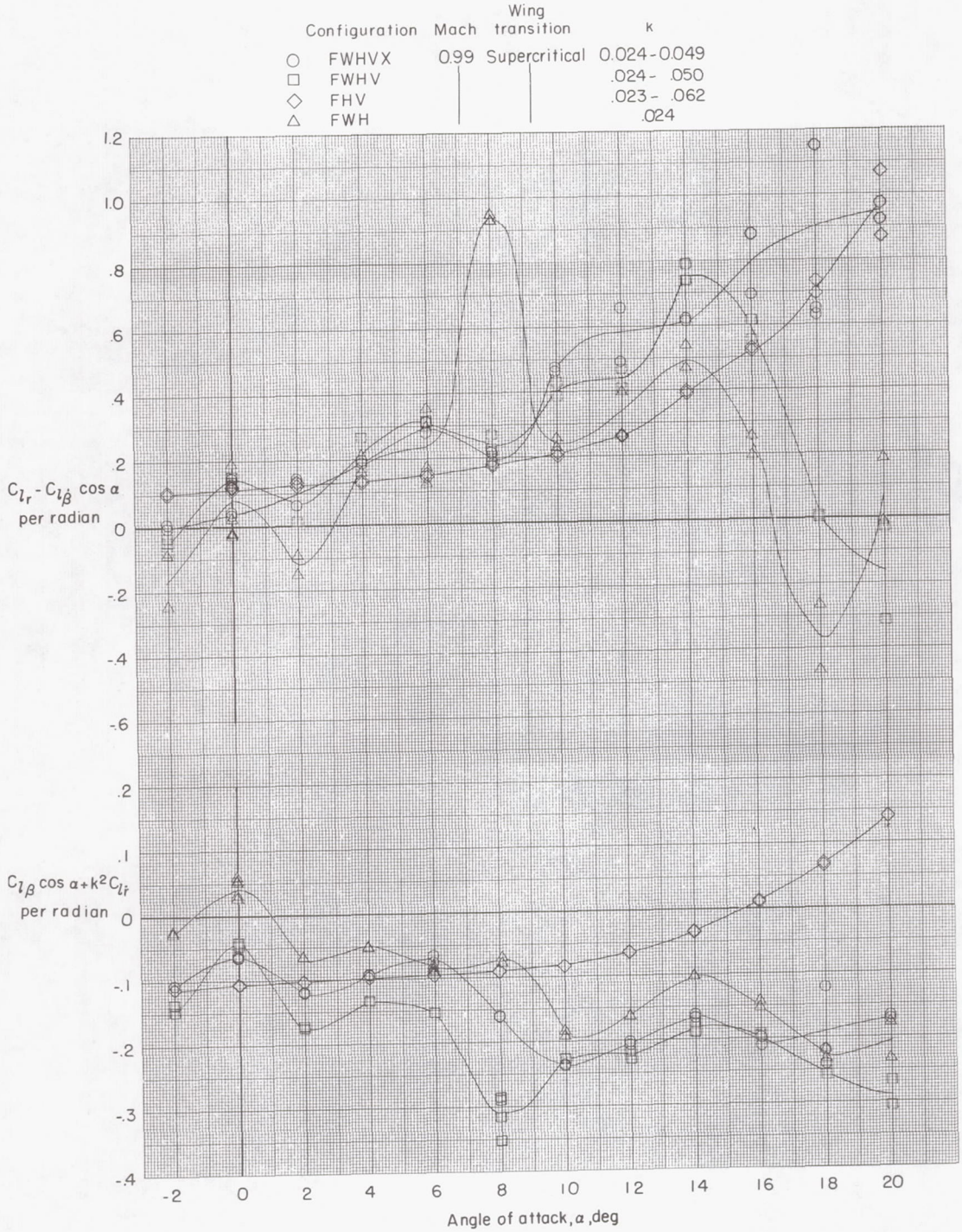

(c) M = 0.99.

Figure 18.- Continued.

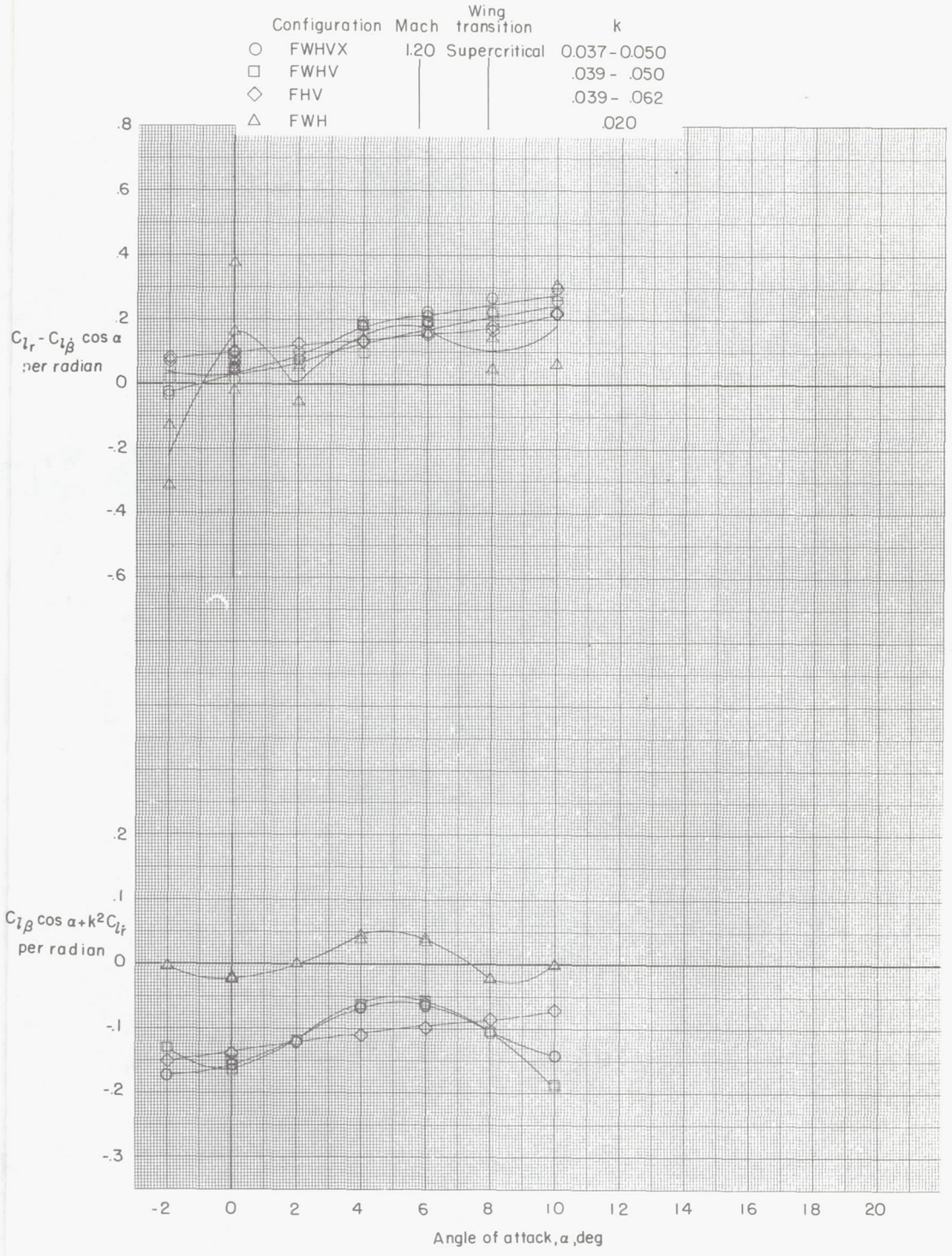

(d) M = 1.20.

Figure 18.- Concluded.

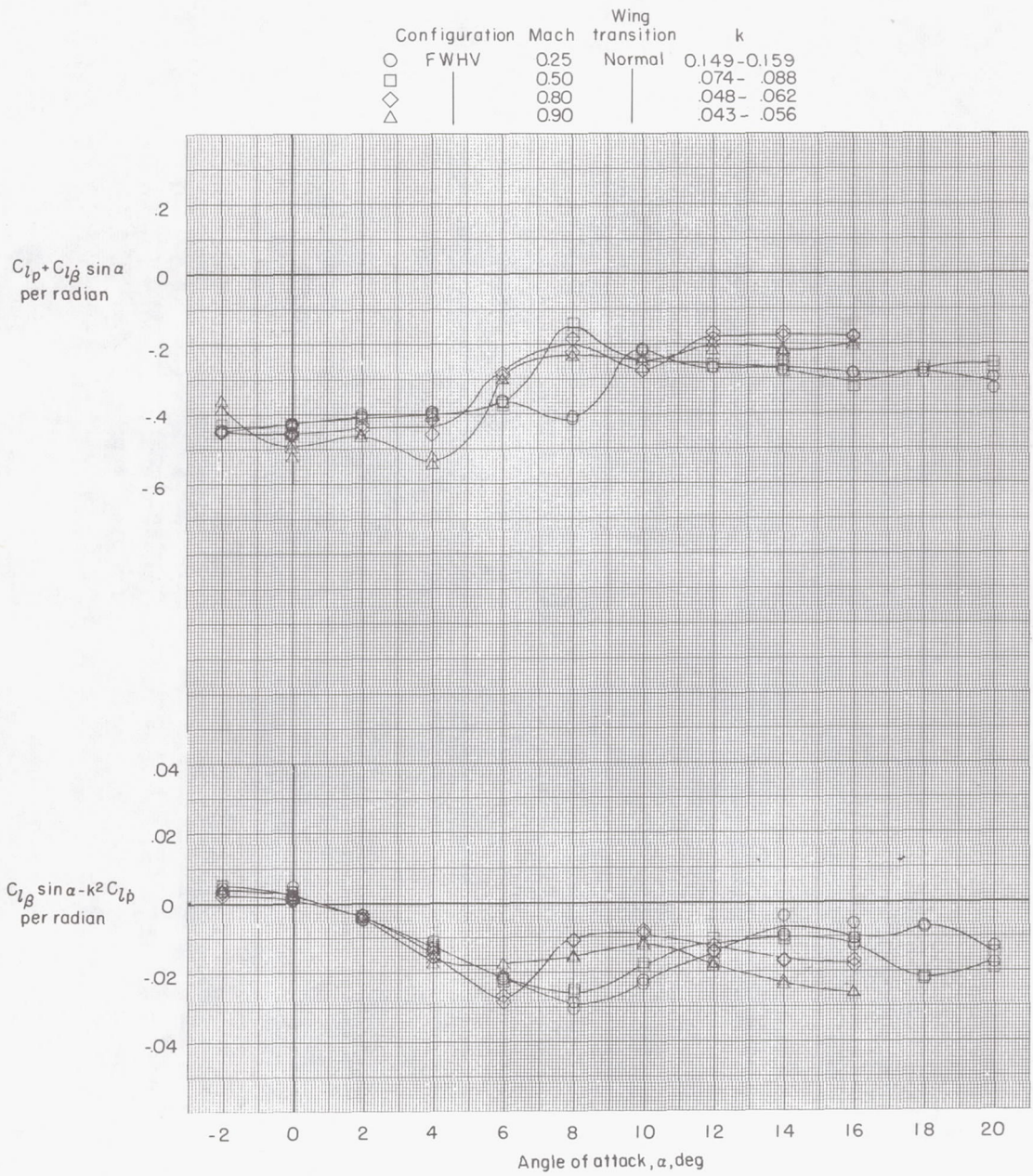

(a) M = 0.25, 0.50, 0.80, and 0.90.

Figure 19.- Variation of damping-in-roll parameter and rolling moment due to roll displacement parameter with angle of attack for basic configuration.

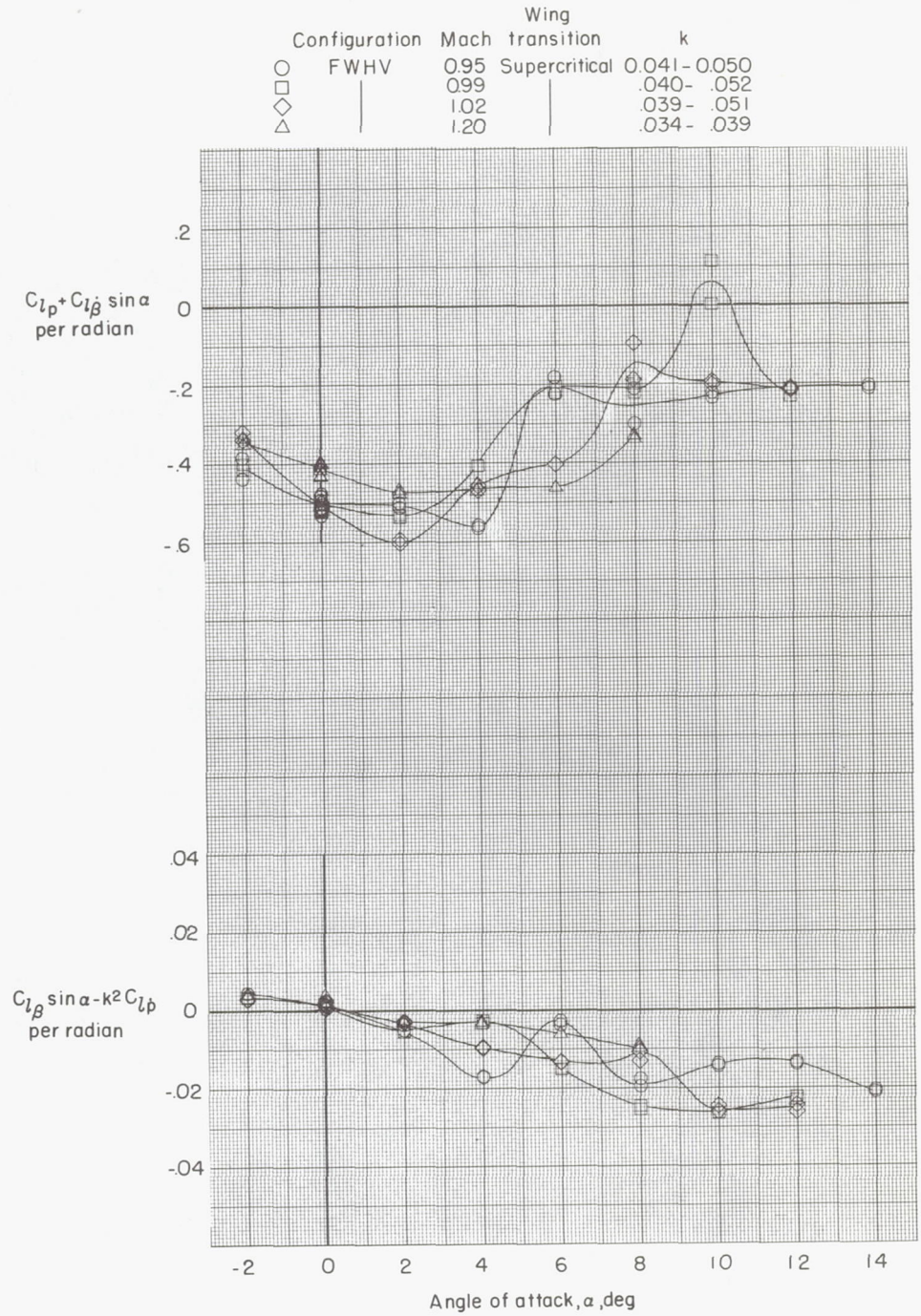

(b) M = 0.95, 0.99, 1.02, and 1.20.

Figure 19.- Concluded.

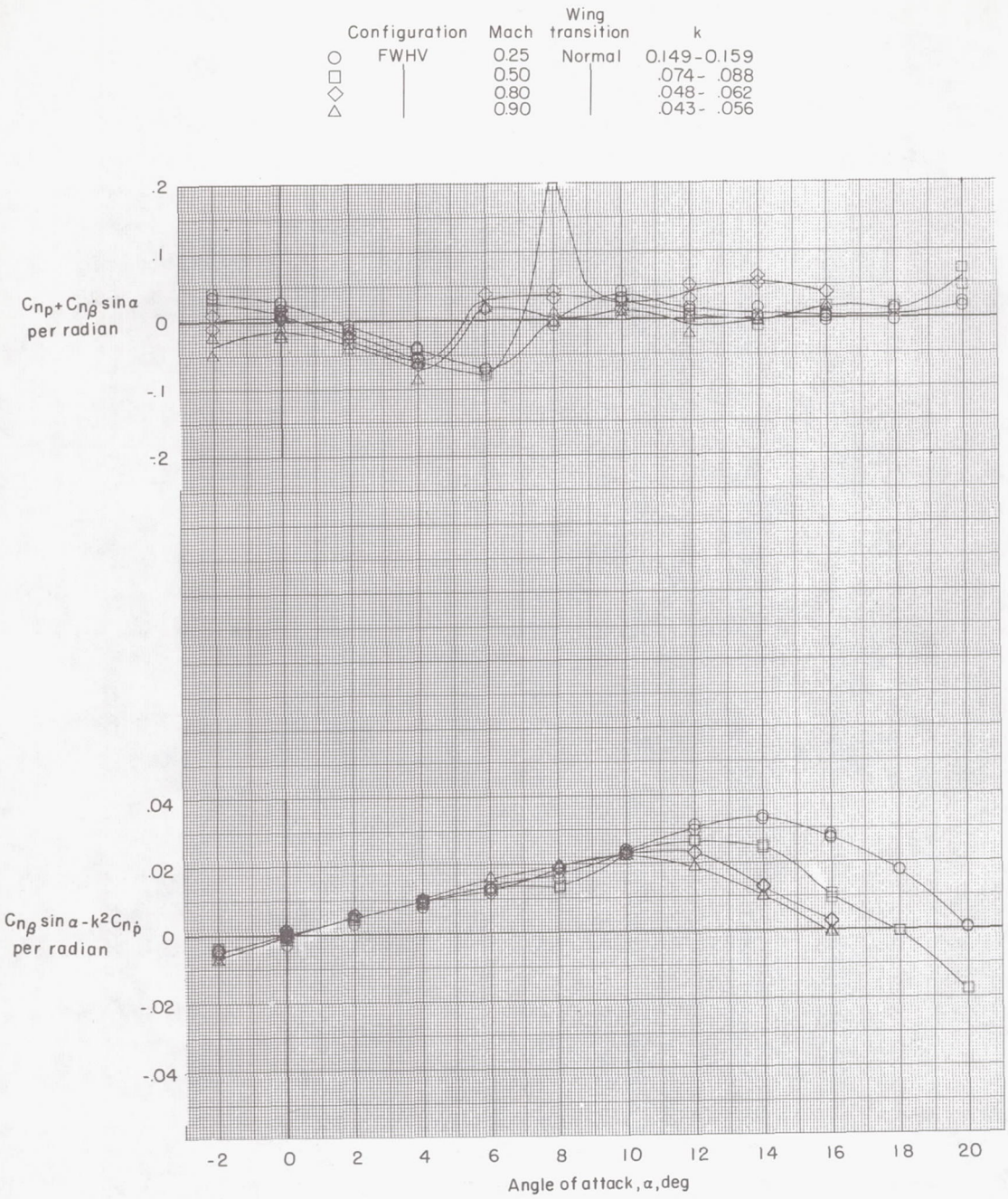

(a) M = 0.25, 0.50, 0.80, and 0.90.

Figure 20.- Variation of yawing moment due to roll rate parameter and yawing moment due to roll displacement parameter with angle of attack for basic configuration.

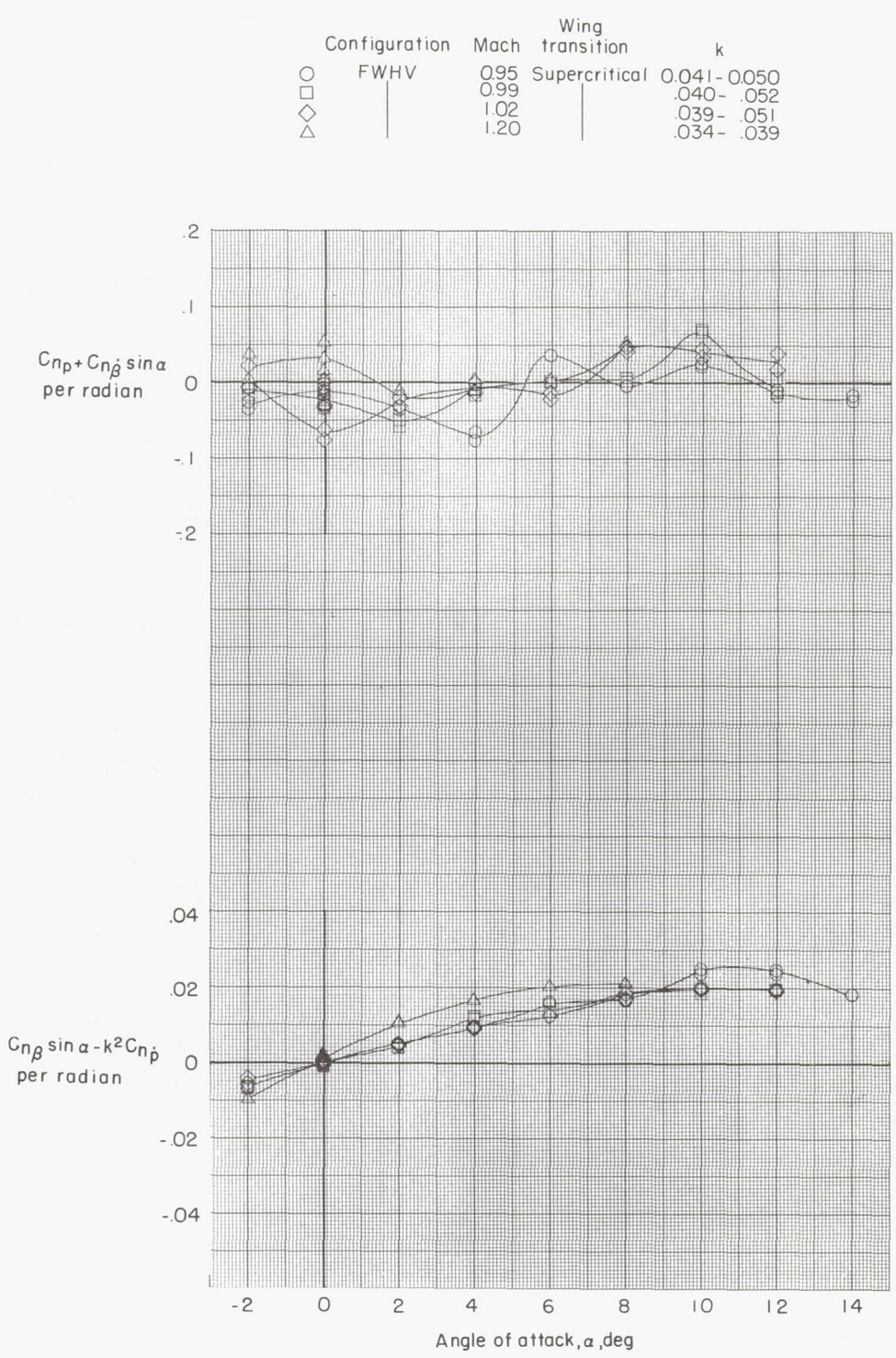

(b) M = 0.95, 0.99, 1.02, and 1.20.

Figure 20.- Concluded.

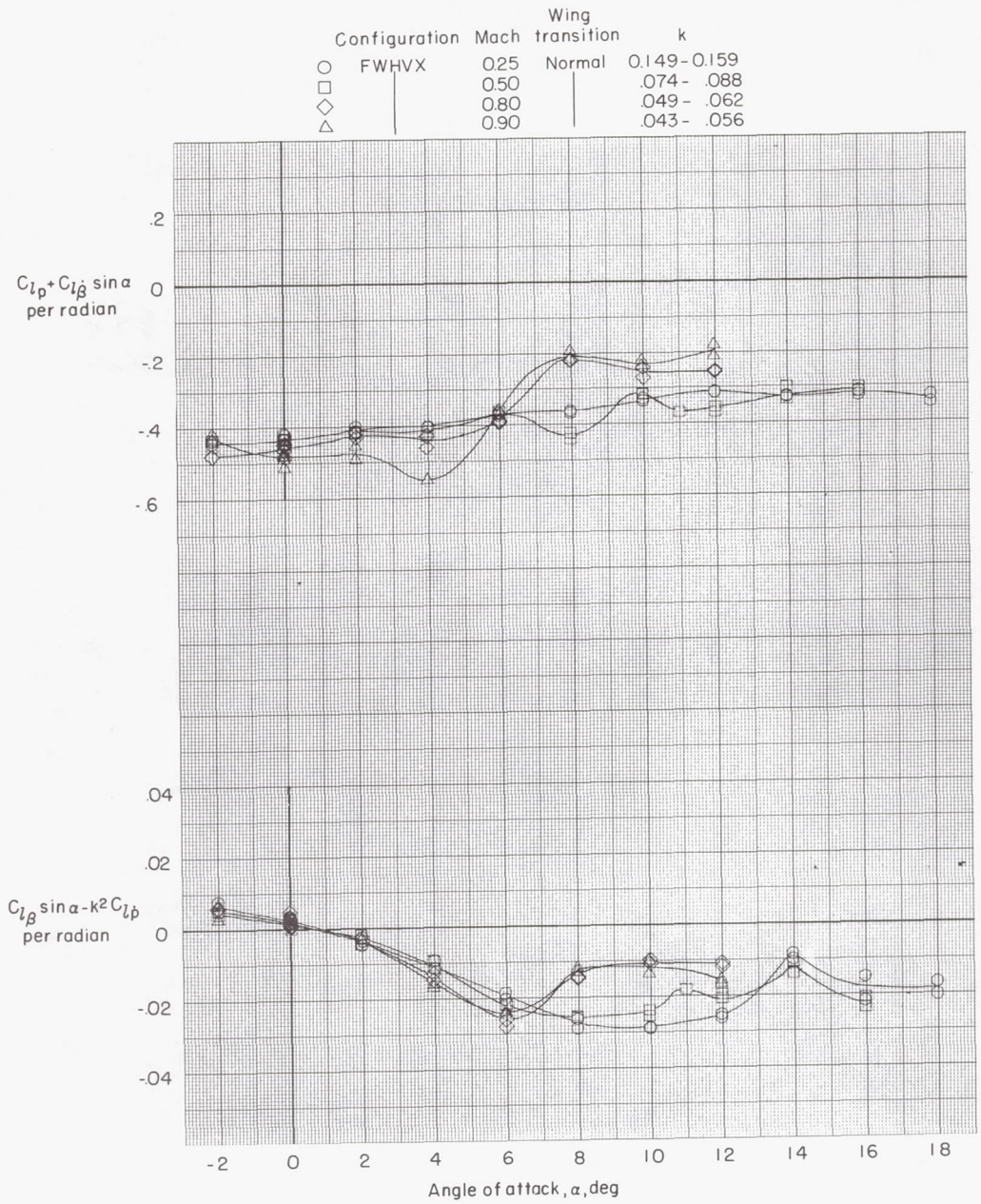

(a) M = 0.25, 0.50, 0.80, and 0.90.

Figure 21.- Variation of damping-in-roll parameter and rolling moment due to roll displacement parameter with angle of attack for basic configuration with vortex generators.

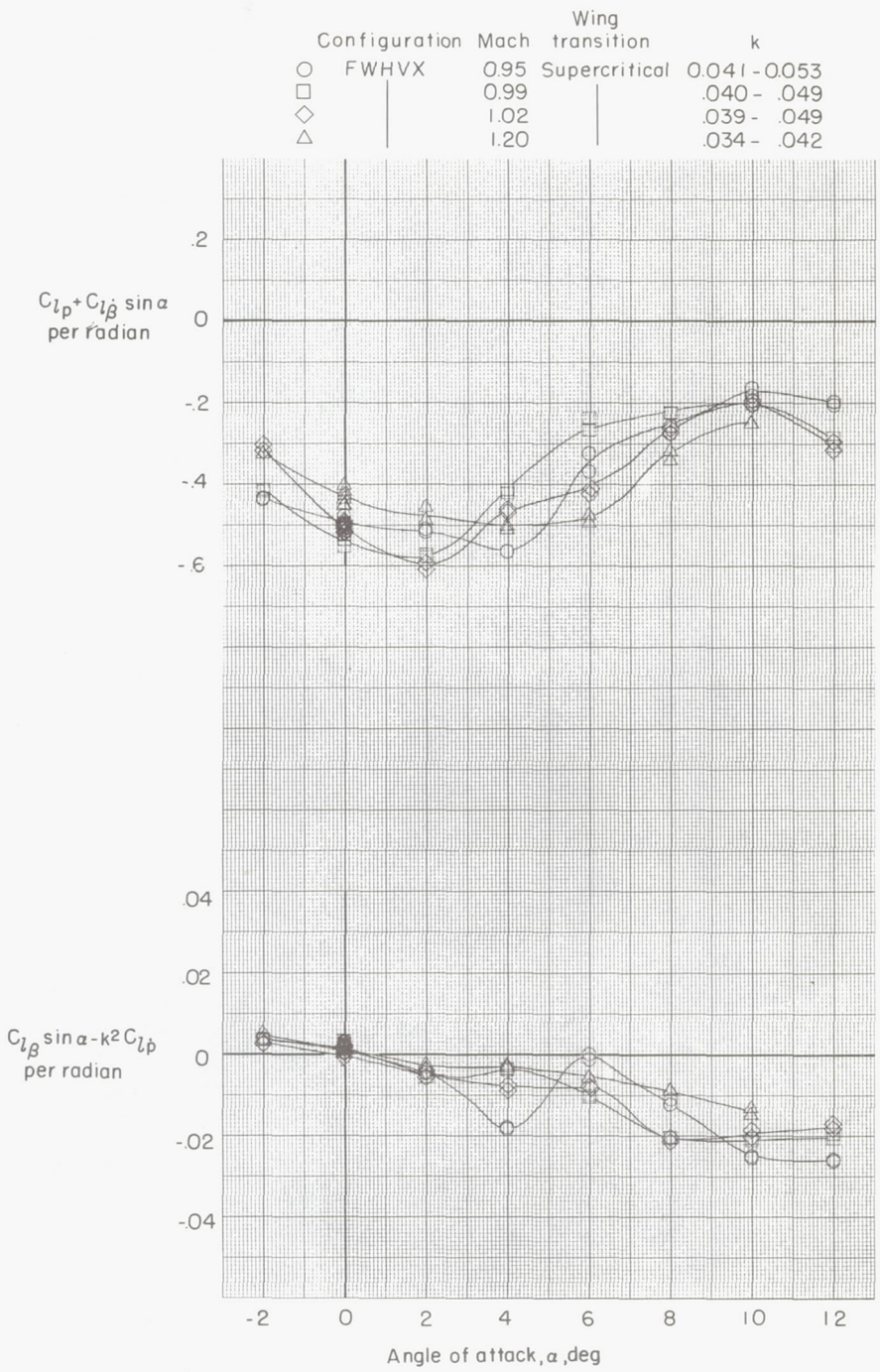

(b) M = 0.95, 0.99, 1.02, and 1.20.

Figure 21.- Concluded.

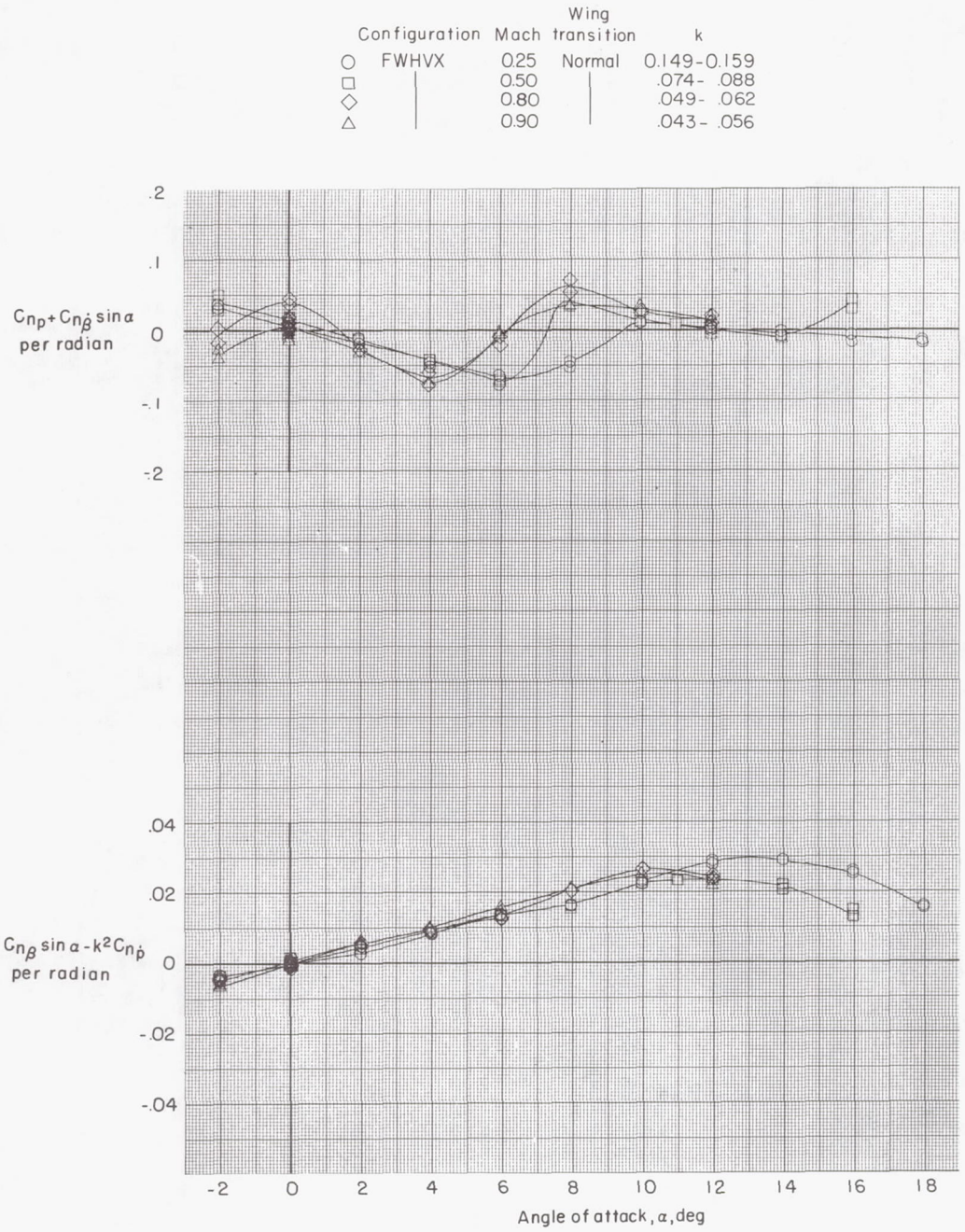

(a) M = 0.25, 0.50, 0.80, and 0.90.

Figure 22.- Variation of yawing moment due to roll rate parameter and yawing moment due to roll displacement parameter with angle of attack for basic configuration with vortex generators.

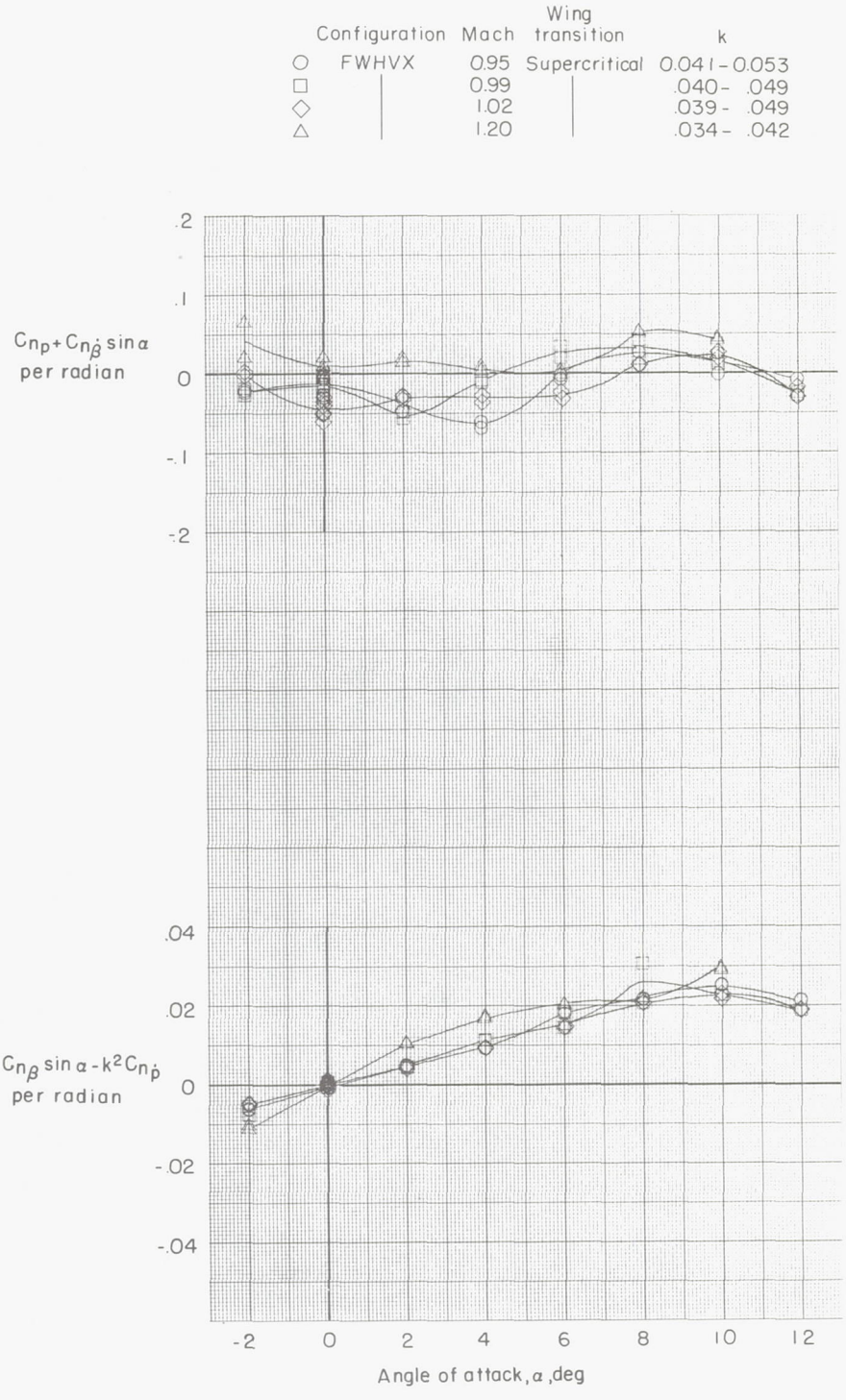

(b) M = 0.95, 0.99, 1.02, and 1.20.

Figure 22.- Concluded.

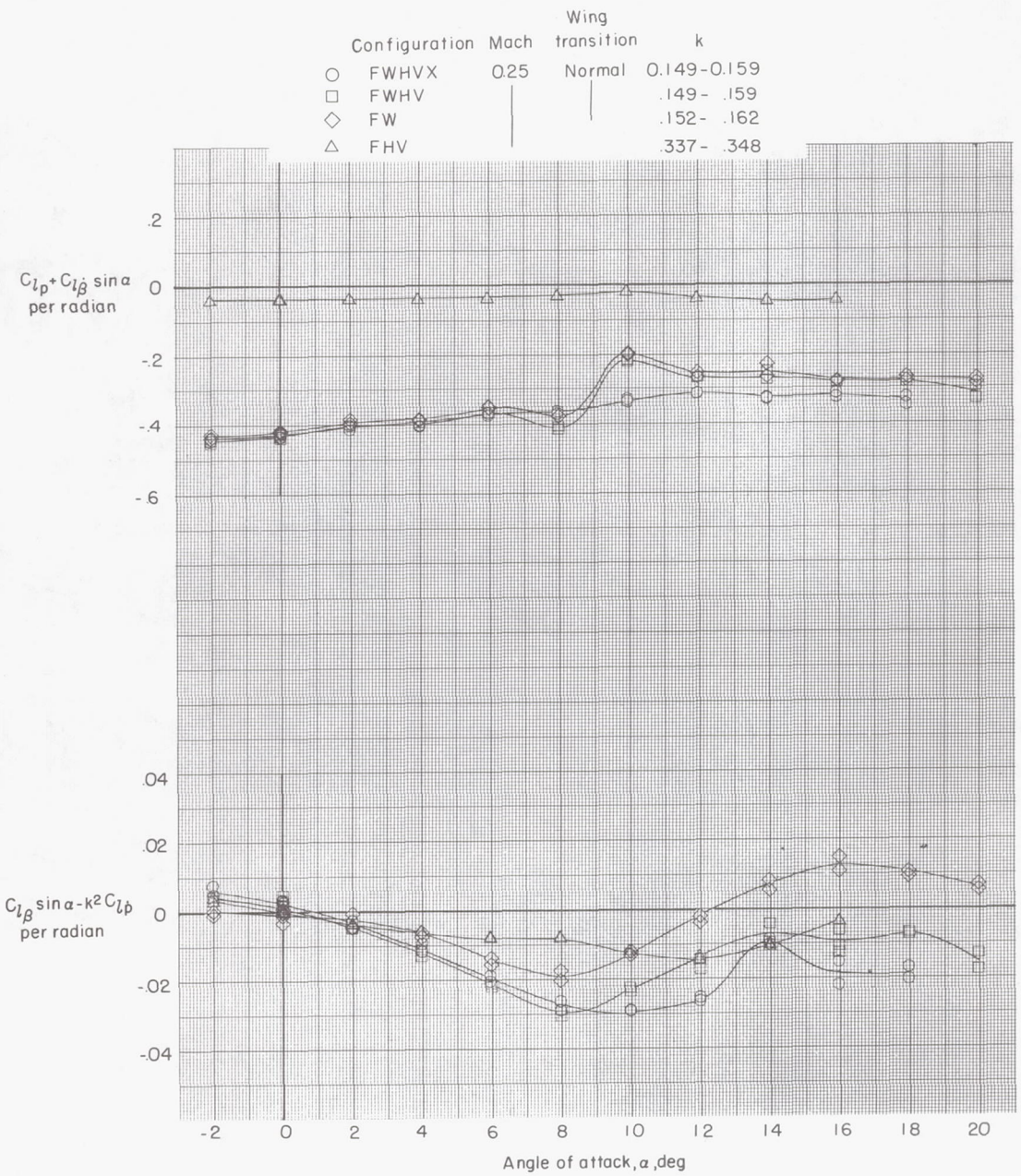

(a) M = 0.25.

Figure 23.- Variation of damping-in-roll parameter and rolling moment due to roll displacement parameter with angle of attack. Configuration component breakdown.

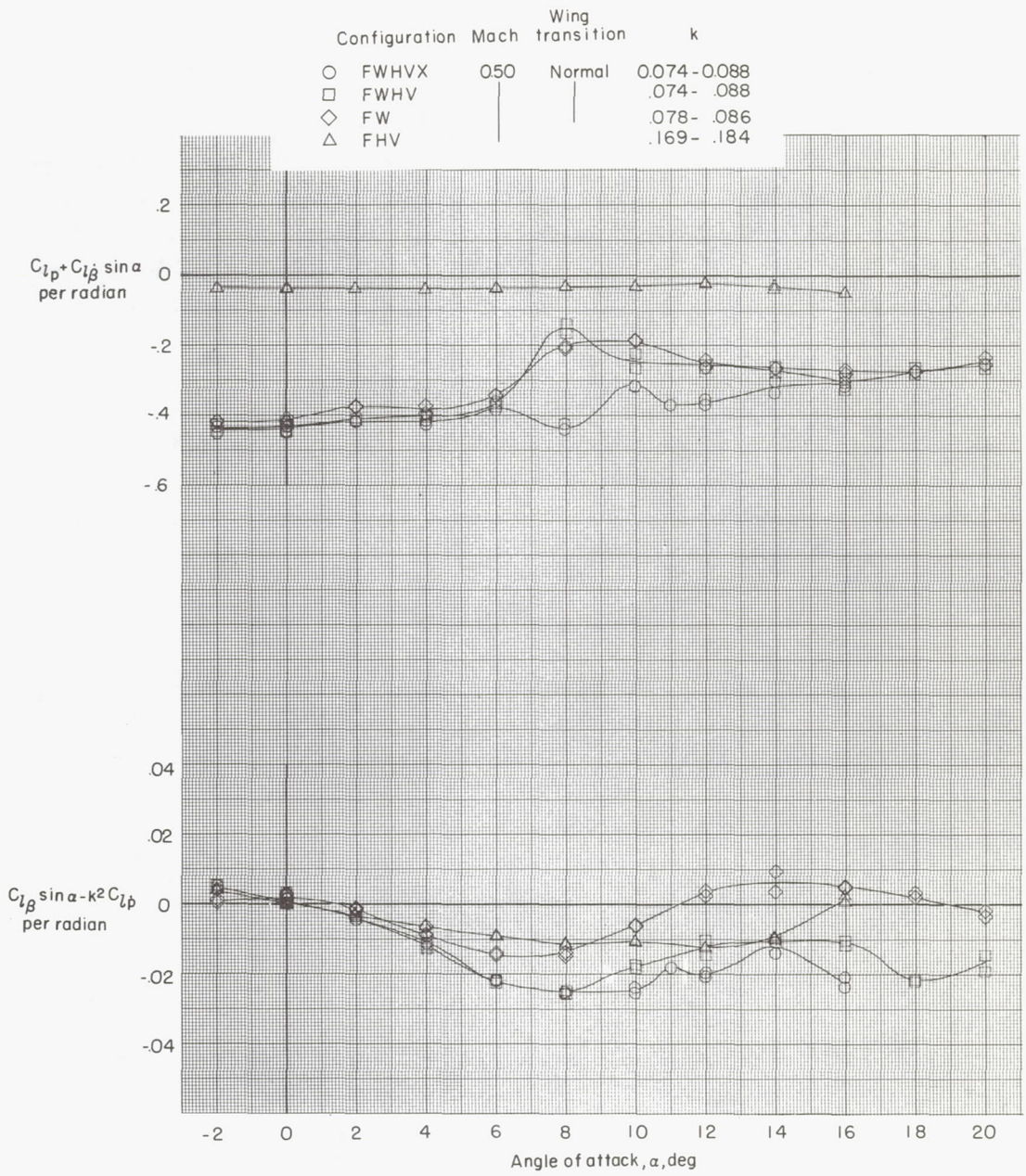

(b) M = 0.50.

Figure 23.- Continued.

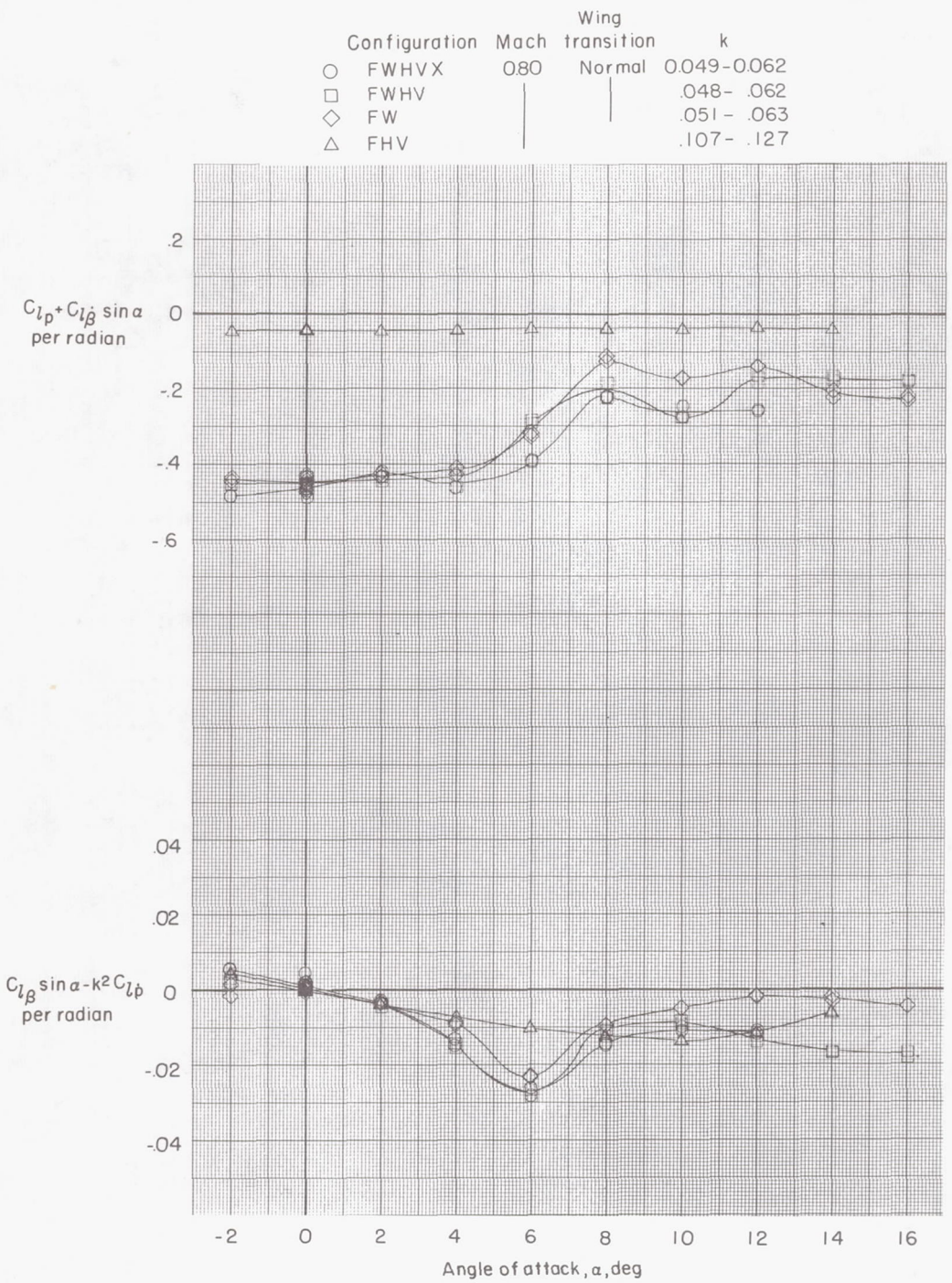

(c) M = 0.80.

Figure 23.- Continued.

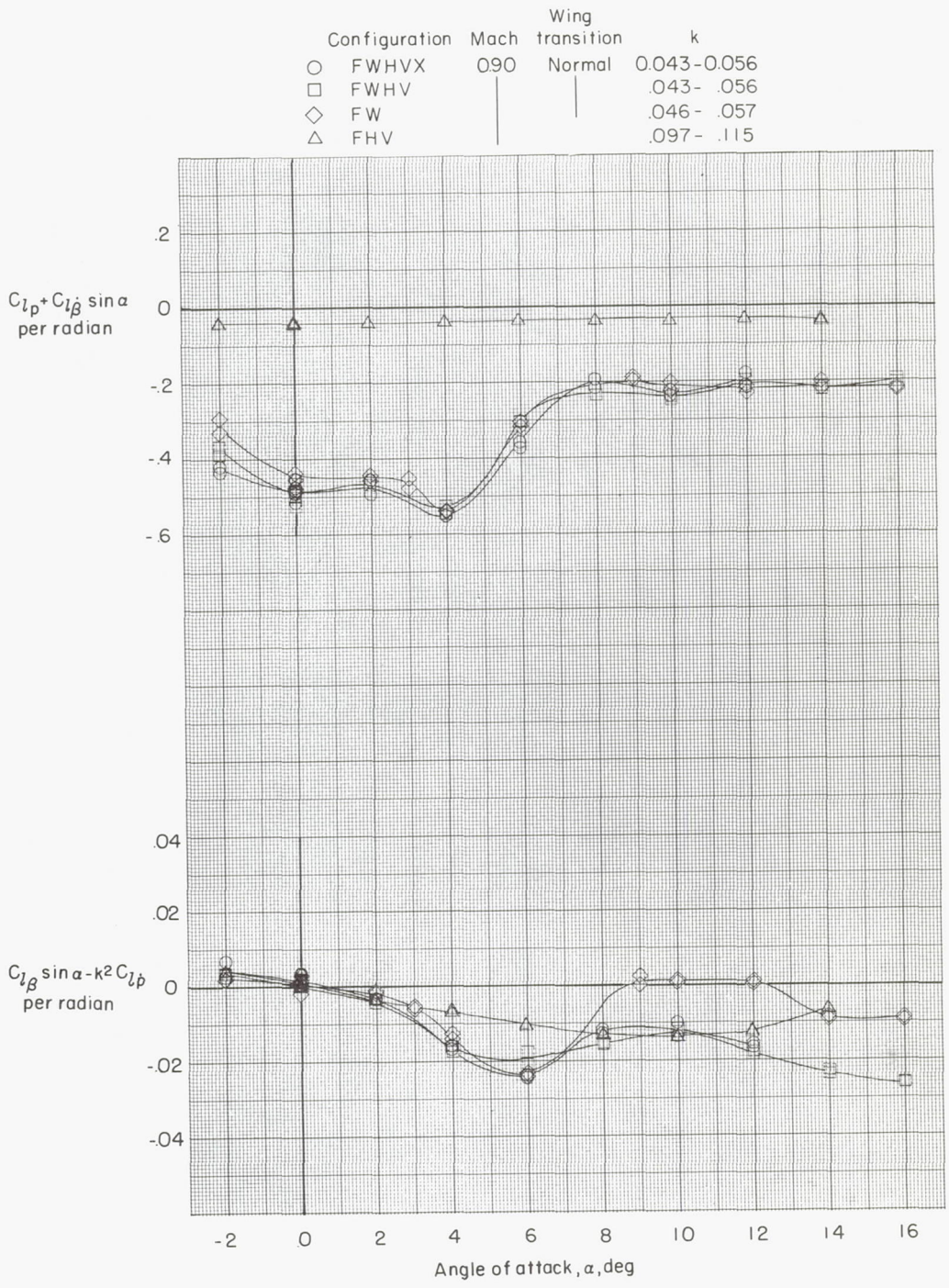

(d) M = 0.90.

Figure 23.- Continued.

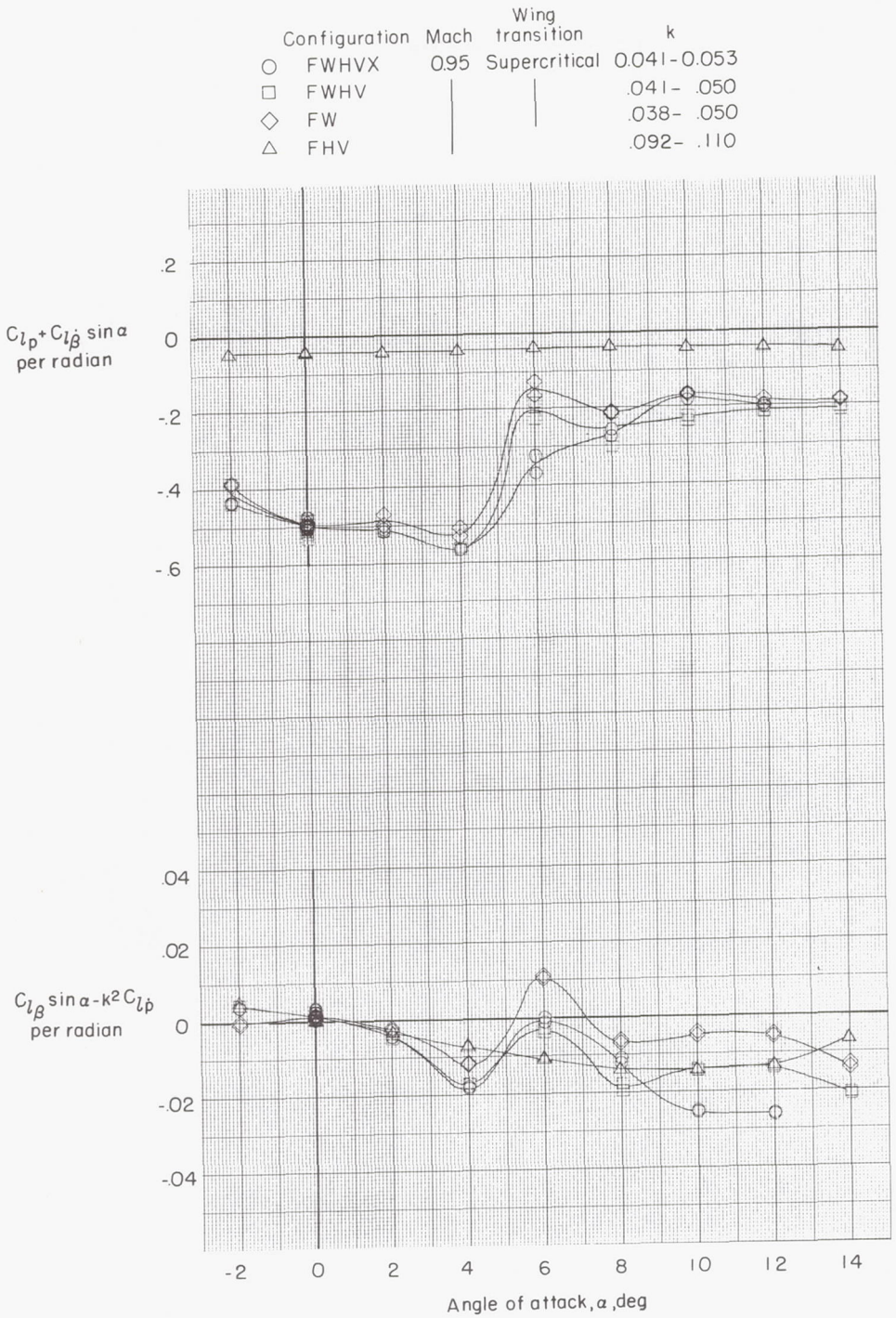

(e) M = 0.95.

Figure 23.- Continued.

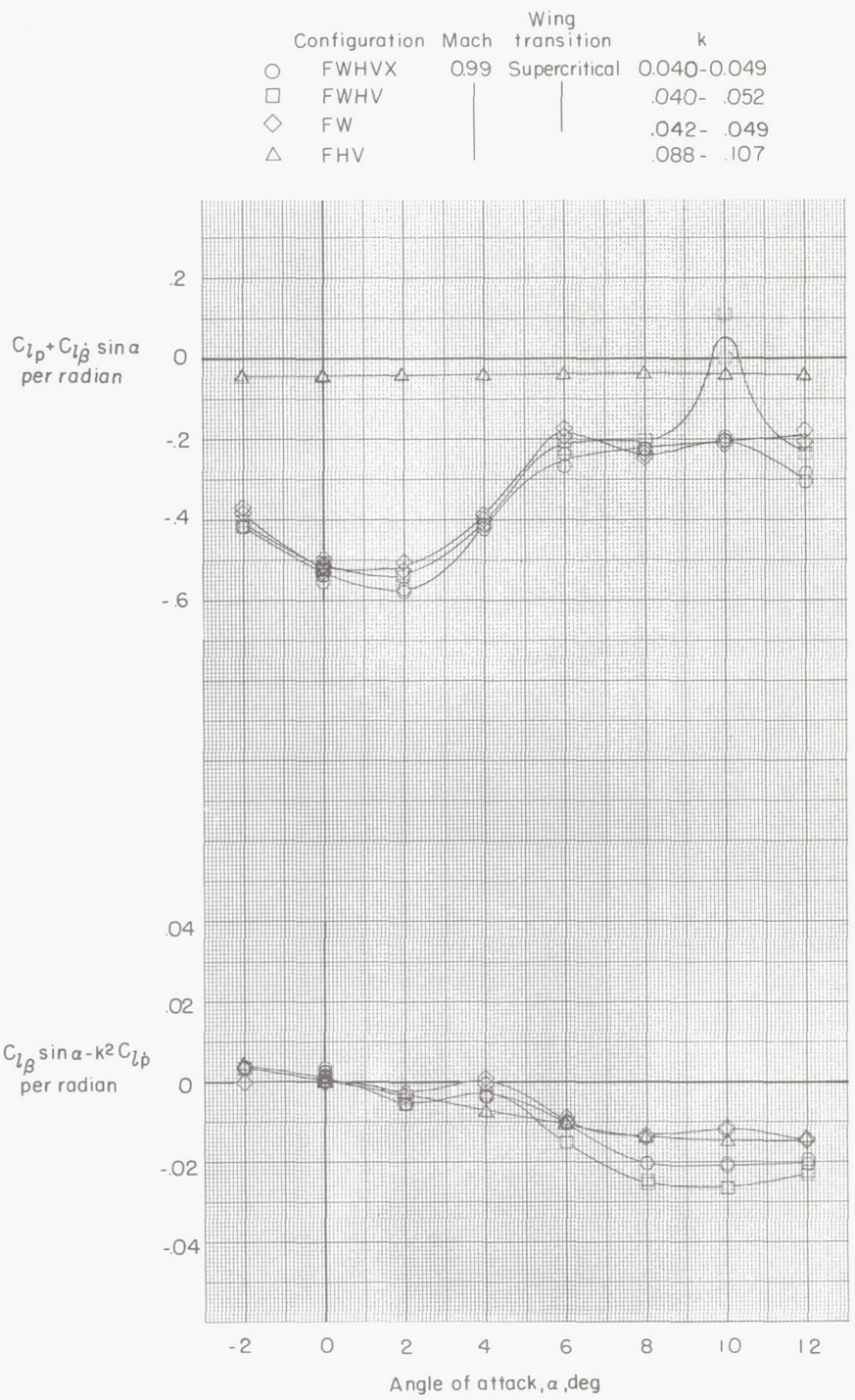

(f) M = 0.99.

Figure 23.- Continued.

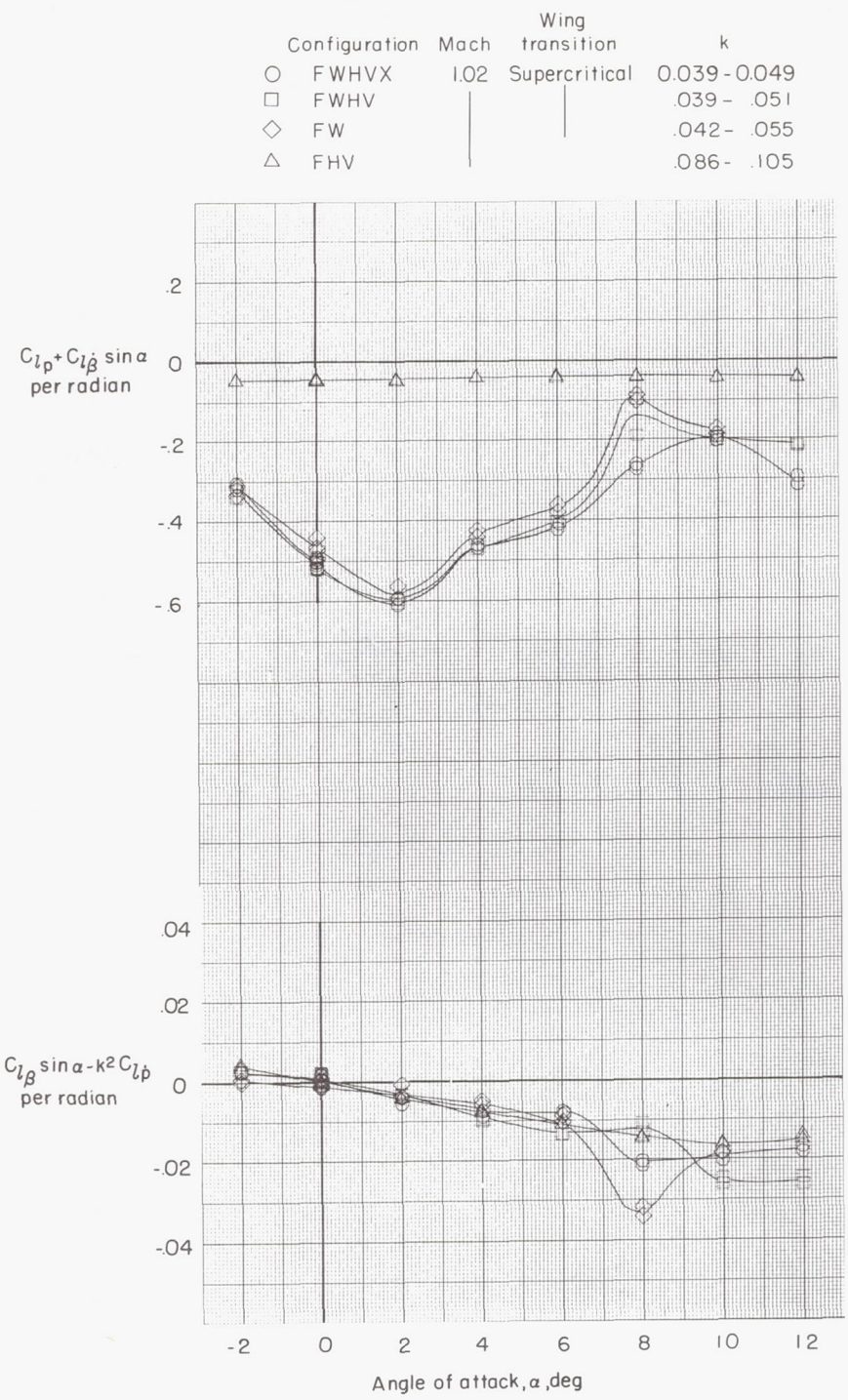

(g) M = 1.02.

Figure 23.- Continued.

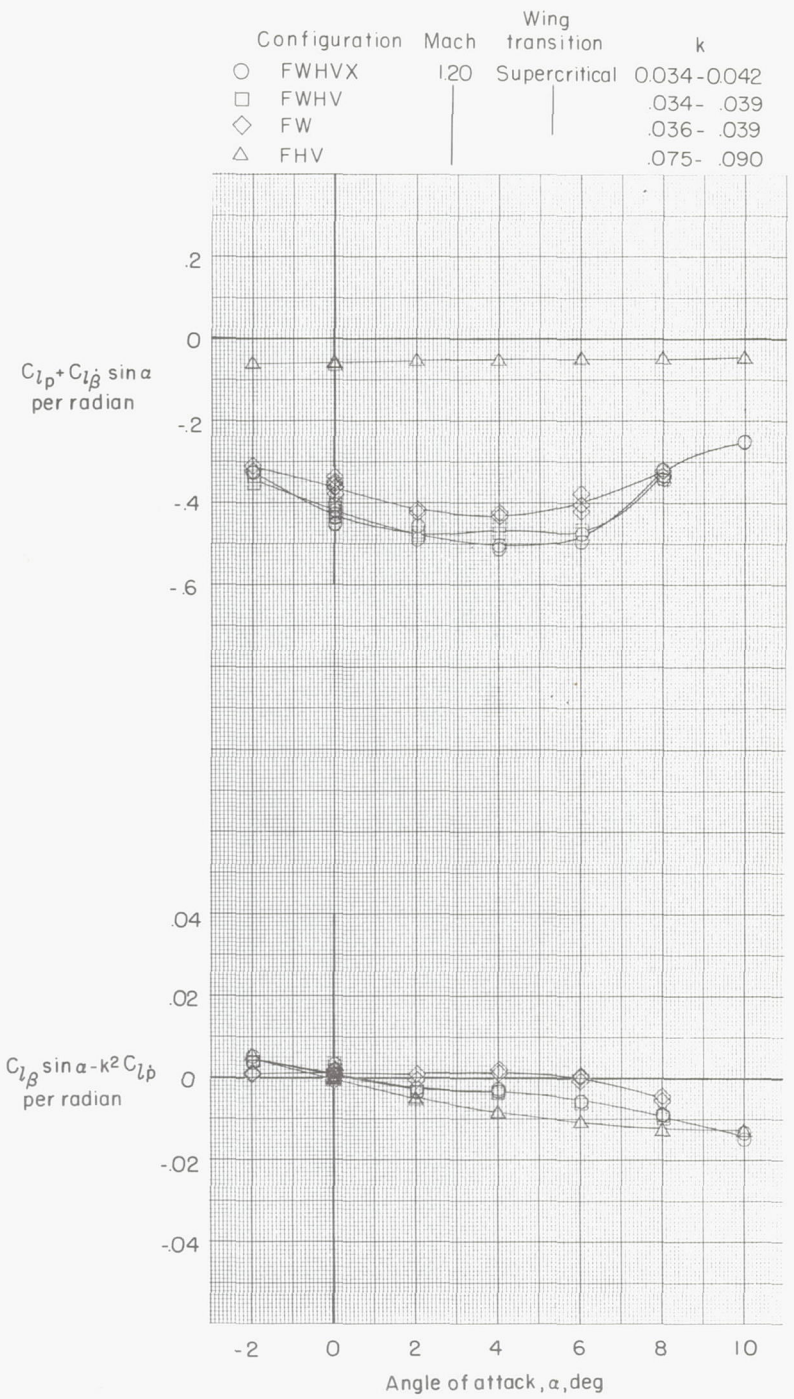

(h) M = 1.20.

Figure 23.- Concluded.

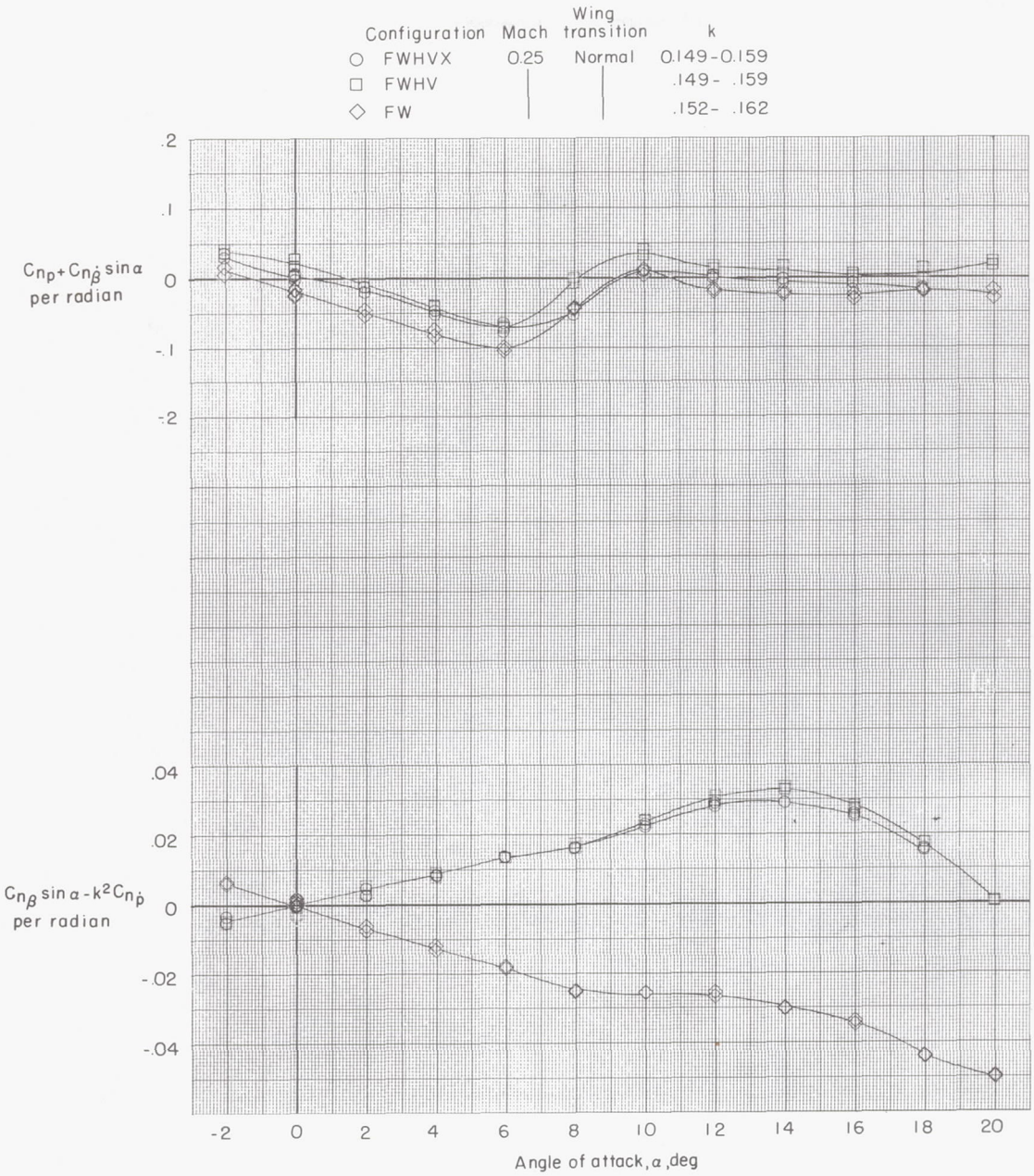

(a) M = 0.25.

Figure 24.- Variation of yawing moment due to roll rate parameter and yawing moment due to roll displacement parameter with angle of attack. Configuration component breakdown.

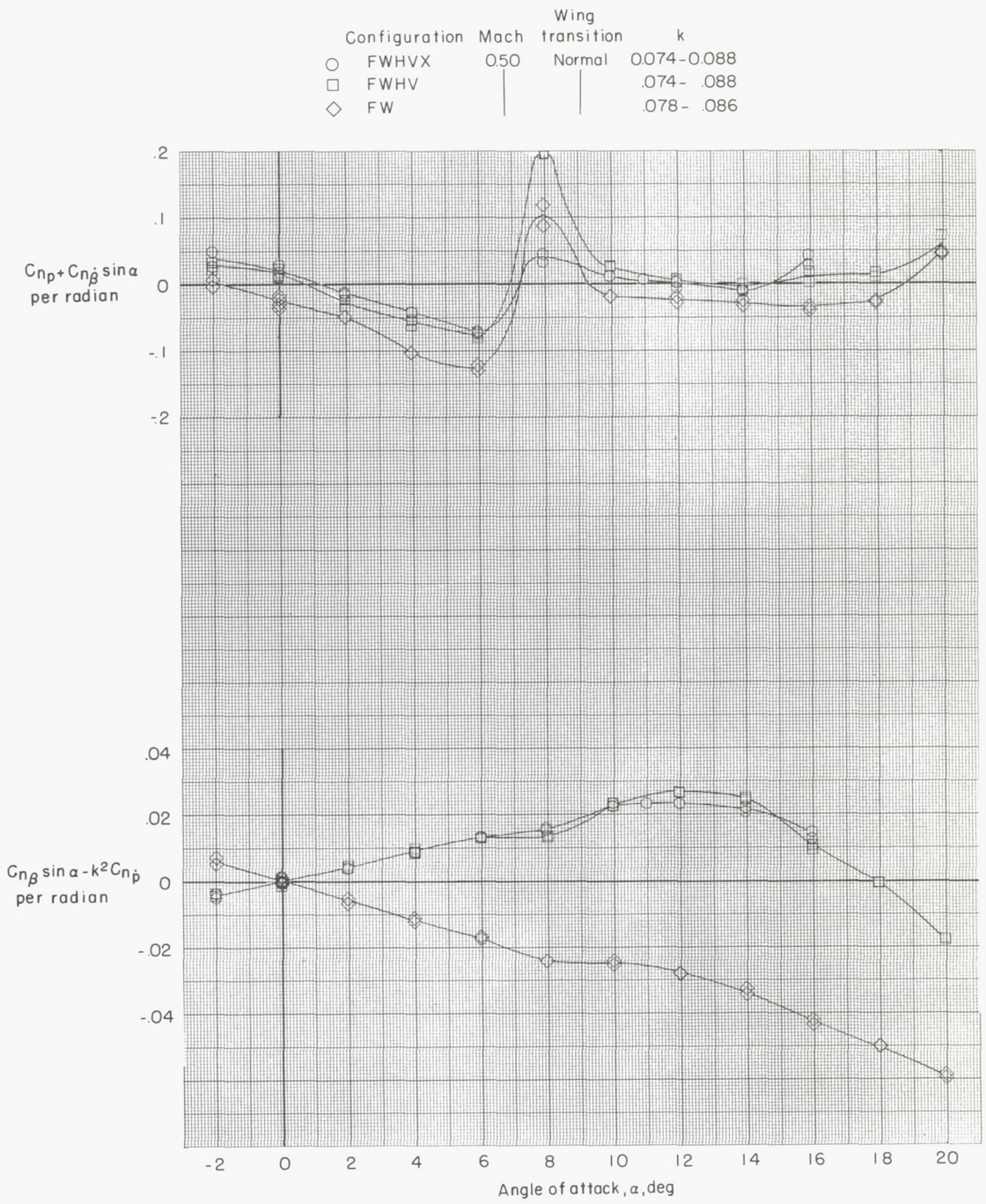

(b) M = 0.50.

Figure 24.- Continued.

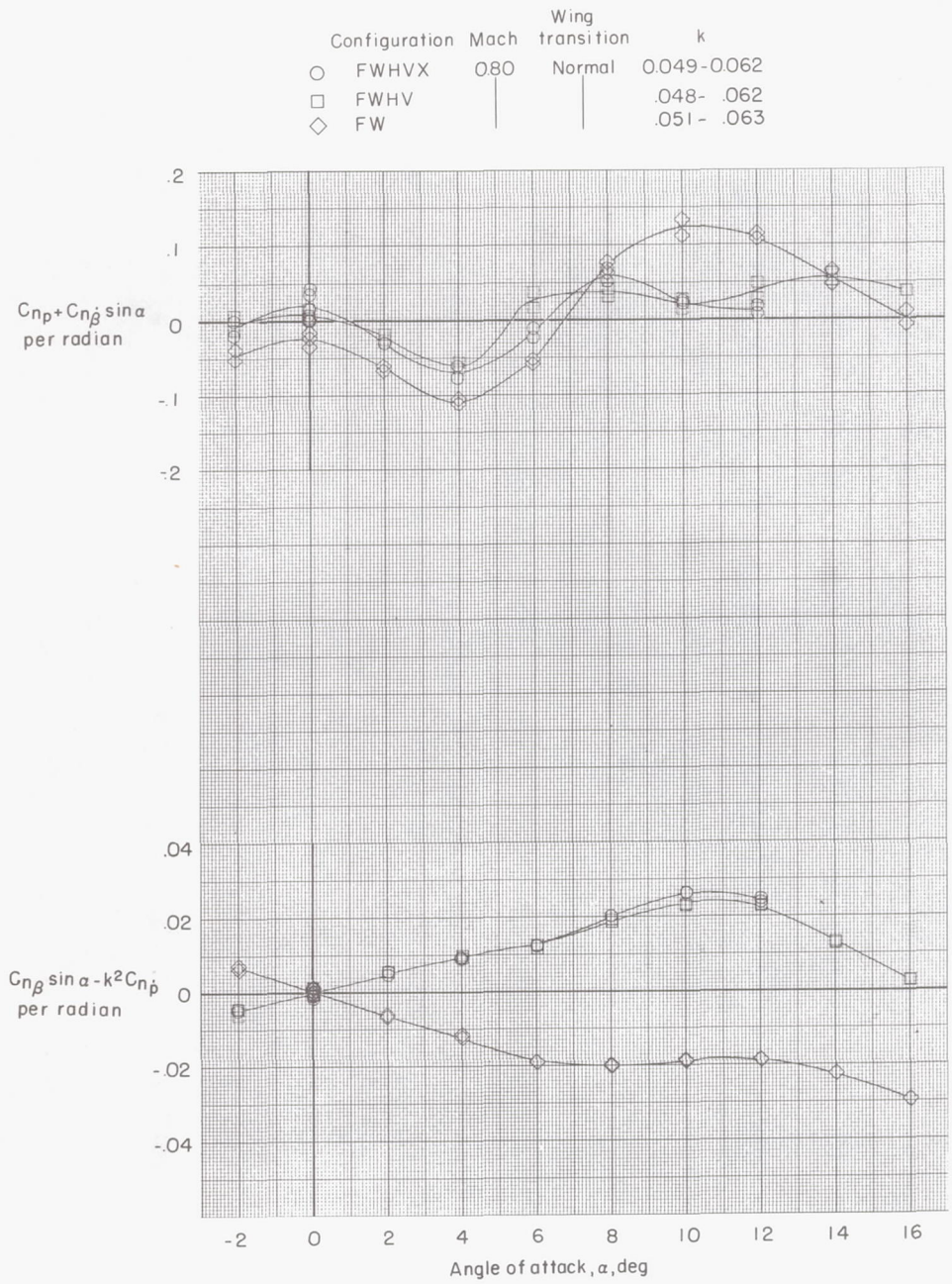

(c) M = 0.80.

Figure 24.- Continued.

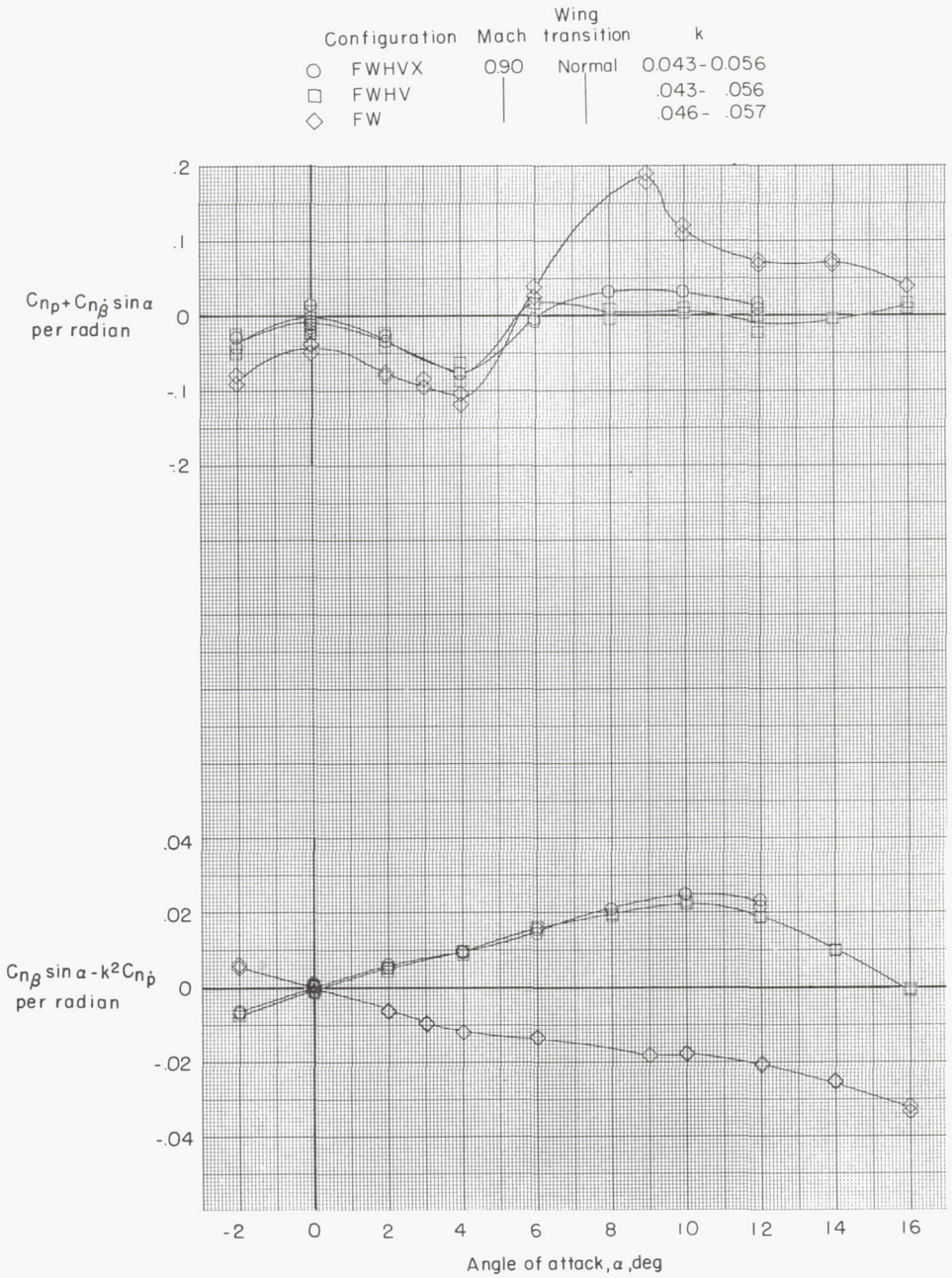

(d) M = 0.90.

Figure 24.- Continued.

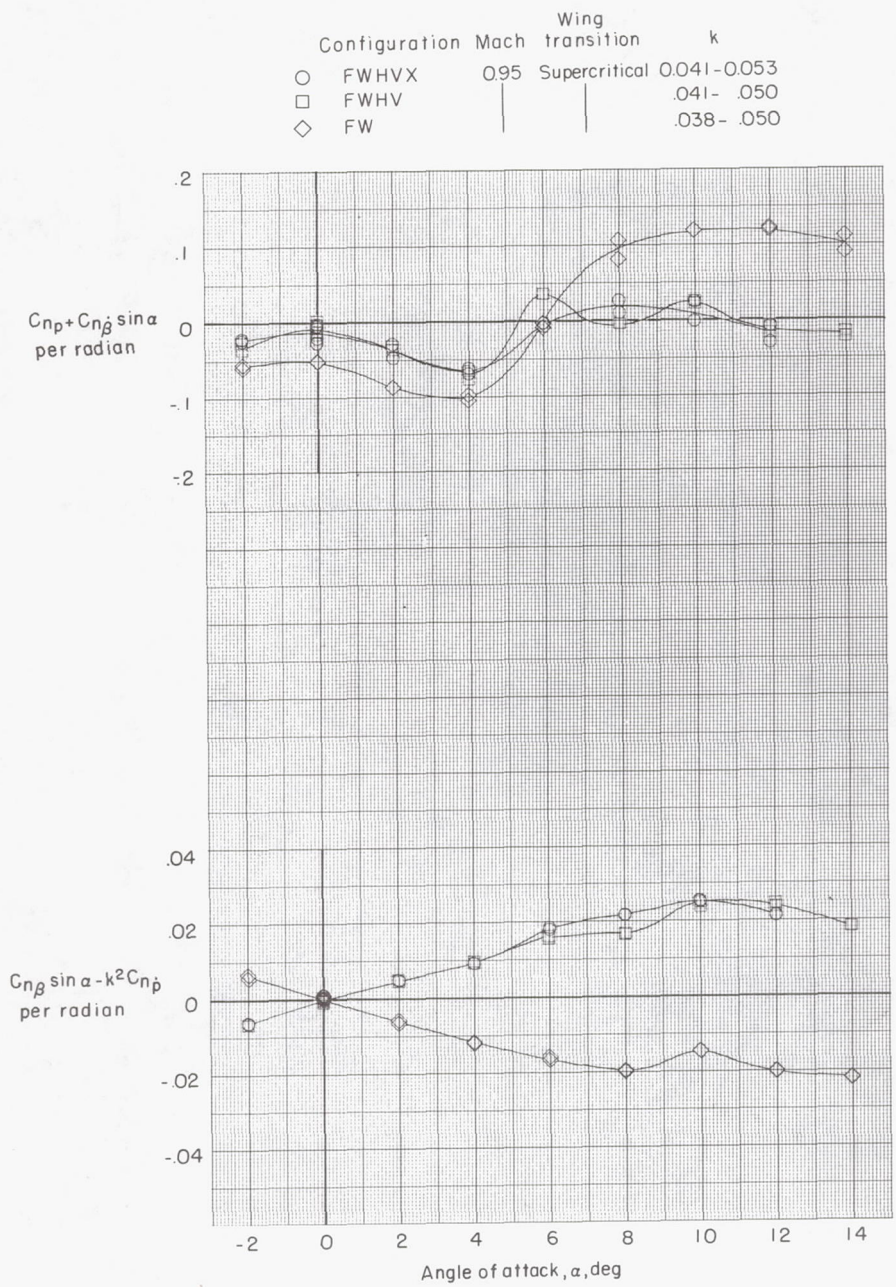

(e) M = 0.95.

Figure 24.- Continued.

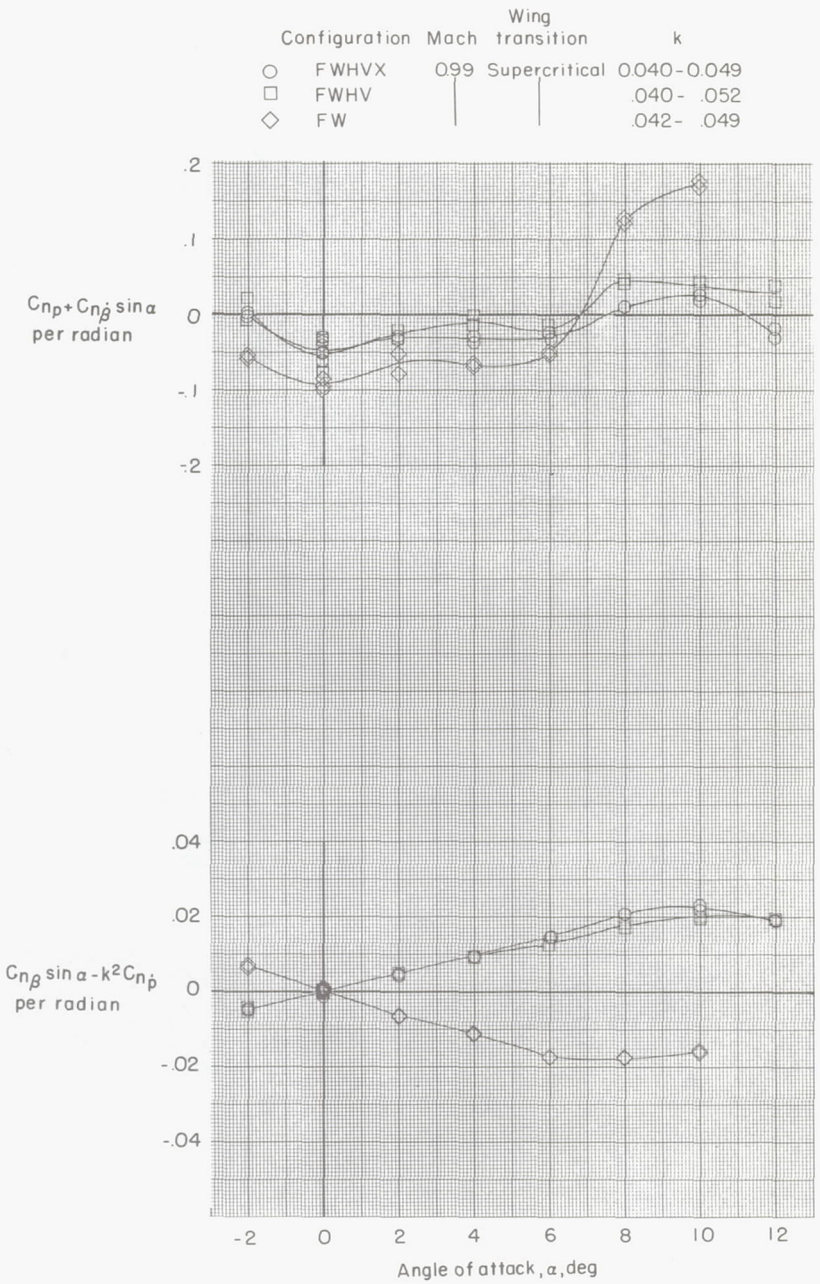

(f) M = 0.99.

Figure 24.- Continued.

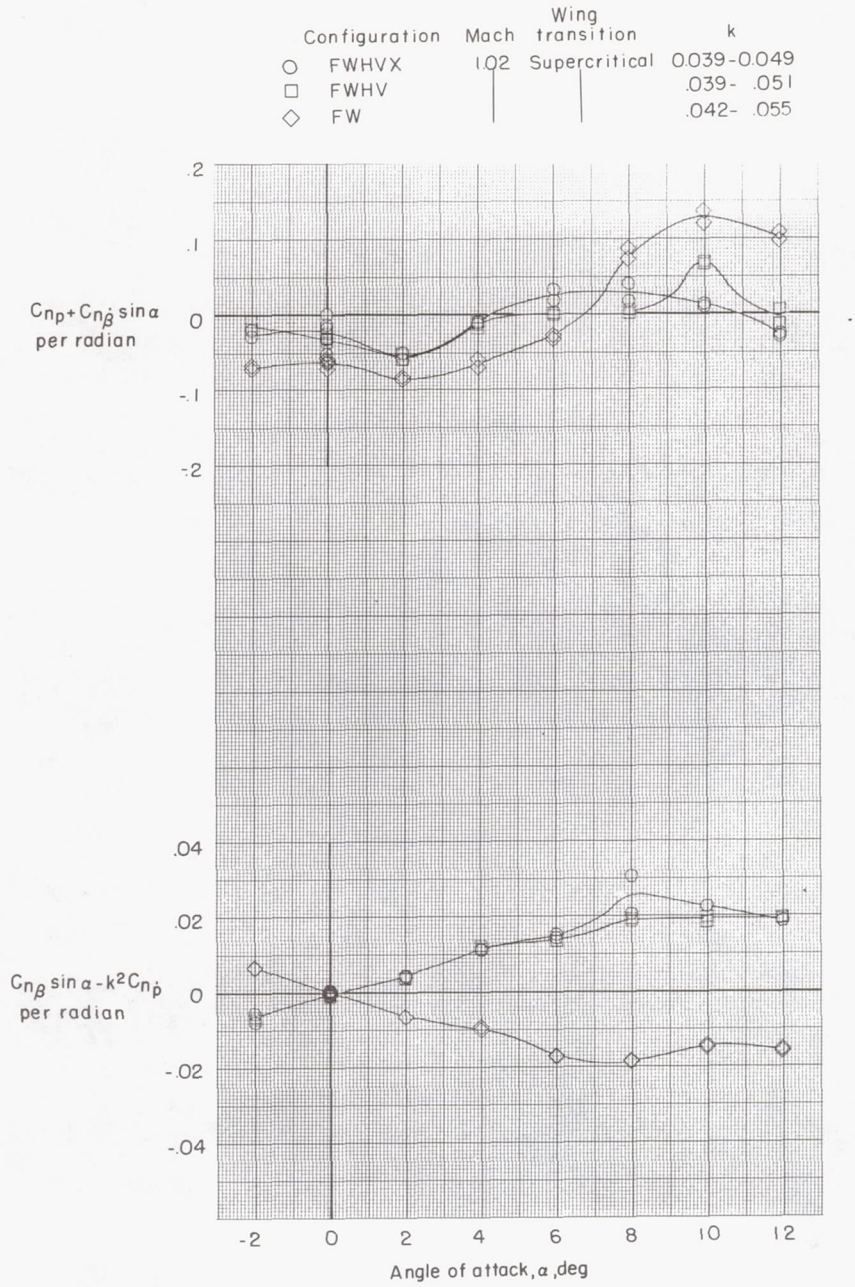

(g) M = 1.02.

Figure 24.- Continued.

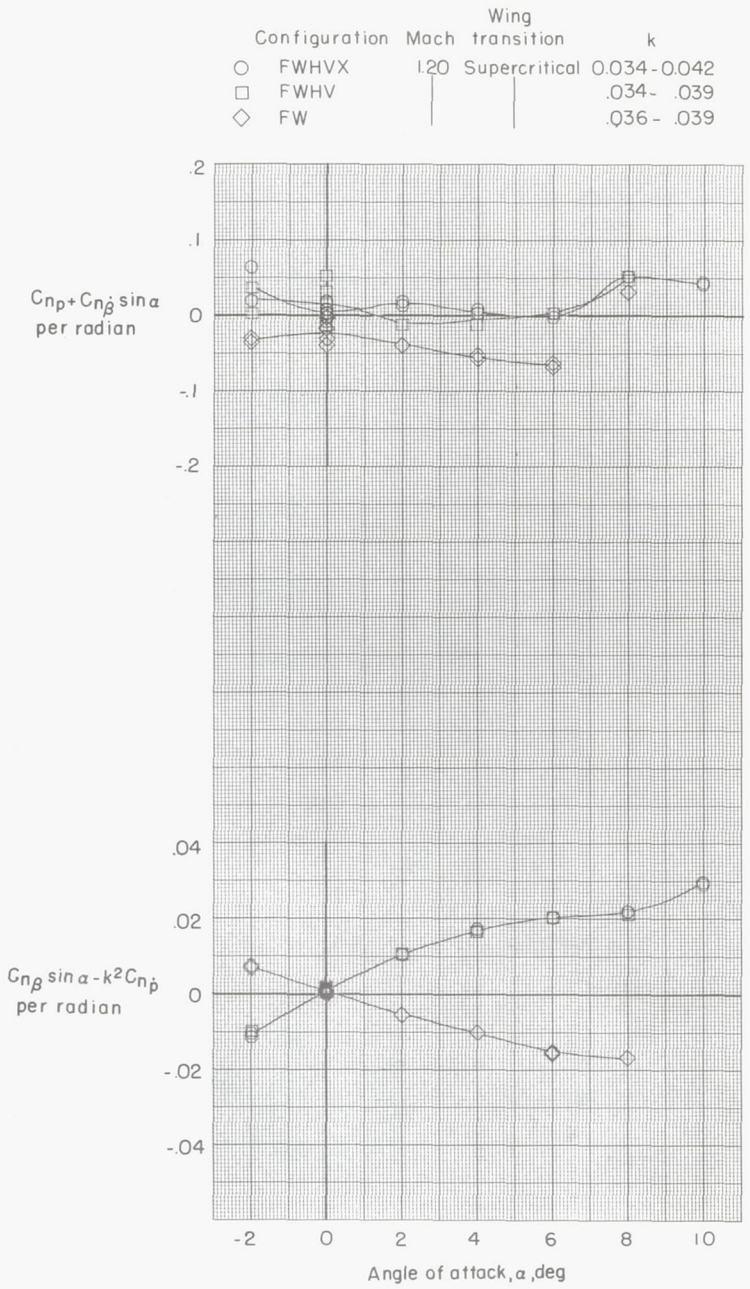

(h) M = 1.20.

Figure 24.- Concluded.

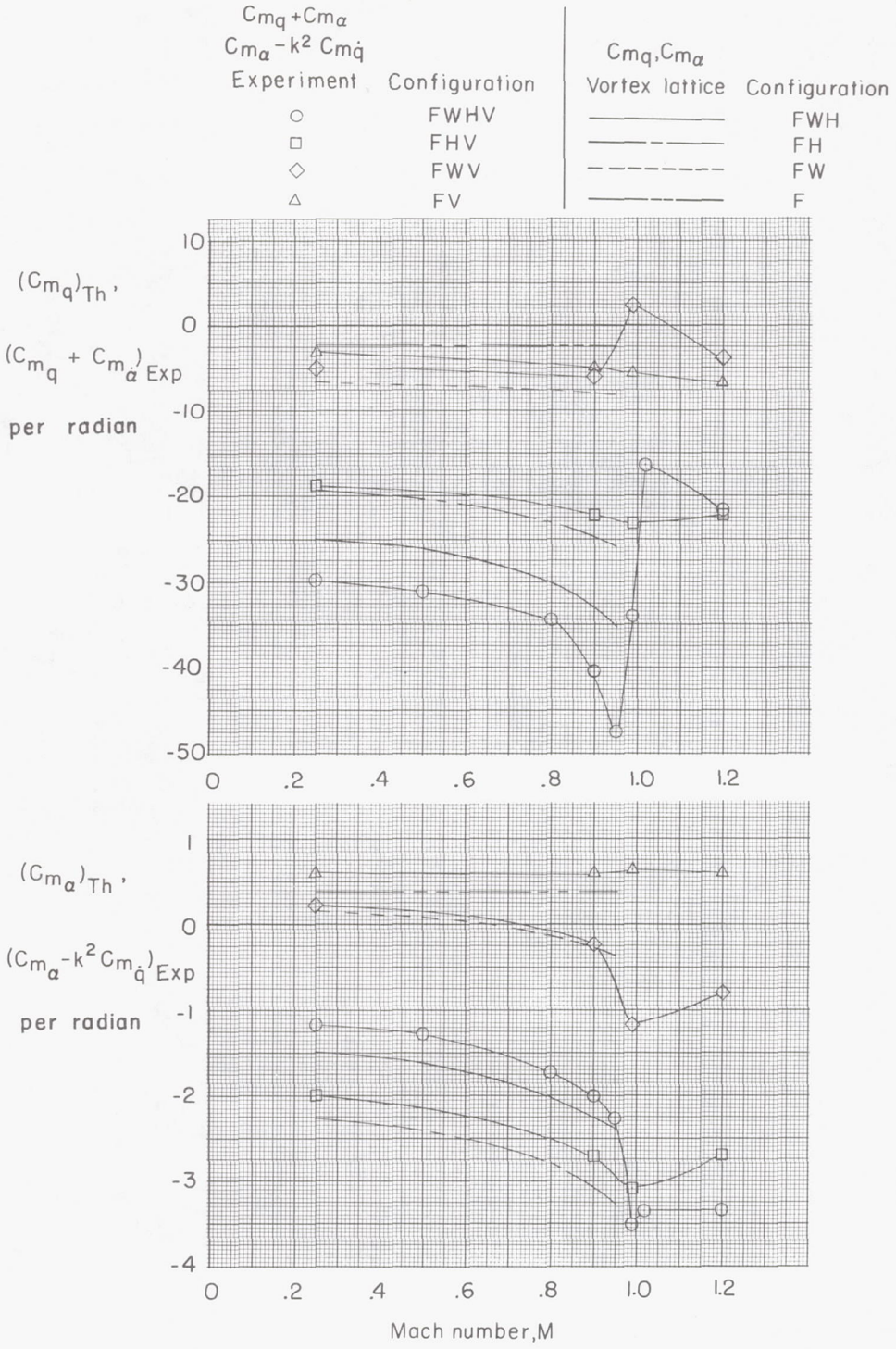

(a) Damping in pitch and longitudinal stability.

Figure 25.- Comparison of experiment with vortex-lattice prediction. $\alpha = 0^{\circ}$.

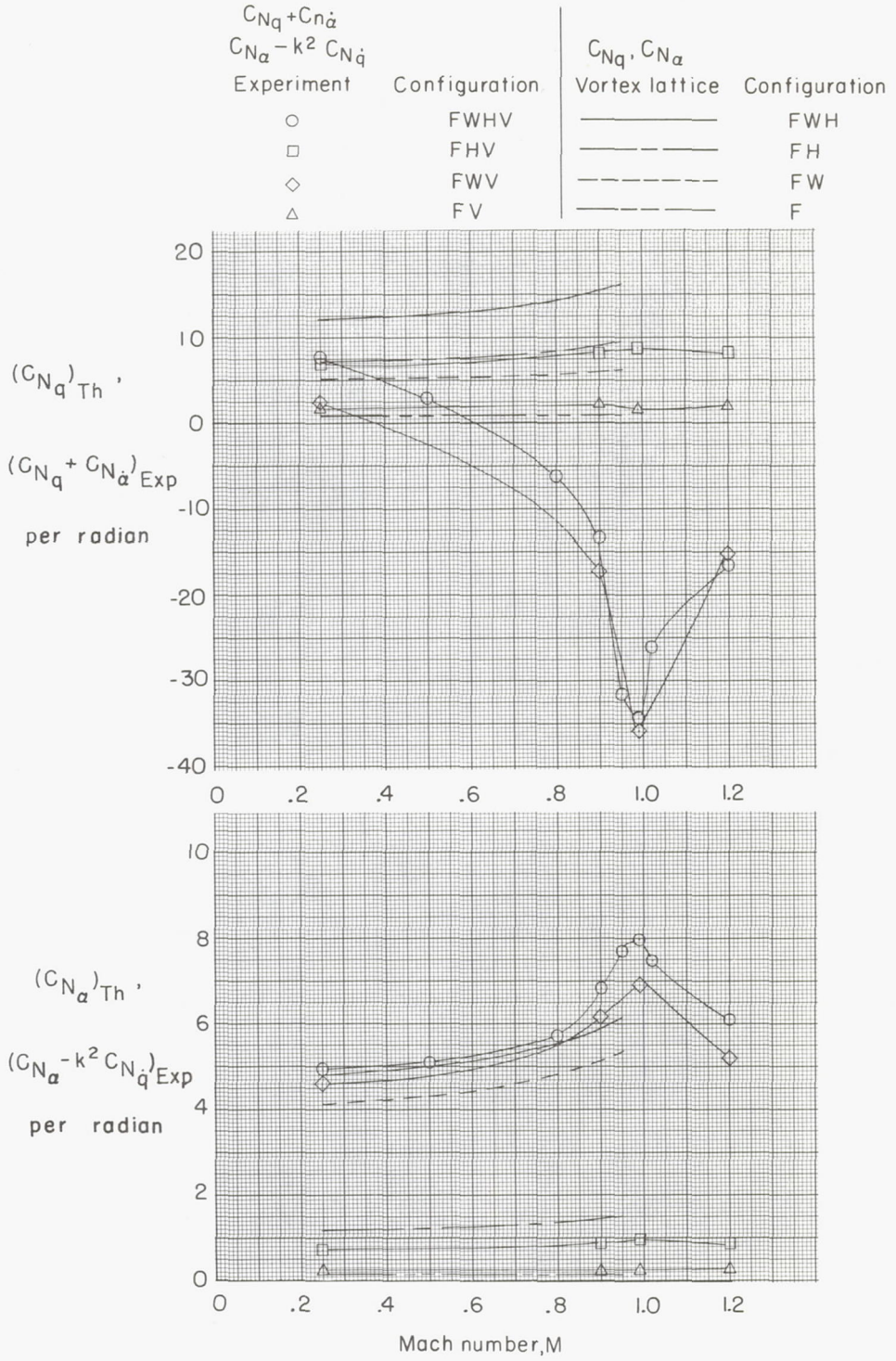

(b) Normal force due to pitch rate and normal force due to pitch displacement.

Figure 25.- Continued.

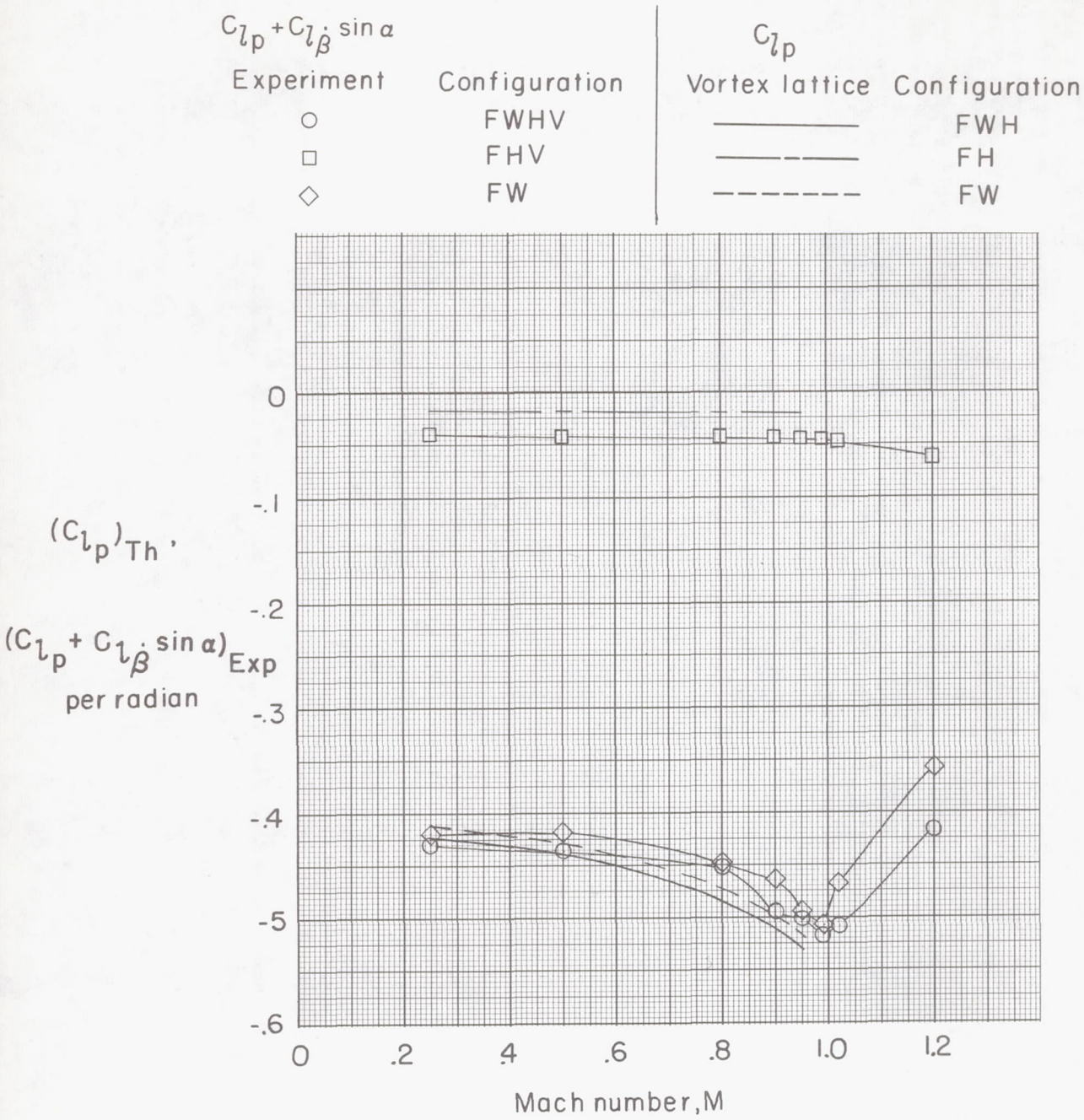

(c) Damping in roll.

Figure 25.- Concluded.

"The aeronautical and space activities of the United States shall be conducted so as to contribute . . . to the expansion of human knowledge of phenomena in the atmosphere and space. The Administration shall provide for the widest practicable and appropriate dissemination of information concerning its activities and the results thereof."

—NATIONAL AERONAUTICS AND SPACE ACT OF 1958

NASA SCIENTIFIC AND TECHNICAL PUBLICATIONS

TECHNICAL REPORTS: Scientific and technical information considered important, complete, and a lasting contribution to existing knowledge.

TECHNICAL NOTES: Information less broad in scope but nevertheless of importance as a contribution to existing knowledge.

TECHNICAL MEMORANDUMS: Information receiving limited distribution because of preliminary data, security classification, or other reasons.

CONTRACTOR REPORTS: Scientific and technical information generated under a NASA contract or grant and considered an important contribution to existing knowledge.

TECHNICAL TRANSLATIONS: Information published in a foreign language considered to merit NASA distribution in English.

SPECIAL PUBLICATIONS: Information derived from or of value to NASA activities. Publications include conference proceedings, monographs, data compilations, handbooks, sourcebooks, and special bibliographies.

TECHNOLOGY UTILIZATION PUBLICATIONS: Information on technology used by NASA that may be of particular interest in commercial and other non-aerospace applications. Publications include Tech Briefs, Technology Utilization Reports and Notes, and Technology Surveys.

Details on the availability of these publications may be obtained from:

SCIENTIFIC AND TECHNICAL INFORMATION OFFICE
NATIONAL AERONAUTICS AND SPACE ADMINISTRATION
Washington, D.C. 20546